NADPH:Protochlorophyllide Oxidoreductase (POR) – Advanced Insight into the Catalytic Mechanism of the Two Plant Isozymes POR A and POR B

Dissertation

To fulfil the requirements for the title
"Doctor rerum naturalium" (Dr. rer. nat.)

seit 1558

Submitted to the council of the Faculty of Biology and Pharmacy of the Friedrich Schiller University

by Alessio Garrone (MSc Industrial Biotechnology)
born on 23.09.1985 in Ciriè (IT)

Reviewers:

PD Dr. Gudrun Hermann, Friedrich-Schiller-University Jena

apl. Prof. Dr. Michael Schmitt, Friedrich-Schiller-University Jena

Prof. Dr. Jörg Matysik, University of Leipzig

Day of the examination: 20th of October 2017

Table of abbreviations

Abbreviation	Extended form	Abbreviation	Extended form
3-D	three dimensions	Lys - K	lysine
ALA	5-aminolevulinic acid	mg	milligram
ACN	acetonitrile	Mg	magnesium
Ala – A	alanine	min	minute
Asp - D	aspartic acid	ml	millilitre
C	Celsius	NADPH	nicotinamide adenine dinucleotide phosphate
Chla	chlorophyll a	ns	nanosecond
Chlide	chlorophyllide a	ON	over night
Cys - C	cysteine	PChlide	protochlorophyllide a
DPOR	dark operative protocholorophyllide oxidoreductase	PDB	Protein Data Bank
DTT	dithiothreitol	Phe - F	phenylalanine
E_a	activation energy	PLB	pro lamellar body
EFA	exploratory factor analysis	POR	NAPDH: protocholorophyllide oxidoreductase
FPLC	fast protein liquid chromatography	s	second
Glu - E	glutamic acid	SDS-PAGE	sodium dodecyl sulphate polyacrylamide gel electrophoresis
GSA	glutamate-1-semialdehyde	Ser - S	serine
His - H	histidine	S_{ICT}	intramolecular charge transfer state
HOMO	highest occupied molecular orbital	SVD	singular value decomposition
HPLC	high-performance liquid chromatography	t	time
IR	infrared	TLC	thin layer chromatography
K	Kelvin	Tyr - Y	tyrosine
k_{cat}	catalytic constant	UV-Vis	ultra violet - visible spectroscopy
kDa	kilo Dalton	V_{max}	maximal velocity
K_M	Michaelis-Menten constant	v_o	initial velocity
LHPP	light harvesting POR PChlide complex	W	Watt
LUMO	lowest unoccupied molecular orbital		

Abstract

NADPH:protochlorophyllide oxidoreductase (POR), EC 1.3.1.33, is a key enzyme in the biosynthesis of chlorophyll in all organisms with oxygenic photosynthesis. POR catalyses the reduction of protochlorophyllide (PChlide) to chlorophyllide (Chlide) by the absorption of light and in the presence of the cofactor NADPH.

In plants, two different isoenzymes are found, POR A and POR B. POR A is transiently active in etiolated plant seedlings, whereas POR B is predominantly active throughout the greening process and in greened and adult plants. The two plant POR isoenzymes are compared with respect to their catalytic efficiency and their reaction mechanism in experiments using highly purified recombinant POR from barley (*Hordeum vulgare L.*) heterologously expressed in *Escherichia coli*. POR B shows a 3-fold higher binding affinity (K_M) when compared with POR A and a 6-fold higher catalytic efficiency (k_{cat}/K_M). Based on the reaction intermediates, which can be trapped at low temperatures, the same reaction mechanism operates in both POR A and POR B but a different temperature dependence of the dark reactions suggests a higher conformational flexibility of POR B in the surrounding of the active centre. Therefore, the increased catalytic efficiency of POR B as compared to POR A is attributed to the higher substrate binding affinity and a well-adapted enzyme dynamics of POR B. The initial light-driven step, which occurs at temperatures below 180 K, already produces enzyme-bound Chlide. In contrast with cyanobacteria POR from *Synechocystis*, which can be seen as phylogenetic ancestor of all other POR enzymes, the hydride and proton transfer reactions evidently occur in a coupled reaction step, most likely as a result of in optimized active site architecture in the higher-organism plant PORs.

With the aim of gaining a deeper insight into the active-site architecture a 3-D model is predicted for POR B by using in silico homology modelling techniques. The first prediction of a structural model for POR B including the docking the PChlide substrate and NADPH cofactor by adequate methods identifies His-138, Ser-164, Lys-216 and Tyr-299 as important residues for the correct positioning of the PChlide substrate within the active site. His-138 and Lys-216 interact with the propionic acid side chain at C(17) of PChlide through electrostatic/hydrogen bonding. Ser-164 undergoes formation of a coordinative bond to the central Mg^{2+} ion resulting in a pentocoordinated Mg^{2+} complex. Tyr-299 is most probably involved in interactions with the C(13')=O group of PChlide via hydrogen bonding. This active site architecture of POR B is validated by the replacement of the respective amino

acids in point mutation experiments. Moreover, the active site Tyr-212 and Lys-216 also play a key role in PChlide binding. Mutations to those residues compromise PChlide binding significantly, whereas mutation of Lys-216 has a more dramatic effect. Tyr-212 is also shown to take part in the proton transfer to the C(18) position of PChlide. This is the first evidence for the role of Tyr- 212 as proton donor in the photoreduction of PChlide catalysed by POR B.

The remaining residues within the catalytic motif, Lys-213, Asp214 and Ser-215 create a polar interaction site, which is finely tuned by the cooperation of all three residues to facilitate the proper alignment of PChlide within the active site and to support a highly efficient photochemistry. Only small steric perturbations or changes in the hydrogen bonding tendency of these active site residues affect the photoreaction dramatically.

Several of the active site variants exhibit a profound effect on the fluorescence decay time of the respective ternary complexes. Some mutant forms can correctly bind in the catalytic pocket but their fluorescence decay times are lengthened compared to the wild-type enzymes. The increased decay times indicate that the mutation impairs the photochemical reaction, which finally results in a strongly reduced enzymatic activity. From this result it is concluded that the active site residues are also essential for excited-state interactions that contribute to the stabilization of the intramolecular charge transfer state (S_{ICT}) in the POR photochemistry.

1. Introduction

Life exists on earth because biological systems have evolved and adapted to use the most abundant source of energy: the light coming from the sun. The way nature reaches this goal is called photosynthesis. It is an astonishing synergic combination of molecules capable of absorbing light and micro biological structure able to exploit such a condition to convert light into bio-chemical energy[1–3].

The most abundant photoexcitable molecule in photosynthesis is chlorophyll, a magnesium coordinating chlorin, which is produced via a complex biosynthetic pathway by organisms such as plants, green algae and cyanobacteria (aerobic organisms). In those organisms chlorophyll synthesis involves a series of tightly regulated enzymatic reactions. A key reaction within the pathway is catalysed by the light-dependent enzyme NAPDH: protocholorophyllide oxidoreductase (POR)[4]. POR (EC 1.3.1.33) uses light energy to perform the reduction of protochlorophyllide (PChlide) and to produce chlorophyllide (Chlide). This photoreduction step from PChlide to Chlide is fundamental to chlorophyll biosynthesis in all organisms carrying out oxygenic photosynthesis. Moreover, POR and DNA photolyase[5] are the only two enzymes in nature, which requires light to perform catalysis. This special feature makes POR an interesting model system for studying the reaction mechanism in enzyme reaction at a molecular level[6,7].

In the following, the different components constituting the catalytically active POR enzyme are introduced: the substrate, PChlide; the apoenzyme, POR; and the enzyme complex with the bound cofactor, NADPH, and bound PChlide, the so-called ternary complex.

1.1 The substrate - protochlorophyllide a (PChlide)

1.1.1 The PChlide biosynthetic pathway as part of chlorophyll synthesis

The biosynthesis of PChlide involves a high number of enzymes, which are monomeric or homomultimeric and mainly nuclear-encoded[6]. Biosynthesis starts from an activated glutamate provided in the form of glutamyl-tRNA(Glu), which is reduced to glutamate-1-

semialdehyde (GSA). An amino group at C(2) of GSA is transferred to the neighbouring carbon atom to finalize the formation of 5-aminolevulinic acid (ALA). Two molecules of ALA are condensed to form a monopyrrole called porphobilinogen, then four of these molecules are sequentially polymerized to generate a linear tetrapyrrole, which in turn undergoes cyclization to yield the cyclic tetrapyrrole uroporphyrinogen III. At this point the pathway is branched; one path leads to siroheme and the other one, after decarboxylations and oxidations, to protoporphyrin IX (Figure 1.1). The insertion of Mg^{2+} into protoporphyrin IX starts "the Mg branch". In the Mg branch, Mg-protoporphyrin IX is sequentially modified by methylation, formation of the isocyclic 'fifth' ring and reduction of the 8-vinyl substituent at the pyrrole ring B to an ethyl group. From these reactions PChlide is generated as final product[6].

In the course of chlorophyll synthesis, PChlide is then stereospecifically reduced at the C(17)-C(18) double bond of pyrrole ring D and converted into chlorophyllide a (Chlide). In all chlorophyll-containing organisms this reduction is catalysed in a light-dependent pathway by POR. Whereas angiosperms only possess this light-dependent POR enzyme, cyanobacteria, algae and gymnosperms contain in addition a light-independent enzyme, the so-called dark-operative PChlide oxidoreductase[8]. In a final reaction step Chlide is esterified at the C(18) propionyl group with phytol to complete the structure of chlorophyll a (Chl)[9–11].

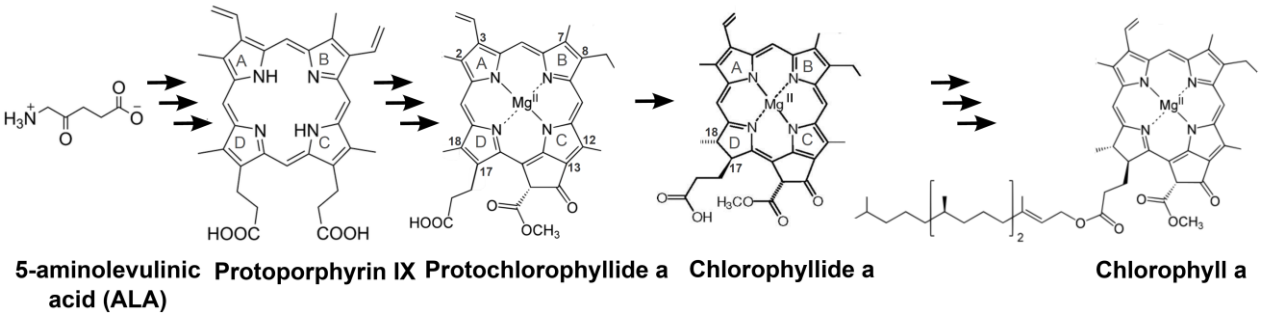

Figure 1.1: Schematic representation of the chlorophyll biosynthetic pathway. Only the first component (5-aminolevulinic acid), two important intermediates (Protoporphyrin IX, Protochlorophyllide a and Chlorophyllide a) and the final product (chlorophyll a) are shown. Black arrows in parallel represent different intermediates which are omitted. Single arrow represents the reduction performed by POR

To allow a balanced synthesis the formation of chlorophyll is strongly controlled for the following reasons: (i) Chlorophyll production must be adjusted to the varying needs during the daily photoperiodic cycle and during different stages of development. (ii) Apart from chlorophyll further tetrapyrroles and products (e.g. siroheme, heme), the requirement of

which is strikingly different from that of chlorophyll, are synthesised through the same pathway. (iii) Many tetrapyrrole intermediates are highly photosensitizing molecules and bear the risk for photooxidative damage or cell death by formation of toxic radicals and highly reactive singlet oxygen species (ROS)[6,12–14].

The regulation of chlorophyll formation is an overall complex process, which includes all levels of control. The most important stimulus is light itself. Briefly summarized, the regulation consists of steps as (i) the daily adjustment of Chl synthesis to the photoperiodic cycle and the perception of light by phytochromes and blue light receptors (ii) the control of transcription at various levels including the post translational level (iii) the control of enzyme activity by regulators, the redox-state, protein-protein interactions and proteolysis[6,12–17].

1.1.2 Spectroscopic characterisation and excited-state chemistry of PChlide

PChlide is a porphyrin-like compound with a central N_4 cavity that coordinates an Mg^{2+} ion whereas different functional groups are substituted at the porphyrin macrocycle: a vinyl group at C(3), an isocyclic fifth ring at C(13)-C(14) and a propionic acid at C(17) (Figure 1.2 A). Apart from the propionic acid all the other substituents are in full conjugation with the π–electron system of the phorphyrin ring and thus contribute to the elongation of the π-electron conjugation path in the macrocycle.

The steady-state absorption spectrum of PChlide (Figure 1.2 B) is very similar to a typical

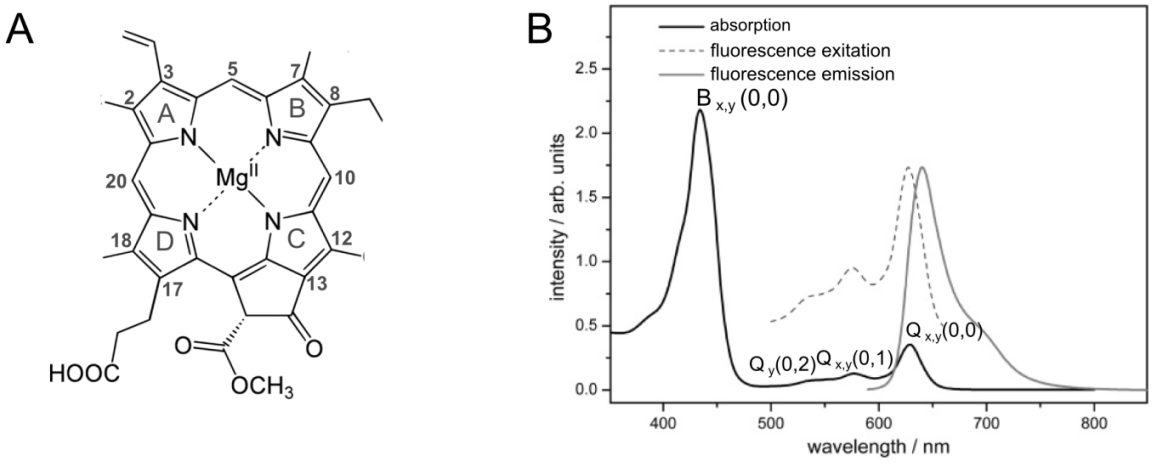

Figure 1.2: **(A)** molecular structure of PChlide a. **(B)** Steady-state absorption, fluorescence and fluorescence excitation spectra of PChlide in methanol. Fluorescence was measured at λ_{exc} = 627 nm and fluorescence excitation at λ_{em} = 641 nm. The assignment of the absorption bands on the basis of the "four-orbital" model of Gouterman is also indicated[18]. Figure modified from Dietzek at al. [20]

porphyrin spectrum, with a Soret or B band at 434 nm accompanied by weaker Q absorption bands at 543, 576 and 629 nm. Based on the theory of M. Gouterman the B- and Q- bands result from the transition between four orbitals, two highest occupied π-orbitals (HOMO-1 and HOMO) and two lowest unoccupied π*-orbitals (LUMO and LUMO+1)[18,19].

The photophysical and photochemical properties of PChlide were intensely investigated in the past years[20–23]. Thus, the excited-state dynamics of free, non-bound PChlide was studied by time-resolved absorption and fluorescence spectroscopy. According to those studies PChlide is an intrinsically reactive molecule and the excited-state dynamics is strongly dependent on solvent polarity[20]. To describe the multi-exponential dynamics both a branched and sequential reaction model were proposed (Figure 1.3). On the basis of the branched reaction model photoexcitation of PChlide is followed by a bifurcation of the exited-state population into two reaction pathways referred to as non-reactive and reactive path (Figure 1.3 A). Along the non-reactive path, vibrational relaxation and vibrational energy redistribution of the initially excited state leads within 3-4 ps to the population of the thermally equilibrated S_1-excited state, which then decays by intersystem crossing within 3.5 ns into a long-lived triplet state[24]. Following the reactive channel, an ultrafast excited-state motion out of the Franck-Condon region into a secondary excited state (S_X) takes place, which in turn converts in 27 ps into an intermediate product. The latter product is non-fluorescent, returns into the initial ground state in 200 ps and, as it is not formed in un-polar solvents[25], proposed to represent an intramolecular charge-transfer state (S_{ICT}). The charge-transfer character of the S_{ICT} state is expected to result from the

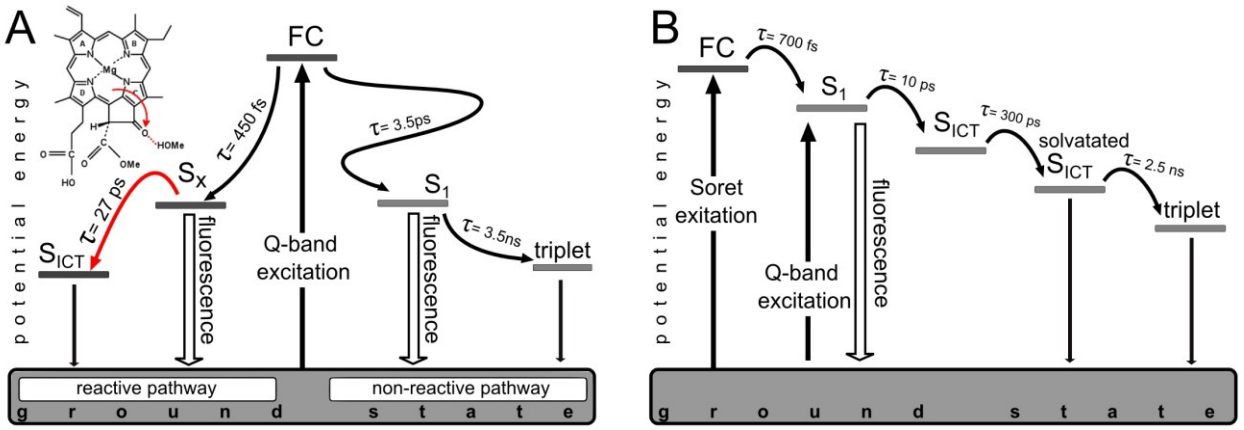

Figure 1.3: Schemes of the relaxation processes in PChlide a. **(A)** Branched reaction model.[25] In the insert the electron withdrawing effect of the C(13')=O keto group is highlighted with an arrow. **(B)** Sequential reaction model as proposed by Sytina et al.[23]

electron withdrawing effect of the C(13')=O keto group at the isocyclic fifth ring of the PChlide molecule because it is substituted in full conjugation with the porphyrin macrocycle[26] (Figure 1.3 A).

The sequential reaction model was introduced on the basis of the finding that the S_{ICT} state was formed regardless of the H-donating properties of the solvent and therefore should represent an intrinsic property of the PChlide molecule itself[23]. Accordingly, the initially excited state undergoes decay into the S_{ICT} state, which subsequently forms via solvation of the S_{ICT} intermediate the triplet state on the nanosecond timescale (Figure 1.3 B).

Further experimental evidence supports the charge-transfer character of the S_{ICT} intermediate: (i) This intermediate is not observed in the excited-state dynamics of magnesium octaethylporphyrin, which is structurally related to the porphyrin skeleton in PChlide but lacks the isocyclic fifth ring and thus the electrophilic substituent[27]. (ii) Moreover, transient IR measurements on the sub-picoseconds time scale indicate a significant red shift in the vibrational frequency of the C(13')=O keto group during creation of the S_{ICT} state[26]. This frequency shift can be brought into line with a decrease in the double bond character of the C(13')=O bond caused by the charge-transfer character of the S_{ICT} state.

1.2 The enzyme – NADPH:protochlorophyllide oxidoreductase (POR)

1.2.1 Origin of POR and relationship with the family of short chain dehydrogenases/reductases

The light-dependent POR is the main enzyme for the reduction of PChlide to Chlide in all chlorophyll-containing organisms that perform oxygen-evolving photosynthesis[28–30]. However, while in angiosperms POR is the only enzyme for PChlide reduction, gymnosperms, cyanobacteria and green algae make in addition use of a separate, light-independent protochlorophyllide reductase (DPOR) that operates in the dark. On the contrary, anoxygenic photosynthetic bacteria using bacteriochlorophyll rely only on the dark-operative DPOR[31]. Since the biochemical pathway, which leads to production of chlorophyll and bacteriochlorophyll is similar in most of the early reaction steps, except for PChlide reduction, the question arises why POR has evolved in addition to DPOR to catalyse the same reaction. At present it is generally accepted that the reason for POR

evolution lies in the transition from the anaerobic to the aerobic atmosphere on earth[4,32,33]. DPOR, or more precisely, the L-protein representing the reductase component of DPOR, is extremely oxygen-sensitive and irreversibly inhibited by molecular oxygen[34,35]. That means that free PChlide would accumulate under O_2-rich conditions and then generate free, toxic radicals and reactive oxygen species in the light, which in turn causes photooxidative damage and cell death unless no precautions are taken. Therefore, it seems likely that oxygen stress has resulted in the evolution of the oxygen-insensitive POR enzyme[36]. POR has at least two advantages over DPOR (i) it is insensitive to oxygen and (ii) the tight binding of PChlide and the transformation into Chlide in the light constitutes an efficient protection mechanism against the potential photooxidation risk. During evolution different paralogous forms of POR as POR A, POR B and POR C have been developed, the appearance of which suggests that new rounds of gene duplication and diversification events have occurred to enable optimal adaption of PChlide reduction on the prevailing light

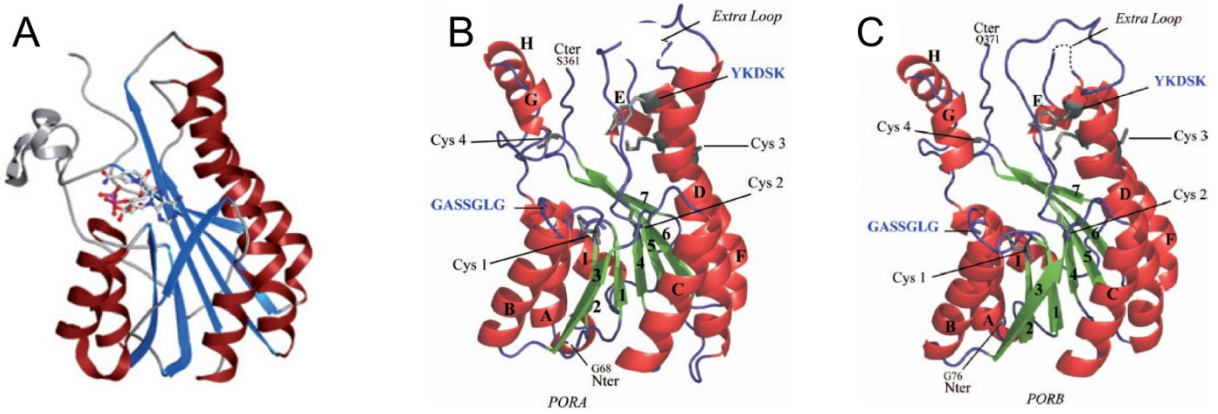

Figure 1.4: Comparison of the 3D structure of SDR enzymes. **(A)** Classic SDR enzyme. **(B)** POR A from barley. **(C)** POR B from barley. The structure of the SDR enzyme shown in (A) corresponds to crystal structure of 3α,20ß-hydroxysteroid dehydrogenase PDB ID: 2HD [113]. The structures of POR A and POR B were derived from modelling studies using 7-α-hydroxysteroid dehydrogenase (AHI) from *Escherichia coli* as template[45]. Figure modified from Kavanagh et al.[113] and Buhr et al.[45].

conditions and to ensure thereby effective photoprotection[36].

Based on the amino acid sequence, POR enzymes show similarities to the so-called short-chain dehydrogenase/reductase (SDR) superfamily, especially when features of the secondary structure of established crystal structures are compared[7,28,37]. The SDR enzymes constitute a large family of $NAD(P)^+$ or NAD(P)H-dependent oxidoreductases, which only show a low pairwise sequence identity but share common sequence motifs in particular at the substrate and cofactor binding sites[38]. They generally occur as homodimers or

homotetramers. The secondary structure is made up of about 7 β sheets connected by 8-9 α helices, i.e. secondary structural elements, which are termed the Rossmann fold[39] (Fig. 1.4). The majority of SDR enzymes utilize a tetrad of amino acids, N-S-Y-K, as catalytic residues, whereas the cofactor binding site includes a glycin-rich motif GxxxGxG[40]. Within the active tetrad the OH-group of tyrosine is proposed to be the proton donor/proton acceptor in the electrophilic/nucleophilic attack on the substrate. The ε-amino group of the adjacent lysine is suggested to affect the pKa of the tyrosin-OH group in order to promote the desired reaction[41]. Moreover, the role of the serine encompasses the stabilization of the bound substrate within the binding cleft, whereas the asparagine seems to interact with the active lysine, the position of which is maintained in the active site to enable an efficient proton relay mechanism.[42].

As shown for SDR enzymes, POR also contains the glycin-rich GxxxGxG nucleotide binding motif. It is located at the N-terminal region and embedded in the Rossmann fold. Moreover, the catalytic site accommodates the highly conserved YxxxK motif characteristic in particular of the tyrosine-dependent oxidoreductases within the SDR enzyme family[37].

Structural models of POR generated by using closely related SDR enzymes as template and adequate modelling tools reveal that typical Rossmann fold is made up of a central seven-stranded ß-sheet which is surrounded by nine α-helices (Fig. 1.4)[7,43–45].Two central helix bundles form the outer wall of a cleft that includes the catalytic YxxxK motif and accommodates the substrate, whereas the cofactor is placed at the Rossmann fold in close proximity to the substrate. An additional segment of ~30 amino acids unique to POR but not to other SDR enzymes is inserted as extra loop region between the fifth and sixth ß-sheet, just before the conserved YxxxK motif. It is assumed that this "extra loop" insertion protrudes from the protein surface and represents an oligomerization domain for POR in barley[7,46]. Thus, the loop region is likely to be involved in the POR A-POR B interactions upon formation of the "light-harvesting POR:PChlide (LHPP) complexes"[47].

1.2.2 POR isoforms

POR exists in different isoforms. While only one POR enzyme has been identified in cyanobacteria, in which the complete genome sequence was determined, three distinct isoforms of POR have been verified in angiosperms. They include the two isoenzymes POR A and POR B, which were first identified in barley (*Hordeum vulgare*) and *Arabidospsis*

thaliana, but exist in other plant species, too[48–50]. The third isoenzyme is POR C, which so far has only been found in *Arabidopsis* in addition to the POR A and POR B isoforms[51,52]. The different isoenzymes are differently controlled both by light and the developmental stage. At present, POR C represents the simplest case in that it is only expressed in light-adapted plants. For POR A and POR B, however, the situation is quite different. POR A is highly abundant in etiolated plants and mainly active in PChlide reduction during seedling de-etiolation as its mRNA stability and transcription are strongly reduced in the light. Thus, POR A selectively disappears in the light while POR B becomes the predominant species. In contrast to POR A, the POR B encoding gen is not negatively regulated by light but constitutively expressed both in etiolated and light-adapted plants. Therefore, in greened and adult plants, POR B is the only POR enzyme, which operates in chlorophyll synthesis[46,47]. Apart from differences in the expression pattern, POR A and POR B vary in the reaction quantum yield of Chlide formation[53] and the mechanism by which their nuclear-encoded precursor proteins are imported into plastids (see below).

In eukaryotic phototrophs, POR A and B are nuclear-encoded proteins, synthesized in the cytoplasm as precursor proteins and post-translationally imported into plastids, where they accumulate in large aggregates, termed prolamellar bodies, within the etioplasts [54,55]. In the cytoplasmic precursor form, POR A and POR B contain a transit peptide at the N-terminus, which is cleaved during import into the plastids giving their mature size of approximately 36 kDa[56]. For the plastid transition POR A and POR B use different pathways. Whereas POR B is imported through the general protein import apparatus TIC/TOC (translocon of the inner/outer chloroplast envelope membrane)[49,57] while POR A translocates by using a PChlide dependent translocon complex (PTC)[58].

To explain the existence of the POR A and POR B isoenzymes and to understand their different biochemical and photochemical properties, it has been suggested that POR A and POR B constitute the so-called light-harvesting POR:PChlide complexes (LHPP) in a of 5:1 stoichiometry of POR A to POR B. In these complexes light is thought to be absorbed by PChlide b bound to POR A in the periphery of the LHPP complex and transferred to POR B- bound PChlide a in the core of the complex. Based on this arrangement LHPP complexes should contribute to an effective light trapping, similar to the antennae of the photosynthetic apparatus, and provide a powerful photoprotection mechanism that keeps the risk of triplet formation in PChlide and thus the production of singulet oxygen low[46,47].

Even though there is a great deal of experimental evidence for the formation of LHHP complexes *in vitro*, the existence under *in vivo* conditions is still under debate[4,6].

1.3 The ternary POR complex and mechanism of enzyme catalysis

1.3.1 General aspects

The active POR enzyme exists as a dark-stable ternary complex of the POR apoenzyme, the substrate, PChlide, and the cofactor, NADPH. The early studies on POR catalysis were carried out using POR enzymes from natural sources, i.e., POR still bound to natural membranes or isolated from etiolated plant material[59–61]. In such preparations POR aggregation, pigment-pigment interactions, energy transfer processes between PChlide and Chlide and distinct enzyme-lipid interactions interfere with the photochemistry und thus the catalysis[62,63,64]. Therefore, in actual studies on POR catalysis recombinant monomeric POR enzymes obtained from heterologous expression are used[62]. After recombination with PChlide as substrate and NADPH as cofactor photoactive ternary POR complexes are built-up, which allow a detailed analysis of the molecular reaction mechanism without the difficulties in the data evaluation as in the case of POR aggregates.

The ternary POR-PChlide-NADPH complex including the reaction steps leading from

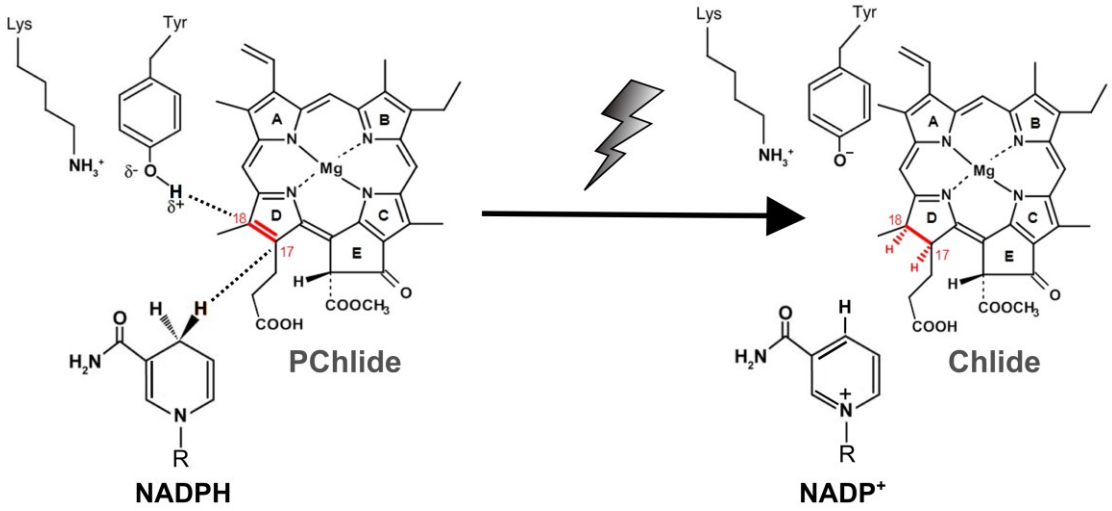

Figure 1.5: Proposed mechanism of the hydride and proton transfer in the reduction of PChlide including the role of the active-site tyrosine and lysine in catalysis. The hydride transferred to the C(17) position of PChlide is derived from the *pro-S* face of NADPH, and the proton at the C(18) position is derived from the catalytic tyrosine, the pKa of which is lowered by the neighbouring lysine.

PChlide to Chlide has been extensively studied. POR catalyzes the endergonic light-driven *trans* addition of hydrogen across the C(17)-C(18) double bond at the D-ring of PChlide to produce Chlide while reducing NADPH to $NADP^+$ (Fig. 1.5A).[65] The hydride is transferred from the *pro-S* face of NADPH to the C(17) position of PChlide, most likely followed/accompanied by an exergonic proton transfer to the free valence at the C(18) position[66–69]. The proton is suggested to be donated by the highly conserved tyrosine residue, which is part of the YxxxK motif at the catalytic site, whereas the pKa of the tyrosine-OH is dramatically lowered by the lysine residue also located at the catalytic site in close proximity to the active-site tyrosine (Fig. 1.5)[28,70,71]. Both the hydride and proton transfer reactions proceed by quantum mechanical tunnelling[69].

In an alternative model it is hypothesised that upon photoexcitation the reaction starts directly with an electron transfer from NADPH to C(17) at the D-ring of PChlide, followed by a rate-limiting proton transfer from the active tyrosine to C(18) and finally terminated by a fast H^+/e^- transfer from NADPH to C(17) to saturate the free valence there[22,72].

From the dependence on the light intensity, the H^-/H^+ transfer is proposed to proceed through a single photon mechanism with a quantum efficiency for PChlide conversion between 0.2 and 0.7 (0.21 for POR from *Synechocystis*, 0.33 for POR A and 0.73 for POR B from barley)[53,70,73,74]. However, evidence was recently provided that the reaction could also involve a two-photon mechanism in that the first photon initiates a conformational change at the active site and turns the enzyme activity 'on' whereas a second photon then triggers the true photochemical reaction[75,76].

1.3.2 Overall view on the complete reaction cycle in POR catalysis

Following the initial photoreaction, the complete POR reaction cycle includes a series of reaction intermediates, which can be trapped at low temperatures. In particular in low temperature absorption and fluorescence measurements, a sequence of ordered product release and cofactor rebinding steps, which are required to complete the catalytic cycle, could be identified (Figure 1.6) [70]. After electronic excitation the first detectable intermediate is $A_{696,}$ with the subscript indicating the absorbance maximum. A_{696} is formed at temperatures below 180 K and ascribed to the primary photoproduct, in which PChlide has received the hydride (H^-) from NADPH and forms an intramolecular charge transfer complex with $NADP^+$ [67,74]. In the subsequent dark reaction, A_{696} converts into A_{681}. A_{681} is attributed to an

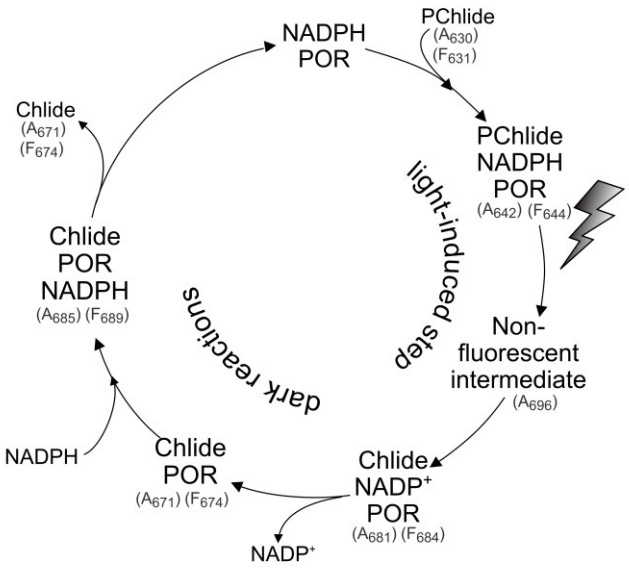

Figure 1.6: Overall scheme for the catalytic cycle of POR. Different reaction intermediates trapped at low temperatures are shown together with the absorbance (A) and fluorescence maximum (F) in nm.

intermediate, in which the partially reduced PChlide (PChlide·H$^-$) has reacted to Chlide by the uptake of a proton from the Tyr-OH group[77]. The following dark reactions include the release of NADP$^+$ ($A_{681}\rightarrow A_{671}$), the rebinding of NADPH ($A_{671}\rightarrow A_{685}$) and, finally, the desorption of Chlide from the active site ($A_{685}\rightarrow A_{671}$).[78] Equivalent reaction steps are also identified in low temperature fluorescence measurements with the exception for the initial light-driven reaction, which escapes the detection because A_{696} is non-fluorescent[77,78].

On one hand, the fact that the primary photoreaction, the hydride transfer, can still proceed well below 180 K implies a lack of large-scale structural rearrangements associated with this reaction step[74]. It is likely to be influenced by only local motions of the catalytically essential side chains within the active site. On the other hand, the proton transfer reaction, resulting in the formation of A_{681}, occurs at temperatures close to the glass transition (from frozen to fluid buffer). It seems to require long-range, solvent-slaved protein motions/conformational rearrangements around the catalytic centre to ensure an optimal proton donor-acceptor distance[79,80]. However, this applies only for prokaryotic cyanobacteria. In eukaryotic POR enzymes (plant/algal enzymes), the large-scale solvent–coupled dynamics is lost. In this case, analogous to the hydride transfer, the proton transfer requires catalysis-linked local motions restricted to the active site only[80]. The final steps in the reaction pathway occur at temperatures above the glass transition. This indicates a significant role for protein dynamics at this stage of catalysis and, consequently, suggests

that the last reactions are assisted by more global conformational changes involving domain movements and/or domain reorganisation[77,78].

1.3.3 The ultrafast reaction dynamics in POR catalysis

The initial ultrafast reaction dynamics within the ternary POR-PChlide-NADPH complex has been extensively investigated because it should directly lead to the photochemistry underlying PChlide reduction and thus to the real chemical reaction steps powered by harnessing light energy.

On the basis of former results, a first intermediate photoproduct, referred to as I675*, is proposed to appear in two parallel reactions with time constants of 3 ps and 400 ps[81]. The one reaction is ascribed to a coupled proton/hydride transfer mechanism with the proton and hydride transfer occurring in 3 ps. The other one is related to a sequential reaction with a 3-ps proton transfer and a subsequent 400-ps hydride transfer. Further on, the rate and quantum yield of I675* formation is found to increase strongly after PChlide had passed the catalytic cycle at least once suggesting that in a two photon mechanism the first photon generates a more favourable conformation at the active site of the POR-PChlide-NADPH complex. Once in an active state, the second photon initiates catalysis to produce Chlide[82]. However, in the mean time the I675* intermediate turned out to represent an excited-state species of PChlide-Chlide dimers/eximers the formation of which is maximized in a 50:50 mixture of the two pigments[83]. In consequence, I675* is not of relevance in POR catalysis but rather an artefact that apparently arises upon thermal denaturation of the ternary POR-PChlide-NADPH complex. In the light of this finding, the two photon mechanism (see above) can also be explained by a first photon that is required to form the PChlide-Chlide dimer/eximer and a second one that triggers energy transfer processes within the dimer/eximer.

A reaction model for the photochemistry in the ternary POR-PChlide-NADPH complex has been suggested based on the use of time-resolved UV/Vis spectroscopy in combination with IR spectroscopy and the inclusion of free PChlide as well as an inactive POR mutant in addition to the ternary POR-PChlide-NADPH complex (Figure 1.7 A)[84]. General aspects of this model are (i) the formation of an intramolecular charge transfer complex (S_{ICT}) and (ii) the bifurcation of the reaction path into a catalytic and non-catalytic branch, whereas the branching occurs after formation of the S_{ICT} state. While along the non-catalytic route the

S_{ICT} state is converted into a solvated S_{ICT} state and subsequently into the triplet state, the catalytic route involves the formation of a so-called "reactive" S_{ICT} state, which goes over into a partially reduced hydride-transfer intermediate (PChlide·H^-) with a time constant of about 500 ns. In the "reactive" S_{ICT} state the electron density across the C(17)-C(18) double bond is postulated to be diminished by the electron withdrawing effect of an excited-state H-bonding interaction between the propionic acid at C(17) of the PChlide structure and the Tyr-OH in the active centre (Figure 1.7 A). It is just this constellation, which is speculated to facilitate the nucleophilic attack of the negatively charged hydride from NADPH to C(17). Nevertheless, it remains to be seen whether (i) the main electron-withdrawing effect, responsible for the regioselective reduction of PChlide in the ternary POR complex, is not due the C(13') carbonyl group at the isocyclic fifth ring (Figure 1.7B) and (ii) the active-site Tyr-OH is really positioned in hydrogen-bonding distance to the C(17) propionic acid and, in consequence, involved in the formation of the reactive S_{ICT} state.

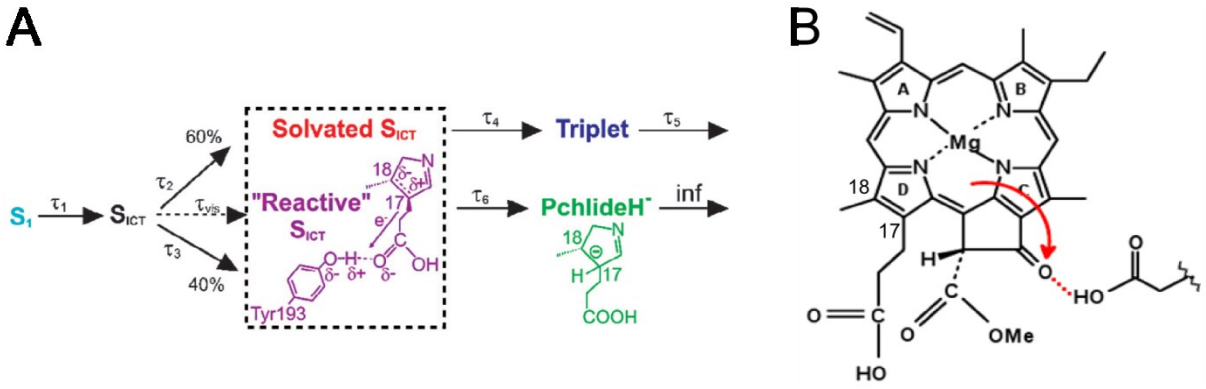

Figure 1.7: Scheme of the reaction mechanism in POR catalysis. **(A)** suggested from a combination of UV/Vis absorption and mid-IR spectroscopy[84]. **(B)** The possible role of the C(13') carbonyl group at the isocyclic fifth ring in creating an electron deficient site at C(17)-C(18) of the PChlide structure is also shown[25,26,85].The figure is modified from Heyes et al. [84].

Evidently, the ultrafast reaction dynamics in the ternary POR complex is affected by the local protein environment, surrounding the enzyme-bound PChlide at the active site. Such protein-substrate interactions have been confirmed by time-resolved fluorescence and pump-probe absorption measurements including the so-called pseudoternary complex composed of the POR enzyme, the substrate, PChlide, and the already reduced cofactor, $NADP^+$ (POR-PChlide-$NADP^+$)[85]. The pseudoternary complex is non-productive, i.e. the photoreaction does not lead to the formation of Chlide. However, the complex should mimic the real protein-PChlide interactions at the active site and the very early excited-state processes in

PChlide, which, in this case, are not masked/disturbed by signals originating from Chlide. Thus it is shown that, in analogy to the PChlide photochemistry, an intramolecular charge-transfer state, S_{ICT}, is formed as intermediate product. A strong blue shift in the excited-state absorption suggests that the S_{ICT} state is significantly stabilized by local interactions with specific protein sites in the catalytic pocket of POR[85]. Similar findings have also been reported from the time-resolved UV/Vis and mid IR spectroscopic study on the enzymatically active POR-PChlide-NADPH complex referred to above[84].

Moreover, when compared with isolated PChlide, the lifetime of the thermally equilibrated S_1-excited state is remarkably lengthened in the pseudoternary POR-PChlide-$NADP^+$ complex. It increases from 3.4 ns in isolated PChlide to 5.6 ns in the pseudoternary complex, whereas the non-radiative rate is decreased by ~40% from $2.8 \cdot 10^8$ s^{-1} to $1.7 \cdot 10^8$ s^{-1} [85]. This effect is attributed to the reduced probability for *intersystem crossing* of S_1-excited PChlide into the triplet state. This in turn indicates that the risk for the accumulation of triplet states and consequently for photosensitized side reactions producing reactive oxygen species (ROS) is kept low by binding PChlide to the POR apoprotein. It therefore seems that the POR complex fulfils an important photoprotective role in chlorophyll biosynthesis.

1.3.4 The role of point mutations in POR sequence for catalysis

To gain an insight into the mechanistic role of specific amino acid residues in POR catalysis also a series of site-directed mutagenesis studies combined with a variety of spectroscopic and kinetic measurements has been undertaken. The residues primarily included in these studies are the tyrosine and lysine at the active site, which are part of the catalytic YxxxK motif that is highly conserved between different POR enzymes. To determine the function of these residues Tyr was replaced by Phe, Cys, Ala and Ser, whereas the active site Lys was mainly substituted by Arg, Ala, and Asn[28,84,86,87].

The mutations of both residues confirm the model proposed for POR catalysis (Chapter 1.3.1, Figure 1.5) whereby Tyr donates the proton to the C(18) position of the PChlide macrocycle after the hydrogen has been perceived from NADPH and Lys lowers the pKa of the Tyr-OH. In addition, Tyr and Lys have a key role in PChlide binding, they are responsible for maintaining specific interactions between PChlide, NADPH and the protein sites within the active centre and they stabilize the photoexcited state in POR.

Moreover three cysteine residues are absolutely conserved throughout all POR enzymes. Site-directed variants with Cys→Ala and Cys→Ser exchanges[72,88], provide evidence that one of them, which is in close proximity to the nucleotide binding domain, is responsible for the proper positioning of NADPH and, in addition, has a cooperative effect on NADPH binding[72]. Another Cys, which is located near to the catalytic centre, is shown to play a major role for the catalytic mechanism. It is involved in the binding of PChlide and in maintaining an optimal alignment with the NADPH cofactor and the proton donor[72,88]. Interestingly, the corresponding Cys→Ser mutant uses a different catalytic mechanism as compared to the wild type form. The charge-transfer intermediate, which arises as a result of the hydride transfer from NADPH, is not formed as primary photoproduct but instead a concerted hydride/proton transfer mechanism appears to be realized[72]. Moreover, for plant PORs from barley an additional Cys present in both POR A and POR B has been identified. This Cys constitutes a second, low-affinity PChlide binding site, which is suggested to be involved in the assembly of POR A:POR B complexes and to allow for the resonance energy transfer in the light-harvesting POR:PChlide complexes (LHPP)[88].

Table 1.1 summarizes the main studies, thus far known, on site-directed mutations of POR enzymes and describes their effects on the binding of PChlide/NADPH and on the catalytic mechanism as well.

Table 1.1: Site-directed mutagenesis studies on POR enzymes – summary of the effect of different amino acid substitutions on POR catalysis.

point mutation	source of POR	implications for the reaction mechanism	reference
Y275F Y275C K279R K279I	*Pisum sativum L.*	- Tyr-275 and Lys-279 are critical for the catalytic activity. The mutations give rise to inactive enzymes.	Wilks and Timko [28]
Y275F K279I K279R	*Pisum sativum L.*	- Tyr-275 and Lys-279 increase the probability for the formation of the photoactive state after binding of PChlide and NADPH. They are also responsible for the positioning of the substrate and cofactor in the proper orientation at the catalytic site. - Neither Tyr-275 nor Lys-279 are crucial for the binding of the substrate or the cofactor - Tyr-275 is necessary for the second "dark" step of PChlide reduction (the molecular nature of this reaction step is not defined).	Lebedev et al.[89]
Y189F K193R	*Synechocystis*	- PChlide reduction is totally abolished in both the Y-189 and K-219 mutants, indicating that the two residues are crucial for enzyme activity. - K-193 is also involved in the binding of	Heyes et.al[90]

		NADPH. The K_D value for NADPH binding is significantly higher in the K193R mutant than in the wild-type POR	
C104A C166A C276A C303A C276A-C303A	*Hordeum vulgare L.* POR B	- Neither C-104 nor C-166 impair PChlide and NADPH binding or POR catalysis. C104A and C166A convert PChlide into Chlide. - C-276 has an important impact on enzyme catalysis. C276A is unable to tightly bind and convert PChlide into Chlide. - C-303 is involved in the formation of larger POR A:POR B complexes and is suggested to facilitate the energy transfer between neighbouring POR-pigment complexes.	Reinbothe et.al [88]
Y193F Y193A Y193S K197A K197R K197Q	*Thermosynechococcus elongatus*	- The binding constant, K_D, for PChlide is considerably increased in the Y-193 and K-197 mutants indicating weaker binding. - Most likely, the two residues are involved in the formation of the photoactive ternary POR-PChlide-NADPH complex and responsible for the creation of effective interactions between PChlide, NADPH, and the protein side chains within the active site. - The effect on PChlide binding is more dramatic for K-197 thanY-193 mutants suggesting direct interactions between the positively charged ε-amino group of K-197 and the negatively charged propionic acid side chain at C(17) of PChlide.. - For both the Y-193 and K-197 mutants the reaction quantum yield of Chlide production is remarkably reduced. Based on the impairment of the photochemistry Y-193 and K-197 seem to be involved in the stabilization of the PChlide-excited state and probably also in the quenching of the PChlide triplet state. - Y-193 is most likely the proton donor in PChlide reduction.	Menon et al.[87]
C37S C199S C226S C37S C199S C37S C226S C199S C226S C37S C199S C226S	*Thermosynechococcus elongatus*	- C-37 and C-199 are of minor importance for POR catalysis. The mutant variants retain nearly wild-type levels of the steady-state enzyme activity. - C-226 has a major role in POR catalysis. In all C226S variants the steady-state activity is remarkably reduced. - Mutation of C-226 alters the catalytic mechanism. C226S variants do not form the first charge-transfer intermediate, which is generated upon hydride transfer from NADPH. Rather, a concerted H-/H+ transfer reaction takes place , which yields POR-Chlide-NADP+ in a single reaction step. - The role of C-226 is most likely to create an optimal alignment between NADPH, PChlide and the Tyr hydroxyl group as	Menon et al.[72]

		proton donor. - C-226 is also important in the binding of PChlide to POR. The dissociation constant, KD, is significantly higher for all C226S variants compared to the wild-type enzyme.	
Y193F	*Thermosynechococcus elongatus*	- The mutant fails at creating a "reactive" excited-state species, which is part of the catalytic pathway in wild-type POR. Y-193 therefore seems to be essential for the formation of that excited-state species, which produces an electron-deficient and thus highly reactive site at the C(17)-C(18) double bond of PChlide. The electron withdrawing effect is speculated to be due to excited-state interactions between Y-193 and the carboxyl group of the propionic acid side chain at C(17) of PChlide..	Heyes et al.[84]
S16C G19A R38V N39V K42A N90A Y94F T145A T147S/F N149V S189A T230A/S/F H236A	*Thermosynechococcus elongatus*	- In contrast to previous homology models, Ser189 and His236 only have a minimal effect on PChlide binding and the catalytic activity of POR. - Asn39, Asn90, Thr145 and Asn149 are important for PChlide binding. As mutations they reduce the catalytic efficiency of POR and the affinity to PChlide. - Ser16, Gly19, Arg38, and Lys42 affect the affinity for NADPH. Mutations to these residues result in a lower affinity for NADPH. - Thr230 is important for the optimal positioning of the NADPH coenzyme at the catalytic site.	Menon et al.[43]

1.4 Aim of the work

As outlined above the enzyme NADPH:protochlorophyllide oxidoreductase (POR), EC1.3.1.33, controls a key regulatory step in the biosynthesis of chlorophyll in all organisms showing oxygenic photosynthesis. The light-driven photoreduction of PChlide into Chlide adapts chlorophyll synthesis to the light environment and helps to avoid photodamage due to the phototoxity of free and excess PChlide.

Against that background, POR has been at the main focus of a great deal of studies in recent years. However, a wealth of studies includes POR enzymes from cyanobacteria. Even though excellent work has also been reported on plant enzymes, there is an obvious gap in the understanding of the catalytic mechanism and reaction dynamics between plant PORs and POR enzymes from cyanobacteria. This applies in particular to POR B, which is the

main active enzyme in green and adult plants and which, therefore is of great importance for the general control of chlorophyll biosynthesis in plants.

In more detail the objectives of the thesis are:

i. The calculation of a new three-dimensional (3-D) structural model for POR B by using actual *ab initio* structure prediction tools and the actual entries of the Protein Data Bank (PDB). This work is a prerequisite for an in-depth understanding of the catalytic mechanism in POR B, as the crystal structure could not be elucidated for any POR enzyme as yet. The best-approached model is to be verified by the generation of a number of appropriate mutants, which stand out through specific interactions between the protein side chains of POR B and enzyme-bound PChlide.

ii. The determination of the enzyme kinetic parameters as well as the catalytic efficiency for POR B in comparison to POR A

iii. The evaluation of the catalytic mechanism in POR B as compared to POR A by trapping reaction intermediates at low temperatures and their characterization by absorption spectroscopy including the assessment of the reaction mechanism on the basis of decay components, which are to be identified in time-resolved fluorescence measurements at low temperatures.

iv. A detailed molecular understanding of the role of the key amino acid residues within the catalytic motif in the reaction mechanism. For this purpose the individual amino acids are to be substituted by site-directed mutagenesis and the POR variants to be examined by their enzymatic activity, substrate binding affinity, and reaction sequence at low temperatures. The mutations have different goals: support experimentally the predicted function and validate the 3-D model of POR B. Elucidate the role of the active site Tyr and Lys (YxxxK) in POR A and POR B as well as provide information on the other three amino acids of the catalytic quintet: Lys, Asp, Ser (Y**K**$_1$**DS**K$_2$).

v. The explanation of the different functions of POR A and POR B on the basis of the results achieved.

2. Material and Methods

2.1 Calculation of the three-dimensional (3-D) protein model for POR B

The calculation of the 3D structural model of the POR B enzyme was performed as follows:

(i) the amino acid sequence of POR B was submitted to different on-line services, which calculated on the basis of specific computing algorithms several possible 3D model structures of POR B.

(ii) The 3D structures were then evaluated by a quality test and the most reliable structural model was chosen for the docking experiment.

2.1.1 From the amino acid sequence to the pdb file

The amino acid sequence of POR B from barley (*Hordeum vulgare*) were downloaded from the data bank of the National Centre for Biotechnology Information (http://www.ncbi.nlm.nih.gov) and submitted to the following on-line services:

- HHpred - http://toolkit.tuebingen.mpg.de/hhpred
- I-Tasser - http://zhanglab.ccmb.med.umich.edu/I-TASSER/
- M4T - http://manaslu.aecom.yu.edu/M4T/
- ModWeb - http://technology.sbkb.org/portal/page/137/
- Swiss-Model - http://swissmodel.expasy.org/

These on-line services work on the basis of different computing algorithms and provide as a result the so-called pdb file, in which the calculated position of all the atoms of the POR protein is given in a table of the "x-y-z" coordinates. Specific programs can be used for the visualization of the 3D models. In this work YASARA (www.yasara.org) was generally employed to meet this task.

In order to judge the goodness of the calculated structures, the 3D models were evaluated using a QMEAN scoring function integrated in SWISS-MODEL (http://swissmodel.expasy.org/qmean/cgi/index.cgi). The software performed an estimation of the quality of a modelled 3D structure by assigning a "global score", which is

based on the entire structure of the model and a "local score", which estimates the error for the individual residues along the full-length sequence. The global "QMEAN score" was used as first indication for an adequate fit of the model.

2.1.2 Docking of the substrate, PChlide, and the cofactor, NADPH, at the POR catalytic site

The docking of the coenzyme, NADPH, and the substrate, PChlide, was also carried out by using the software YASARA. The docking was executed in a step-wise manner, in order to avoid artefacts caused by the calculation.

To test whether the software performs a reliable docking, NADPH was at first placed at the cofactor binding site using the AutoDock tool[91] implemented in YASARA. The POR structure including the docked NADPH was then cross-checked with the crystal structure of porcine testicular carbonyl reductase (1N5D), which also belongs to the class of SDR enzymes and which was co-crystallised with NADPH[92]. In the following the POR-NADPH structure was subjected to an energy minimization step using the YAMBER force field [93]. To increase the chance for a reliable docking result upon substrate binding, the docking of the PChlide molecule was restricted to a 15 Å cubic simulation cell placed near to the hydroxyl group of the catalytically active tyrosine[28]. In a last step the best-docked POR B-NADPH-PChlide structure was submitted to another energy minimization using the YASARA YAMBER force field.

2.2 Sequence alignment

Amino acid sequences of POR from *Thermosynechococcus elongatus*, POR from *Synechocystis sp.* PCC 6803, POR A and B from *Hordeum vulgare L.* were downloaded from the NCBI data base (www.ncbi.nlm.nih.gov) and submitted to the multiple sequence alignment ClustaxOmega (http://www.ebi.ac.uk/Tools/msa/clustalo/). The resulting alignment was then processed by using the Jalview software (www.jalview.org), which provides a graphical representation of the conserved and "consensus" amino acids.

2.3 Preparation and purification of PChlide

PChlide was extracted and purified from etiolated oat seedlings (*Avena sativa L*). according to a modified protocol previously reported by Griffiths et al. [65]. Generally the seedlings were grown in the dark, the coleoptiles were then harvested under dim green light and homogenized in an acetone/Tricin buffer mixture. In a dim light environment the pigment solution was processed by several separation steps using the Nernst's distribution law. Thin layer chromatography and/or HPLC were employed in the last purification process.

In detail, the oat seedlings were germinated on vermiculite in the dark for 6 days. The coleoptiles were harvested and incubated in 15 mM 5-aminolevulinic acid (ALA) dissolved in 35 mM potassium buffer (pH 6.5) for 24 - 48 h. The coleoptiles were homogenized with 600 ml of Tricine/KOH buffer (10 mM, pH 7.5) and 300 ml of acetone. Subsequently, 1.5 l of acetone was added to the homogenate, stirred for 20 min at 4 °C and then centrifuged (20 min, 9 890 x g).

The acetone-PChlide solution was transferred into a separatory funnel. By adding 2.4 l of ether and vigorous shaking, PChlide was transferred into the ether phase. The aceton phase was removed and discarded. In order to separate acetone completely 2.4 l of hexane were added and the again settled acetone phase was discarded. The volume of the ether/hexane phase was determined and 1/10 of the volume of a 4:1 mixture of methanol and 0.01 M ammonia was added. The ether/hexane phase was discarded and the methanolic phase was washed five times with 1/10 of the volume of a 1:1 ether/hexane mixture.

The volume of the methanolic phase was determined. Water, ether and the methanolic phase were layered one above the other at the ratio of 9:3:5. Following shaking out, sodium chloride was added for a better phase separation. The methanolic-aqueous phase was shaken out with ether, until it became yellowish. To complete drying the PChlide containing ether phase, anhydrous Na_2SO_4 was added. Finally, the ether was evaporated at 950 mbar and 40°C.

For further purification of PChlide, a semi-preparative thin layer chromatography (TLC) was performed on pre-coated TLC-plates SIL G-200 (Macherey-Nagel). As eluent ether, ethylacetate and methanol at a ratio of 5:2:1 was used. PChlide was eluted from the

stationary phase with methanol, which was then evaporated at 350 mbar and 40 °C and stored at -20 °C until use.

Alternatively PChlide was dissolved in methanol and purified by HPLC (Jasco DG1580-PU987-UV975) on a C18 semipreparative column (VYDAC-218TP1010 particle size 10 µm, pore diameter 300 Å) previously equilibrated with 40% acetonitril (ACN) in H_2O. The elution of the pigment was performed in a continuous 40% to 100% ACN mobile phase at 1ml/min flow rate. The fractions containing pure PChlide were controlled via UV-Vis spectroscopy, collected and freeze-dried for concentration.

2.4 In vitro site-directed mutagenesis

2.4.1 Cloning of POR genes into the plasmid vector

cDNA of POR A and B from barley (*Hordeum vulgare*) was subcloned into a pRSET A vector (Life Technologies) using BamHI and HindIII as restriction enzymes. cDNA encoding the POR enzyme from *Synechocystis sp.* was also subcloned into pRSET A but using the BamHI and EcoRI cloning sites. The pRSET A vector has the advantage of a high level of protein expression, which is due to the control of the expression by the bacteriophage T7 promotor. Further, it produces His tagged recombinant proteins (6xHis) and for the expression of the T7-regulated genes *E. coli* can be used as host and grown-up in a selecting ampicillin rich medium.

The point mutations in the nucleotide sequence of the POR A and B genes, sub-cloned in the pRSET vector, were introduced according to the procedure detailed in the manual of the QuickChange® Site-Directed Mutagenesis Kit from Agilent Technologies (Stratagene). The POR A mutants Y215F and S218A as well as the POR B mutants Y212F, D214M and S215A make an exception insofar as they were generated by site-directed mutagenesis using the terminal substitution technique. The corresponding mutants were produced by the DNA-Cloning-Service e.K. (Hamburg). The oligonucleotide primers were designed according to the guidelines given in the kit manual. The base triplets, which encode the mutated amino acid, were chosen according to the *E.coli* codon usage to ensure that the desired amino acid will be embedded. The forward and reverse primers used for the introduction of the diverse point mutations are summarized in Table 2.1, 2.2 and 2.3, respectively.

Table 2.1: Sequence of the primers designed for the insertion of point mutations in POR B. The point mutations include the amino acids H-138, Y-299 and S-164, which are of importance for the evaluation of the 3D structural model. The base triplet, which has been modified is shown in bold.

POR	mutation		primer sequence
Mutants generated for the evaluation of the three-dimensional model of POR B			
POR B	$H_{138}F$	forward	5'GGCGTTAATCATTTAGGT**TTT**TTCCTGCTGGCGCGCGAAC 3'
		reverse	5'GTTCGCGCGCCAGCAGGA**AAA**AACCTAAATGATTAACGCC 3'
	$H_{138}Y$	forward	5' CGTTAATCATTTAGGT**TAT**TTCCTGCTGGCGCGCG 3'
		reverse	5' CGCGCGCCAGCAGGAA**ATA**ACCTAAATGATTAACG 3'
	$Y_{299}H$	forward	5'CCCTGACGAAAAGTGGTGTA**CAT**TGGAGCTGGAATAAAAATTCG 3'
		reverse	5' CGAATTTTTATTCCAGCTCCAAT**GTA**CACCACTTTTCGTCAGGG 3'
	$Y_{299}F$	forward	5' CCCTGACGAAAAGTGGTGTA**TTT**TGGAGCTGGAATAAAAATTCG 3'
		reverse	5' CGAATTTTTATTCCAGCTCCA**AAA**TACACCACTTTTCGTCAGGG 3'
	$S_{164}A$	forward	5'CGGTTAATTATTGTAGGC**GCG**ATTACCGGAAACACG3'
		reverse	5'CGTGTTTCCGGTAATCG**CGC**CTACAATAATTAACCG3'
	$S_{164}T$	forward	5'GCAAACGGTTAATTATTGTAGGC**ACC**ATTACCGGAAACACGAATACG 3'
		reverse	5' CGTATTCGTGTTTCCGGTAA**TGG**TGCCTACAATAATTAACCGTTTGC 3'

Table 2.2: Sequence of the primers designed for the insertion of point mutations in the YKDSK motif at the active site of POR A. The triplet, which has been substituted, is indicated in bold within the primer sequence.

POR	mutation		primer sequence
Mutants generated to substitute the amino acids in the YKDSK motif at the active site of POR A			
POR A	$Y_{215}F$	forward	5' **T**AAGGACAGCAAGGTGTGCAACATGC 3'
		reverse	5' **AA**CGCCTTGGCGCCGTCGAA3'
	$Y_{215}H$	forward	5' CGACGGCGCCAAGGCG**CAC**AAGGACAGCAAGG 3'
		reverse	5' CCTTGCTGTCCTT**GTG**CGCCTTGGCGCCGTCG 3'
	$K_{216}R$	forward	5' GGCGCCAAGGCGTAC**CGT**GACAGCAAGGTGTGC 3'
		reverse	5′ GCACACCTTGCTGTC**ACG**GTACGCCTTGGCGCC 3′
	$K_{216}Q$	forward	5' GGCGCCAAGGCGTAC**CAG**GACAGCAAGGTGTGC 3'
		reverse	5' GCACACCTTGCTGTC**CTG**GTACGCCTTGGCGCC 3'
	$D_{217}A$	forward	5' CCAAGGCGTACAAG**GCG**AGCAAGGTGTGCAACATGC 3'
		reverse	5' GCATGTTGCACACCTTGCTCGCCTTGTACGCCTTGG 3'
	$D_{217}E$	forward	5' CCAAGGCGTACAAG**GAA**AGCAAGGTGTGCAACATGC 3'
		reverse	5' GCATGTTGCACACCTTGCT**TTC**CTTGTACGCCTTGG 3'
	$D_{217}N$	forward	5' CCAAGGCGTACAAG**AAC**AGCAAGGTGTGCAACATGC 3'
		reverse	5' GCATGTTGCACACCTTGCT**GTT**CTTGTACGCCTTGG 3'
	$S_{218}A$	forward	5' **CG**AAGGTGTGCAACATGCTGACCA 3'
		reverse	5' **C**GTCCTTGTACGCCTTGGCGC3'
	$S_{218}G$	forward	5' CCAAGGCGTACAAGGAC**GGC**AAGGTGTGCAACATGC 3'
		reverse	5' GCATGTTGCACAC**CTT**GCCGTCCTTGTACGCCTTGG 3'
	$S_{218}T$	forward	5' CCAAGGCGTACAAGGAC**ACC**AAGGTGTGCAACATGC 3'
		reverse	5' GCATGTTGCACA**CCT**TGGTGTCCTTGTACGCCTTGG 3'
	$K_{219}R$	forward	5' GGCGTACAAGGACAGC**CGT**GTGTGCAACATGCACC 3'
		reverse	5' GGTGCATGTTGCACAC**ACG**GCTGTCCTTGTACGCC 3'
	$K_{219}Q$	forward	5' GGCGTACAAGGA**CAG**CCAGGTGTGCAACATGCACC 3'
		reverse	5' GGTGCATGTTGCACAC**CTG**GCTGTCCTTGTACGCC 3'

Table 2.3: Sequence of the primers designed for the insertion of point mutations in the YKDSK motif at the active site of POR B. The triplet, which has been modified, is indicated within the whole primer sequence in bold.

POR	mutation		primer sequence
Mutants generated to substitute the amino acids in the YKDSK motif at the active site of POR B			
POR B	$Y_{212}F$	forward	5' GATGGCGCCAAAGCC**CAC**AAAGATAGTAAGGTTTGTAAC 3'
		reverse	5' GTTACAAACCTTACTATCTTT**GTG**GGCTTTGGCGCCATC 3'
	$Y_{212}H$	forward	5' GATGGCGCCAAAGCCC**ACA**AAGATAGTAAGGTTTGTAAC 3'
		reverse	5' GTTACAAACCTTACTATCTTT**GTG**GGCTTTGGCGCCATC 3'
	$K_{213}R$	forward	5' GATGGCGCCAAAGCCTAT**CGT**GATAGTAAGGTTTGTAACATGC 3'
		reverse	5′ GCATGTTACAAACCTTACTATC**ACG**ATAGGCTTTGGCGCCATC 3′
	$K_{213}Q$	forward	5' GATGGCGCCAAAGCCTAT**CAG**GATAGTAAGGTTTGTAACATGC 3'
		reverse	5' GCATGTTACAAACCTTACTATC**CTG**ATAGGCTTTGGCGCCATC 3'
	$D_{214}M$	forward	5' AGTAAGGTTTGTAACATGCTGACTATGC 3'
		reverse	5' **CAT**TTTATAGGCTTTGGCGCCATCAAA 3'
	$D_{214}A$	forward	5' GCGCCAAAGCCTATAAA**GCG**AGTAAGGTTTGTAACATGC 3'
		reverse	5' GCATGTTACAAACCTTACT**CGC**TTTATAGGCTTTGGCGC 3'
	$D_{214}E$	forward	5' GCGCCAAAGCCTATAAA**GAA**AGTAAGGTTTGTAACATGC 3'
		reverse	5' GCATGTTACAAACCTTACT**TTC**TTTATAGGCTTTGGCGC 3'
	$D_{214}N$	forward	5' GGCGCCAAAGCCTATAAA**AAC**AGTAAGGTTTGTAACATGCTG 3'
		reverse	5' CAGCATGTTACAAACCTTACT**GTT**TTTATAGGCTTTGGCGCC 3'
	$S_{215}A$	forward	5' **CG**AAGGTTTGTAACATGCTGACTATGC 3'
		reverse	5' **C**ATCTTTATAGGCTTTGGCGCCATC 3'
	$S_{215}G$	forward	5' GCGCCAAAGCCTATAAAGAT**GGC**AAGGTTTGTAACATGC 3'
		reverse	5' GCATGTTACAAACCTT**GCC**ATCTTTATAGGCTTTGGCGC 3'
	$S_{215}T$	forward	5' GGCGCCAAAGCCTATAAAGAT**ACC**AAGGTTTGTAACATGC 3'
		reverse	5' GCATGTTACAAACCTT**GGT**ATCTTTATAGGCTTTGGCGCC 3'
	$K_{216}R$	forward	5' GGCGCCAAAGCCTATAAAGATAGT**CGT**GTTTGTAACATGCTGAC 3'
		reverse	5' GTCAGCATGTTACAAAC**ACG**ACTATCTTTATAGGCTTTGGCGCC 3'
	$K_{216}Q$	forward	5' CCAAAGCCTATAAAGATAGT**CAG**GTTTGTAACATGCTG 3'
		reverse	5' CAGCATGTTACAAACCT**GAC**TATCTTTATAGGCTTTGG 3'

To introduce the desired mutation into the POR A/POR B gene the PCR technique was used. In more detail, the corresponding wild type plasmid DNA, subcloned into the pRSET A vector, was amplified in the presence of a pair of the complementary mutagenic primer using the high-fidelity DNA polymerase *Pfu Turbo*®) for replication of both plasmid strands.

The components of the reaction mixture and the amplification protocol are listed in Table 2.4.

Table 2.4: **(A)** components of the PCR reaction mixture. **(B)** the parameters of the PCR reaction for the amplification of the dsDNA template

A | PCR reaction mixture for mutagenesis

reaction content	amount
10x reaction buffer	5 µl
30 ng dsDNA template	1 µl
125 ng forward primer	2 µl
125 ng reverse primer	2 µl
dNTP mix	0.5 µl
Pfu Turbo DNA polymerase (2.5 U/ µL)	1 µl
Milli-Q H_2O	38.5 µl
total Volume	50 µl

B | cycling parameters of the PCR reaction

temperature	time	cycle
95°C	30 s	1
95°C	30 s	16
55°C	1 min	
72°C	5 min	
72°C	3 min	1

After temperature cycling the reaction mixture contains both, the mutated and non-mutated DNA (template DNA). To separate the two, a digestion with the endonuclease *Dpn I* was carried out (1 hour at 37°C). *Dpn I* recognizes and digests only the dam methylated, non-mutated wild type template, whereas the mutated DNA product is non-methylated and therefore not susceptible to *Dpn I*. After digestion the entire reaction volume was used for the transformation into *E. coli* XL1-Blue supercompetent cells (aliquots of 200 µl). After the transformation reaction, the cells were plated on 1.5% LB-agar plates containing ampicillin and incubated at 37°C over night.

2.4.2 Analysis of the mutated POR DNA by colony PCR

To control whether the POR DNA inserts are present in the plasmid construct, the transformants were first screened by colony PCR. A chosen colony with an individual transformant was lysed by suspension in 5 µl of Milli-Q water and short heating at 95°C for 15 min.

After that 20 µl of the PCR master mix were added and the reaction was carried out according to the specifications given in Table 2.5. Following cycling, 6.25 µl of 5x DNA loading dye was added into the PCR reaction mixture, from which 20 µl were then loaded onto an agarose gel (1% agarose, 0.005% ethidium bromide, dissolved in 1x TAE buffer - 40mM Tris, 20mM acetic acid, and 1mM EDTA) and run alongside a DNA size marker for 45 min at 130 V, 0.12 A and 15 W.

Table 2.5: Forward and reverse primers used in the colony PCR for the amplification of the mutated POR A and POR B DNA, respectively **(A)**. In addition, the ingredients of the PCR Master Mix **(B)** and the parameters of the PCR reaction **(C)** are shown

A | colony PCR primers

POR A	forward	5′ TGCAGATGGGCAAGAAGA 3′
	reverse	5′ CACACCTTGCTGTCCTTGTA 3′
POR B	forward	5’ GCTACACCATCGTGCACCTTGATCTGG 3’
	reverse	5′ CCT TGGTGATGTACTTCTGGAACG 3’

B | PCR master mix

reaction content	amount
One Taq 2X Master Mix (NEB)	12.5 µl
forward primer	0.5 µl
reverse primer	0.5 µl
Milli-Q H_2O	6.5 µl
Total Volume	20 µl

C | cycling parameters of the PCR reaction

temperature	time	cycle
94°C	2 min	1
94°C	30 s	35
54°C	30 s	
72°C	1 min	
72°C	10 min	1

2.4.3 Isolation and transformation of the mutated plasmid DNA

The colonies shown to contain the required POR DNA inserts in the colony PCR test were subjected to the isolation of the plasmid DNA and the determination of the full-length POR DNA sequence. For the isolation of DNA, a DNA purification kit (Macherey-Nagel) was used taking into account the guidelines in the provided instructions, whereas the sequence was determined by a professional company (Seqlab Sequence Laboratories GmbH) using the T7-promotor and T7-terminator primers in the sequencing reaction.

The plasmid DNA constructs of the POR A and POR B mutant enzymes containing the correct sequence were transformed into SoluBL21™ competent *E.coli* cells (AMS Biotechnology (Europe) Ltd.). For this purpose, an aliquot of the supplied competent SoluBL21™ cells was thawed on ice followed by the addition of 1 µl of the required plasmid DNA and further incubation on ice for 30 min. Then the transformation mixture was heat-shocked at 42°C for 45 seconds and placed back on ice. Thereafter 800 µl of the sterile medium were added and the transformation reaction was continued at 37°C in a thermomixer (Eppendorf) at maximum shaking speed for 45 min. Finally, the transformation mixture was scratched out on 1.5% LB-agar plates containing the antibiotic ampicillin (100 µg/ml) and incubated overnight at 37°C.

The following day, two colonies were transferred into 2 ml of the M9 minimal medium (see below) containing 100 µg/ml ampicillin and incubated once more at 37°C overnight For storage until use in the refrigerator at -80°C, the overnight culture was mixed with glycerine to give a 50% glycerine culture.

2.5 Overexpression of the POR enzymes

For the expression of the POR proteins 50 ml of the M9 minimal medium containing 100µg/ml ampicillin were inoculated with 500 µl of the desired glycerine culture and incubated overnight at 37°C on a rotary shaker. 50 ml of this starter culture were transferred into 500 ml of the M9 minimal medium with the addition of ampicillin (100µg/ml) and incubated by continuous shaking for about 7h at 24°C until the OD at 600 nm reached a value of ~0.4. After the addition of 500 µl of 1 M IPTG (1 mM final concentration) the cells were further incubated at 24°C overnight. After that incubation period the cells were spin down (20 min, 9 600 x g) and the cell pellets frozen at -20°C until further use.

Table 2.6: Composition of the M9 stock solutions and the preparation of the 1x M9 in different culture volumes.

5x M9 medium (in 1 L Milli-Q H_2O)		**stock solutions**	
$Na_2HPO_4 \cdot 2H_2O$	42.5 g	$MgSO_4$	2 M
KH_2PO_4	15 g	$CaCl_2$	1 M
NH_4Cl	5 g	glycerin	4 %
NaCl	2.5 g	ampicillin	100 mg/ml

1x M9 medium						
tot. culture vol.	Milli-Q H_2O	5x M9 medium	4% glycerine	1M $CaCl_2$	2M $MgSO_4$	ampicillin
50 ml	35 ml	10 ml	5 ml	5 µl	50 µl	50 µl
500 ml	350 ml	100ml	50 ml	50 µl	500 µl	500 µl

2.6 Purification of the POR enzymes

The recombinant POR proteins were purified by affinity chromatography on Ni-NTA agarose (Quiagen). The following buffers were used in the purification:

binding buffer:	50 mM	Tris/HCl
	0.5 M	NaCl
	20 mM	imidazole
	0.1%	Triton X-100
	20%	glycerine
	0.1%	β -mercaptoethanol (ß-MCE)
	pH	7,6

elution buffer:	50 mM	Tris/HCl
	0.5 M	NaCl
	300 mM	imidazole
	0.1%	Triton X-100
	20%	glycerine
	0.1%	β -mercaptoethanol (ß-MCE)
	pH	7,6

measuring buffer:	50 mM	Tris/HCl
	0.3 M	NaCl
	0.1%	Triton X-100
	20%	glycerine
	7 mM	DTT
	pH	7,6

In a first step, the frozen bacterial cells obtained from the protein expression procedure were subjected to cell lysis using the non-denaturating protein extraction formulation CelLytic Express™ (Sigma-Aldrich), which contains both lysozyme and endonucleases. For cell lysis, one batch of the cell pellets (~ 2 g) was thawed on ice and mixed with 5 ml of binding buffer,

0.25 g of CelLytic Express™ and 10 mg of additional lysozyme (added from a stock solution of 100 mg/ml). This mixture was incubated for 30 min at room temperature to ensure efficient lysis. The cleared cell lysate was then loaded onto a Ni-NTA agarose column, whereas for the following chromatographic separation two methods were applied: (i) gravity-flow chromatography and (ii) fast protein liquid chromatography (FPLC).

2.6.1 Gravity-flow chromatography

After prior equilibration with the binding buffer, a column containing 800 µl Ni-NTA agarose (Qiagen), was loaded with the cleared cell lysate. For enhancing the binding capacity of the His-tagged POR proteins the Ni-NTA agarose column was gently shaken for 45 min at room temperature. Following this procedure, the supernatant was passed through the column followed by a washing step with 30 ml of the binding buffer and elution of the bound POR protein with the elution buffer in 500 µl fraction.

In the last purification step the eluted POR protein was desalted by means of PD-10 desalting columns (GE Healthcare) filled with Sephadex G-25 resin. Based on the product instructions the PD-10 column was loaded with 2.5 ml of the purified POR protein, whereas the column was equilibrated before with 40 ml of the measuring buffer. The POR protein was eluted with 3.5 ml of measuring buffer. The protein concentration of the desalted samples was determined by the Bradford assay.

2.6.2 Fast protein liquid chromatography

The conditions elaborated in gravity-flow chromatography for the purification of POR proteins were adopted to the technique of fast protein liquid chromatography (FPLC) in order to automate the manual purification. For FPLC an ÄKTA protein purification system was used in combination with a prepacked 1-ml HisTrap HP column and a 50-ml superloop for sample injection (GE Healthcare Life Sciences).

The HisTrap column was equilibrated with 10 ml of binding buffer. Then, the cleared protein lysate was applied to the column via the superloop. After sample application the column was washed with 30 ml of binding buffer (eluent A) to remove unbound proteins. Finally, the His-tagged POR protein was eluted by using a linear gradient from 0 to 100% in 25 ml of eluent B (elution buffer). If necessary, the collected fractions containing the His-

tagged POR protein were concentrated by fast ultrafiltration in Amicon® Ultra 15 ml centrifugal filters (Merck Millipore) with a molecular weight cut-off of 3 kDa.

2.7 Characterization of POR enzymes

2.7.1 SDS polyacralamide gel electrophoresis

The purity and homogeneity of the isolated POR protein was controlled by SDS gel electrophoresis in 12.5% precast polyacrylamide gels of the size 245 x 110 x 0.5 mm containing 0.1% SDS (ExcelGel™ SDS Homogeneous 12.5, GE Healthcare Life Sciences) under the following conditions:

600 V 50 mA 30 W

gel buffer: 0.12 M Tris, 0.12 M acetate, 1 g/L SDS, pH 6.4
cathode buffer: 0.08 M Tris, 0.8 M tricine, 6 g/L SDS, pH 7.1
anode buffer: 0.45 M Tris, 0.45 M acetate, 4 g/L SDS, pH 6.6

After electrophoresis the separated proteins on the SDS gel were fixed in a solution of 50 % methanol and 10 % of glacial acetic acid for 30 min and subsequently stained for 2 h in a 0.1 % solution of PhastGel Blue R (GE Healthcare Life Sciences). For destaining a solution of 25% methanol and 10% of glacial acetic acid was used. The destaining solution was changed several times until the protein bands were clearly visible.

2.7.2 Assays for the determination of the substrate affinity of POR A and POR B wild types

The initial rates (v_0), the Michaelis-Menten constants (K_M) and the turnover numbers (k_{cat}) were determined in measuring buffer containing 50 mM Tris/HCl, 0.3 M NaCl, 20% glycerol, 0.1% Triton X-100 and 7 mM DTT at pH 7.6. The typical reaction mixture was composed of 10 µM POR, 100 µM NADPH and PChlide added at various concentrations as indicated for the individual experiments. For the evaluation of the initial reaction rate (v_0) the ternary POR-PChlide-NADPH complex was pre-formed by incubation in the dark and then irradiated with a HeNe laser 30-50 (Spindler & Hoyer) at λ_{exc} = 633 nm and a photon flux of $2.5 \cdot 10^{-5}$ mol·m^{-2}·s^{-1} for different time periods. The reaction progress was followed by monitoring the absorption spectra in the UV/Vis region in dependence on the irradiation

time using a Lambda 35 UV/Vis spectrophotometer (Perkin Elmer Instruments). In this set-up, the reaction rate corresponds to the decrease/increase in the PChlide/Chlide concentration. The concentrations were determined in each experiment using molar extinction coefficients of $\varepsilon_{630\ nm}$ = 48 700 l/mol·cm^{-1} for PChlide and $\varepsilon_{670\ nm}$ = 91 000 l/mol·cm^{-1} for Chlide. From the dependence of the initial rate on the originally added concentration of PChlide, the K_M values were estimated according to the Michaelis-Menten equation:

$$\frac{\mathrm{d[Chlide]}}{\mathrm{dt}} = v_0 = \frac{V_{max} \cdot [PChlide]}{K_M + [PChlide]} \qquad \text{Eq. 1}$$

by means of a nonlinear least-squares curve fitting procedure in Matlab. The turnover number, k_{cat}, was derived from maximum enzyme velocity (V_{max}) according to:

$$k_{cat} = \frac{V_{max}}{[E_0]} \qquad \text{Eq. 2}$$

with

$[E_0]$ – total concentration of the POR enzyme.

2.7.3 Kinetic assay of POR A and POR B mutant enzymes

Steady-state activity measurements of the POR A and B mutants were carried out at room temperature as described for the wild type enzymes above (2.7.2) using 10 µM POR mutant, 7 µM PChlide and 100 µM NADPH in measuring buffer. After formation of the ternary mutant complex by pre-incubation in the dark the sample was irradiated with a helium-neon laser 30-50 (Spindler & Hoyer) at λ_{exc}= 633 nm and a photon flux of $1.7 \cdot 10^{-5}$ mol·m^{-2}·s^{-1} . From the produced amount of Chlide as function of the irradiation time, the initial rate, v_0, was determined as long as the remaining enzyme activity allowed such calculations, using the following equation:

$$v_0 = -\frac{d[PChlide]}{dt} = \frac{d[Chlide]}{dt} = constant \qquad \text{Eq. 3}$$

The initial rate, v_0, was derived from the slope of such progress curves, whereas the slope was determined by a linear regression analysis. The ratio of the initial rates of the POR mutant forms to the wild type POR then gives the relative activity, A_{rel}. Finally, the turnover number, k_{cat}, was calculated from the maximum velocity, V_{max}, according to 2.

2.7.4 Low temperature absorption spectroscopy

For the low temperature absorption measurements a UV/Vis spectrophotometer (Jasco V-570) was used in combination with a nitrogen bath cryostat (OptistatDN, Oxford instrument). The low temperature absorption spectra were monitored in measuring buffer containing 60% glycerol in 50 mM Tris/HCl at pH 7.6 with the addition of 0.3 M NaCl, 7 mM DTT and 0.1% Triton X-100.The ternary POR-PChlide-NADPH complexes of the mutant and wild type forms were assembled in the dark by mixing 60 µM POR/mutant protein with 3.5 µM PChlide and 400 µM NADPH. Samples of the pre-formed ternary complexes were then placed into the cuvette of the cryostat, frozen at 180 K and irradiated by an LED cold-light source (Thorlabs, Inc.) at λ_{exc} = (632 ± 9) nm (400 µW) for 20 min to initiate the first light-dependent step in enzyme catalysis. After that the absorption spectrum was registered followed by an increase of the temperature from 180 up to 305 K in steps between 5 and 10 K. After warming the samples were kept for 10 min at the gradually higher temperature in the dark to guaranty temperature equilibration. At each required temperature the absorption spectrum was taken in order to characterize the intermediate trapped at the respective temperature. The temperature was controlled with a thermocouple sensor (100 Ω platinum resistance thermometer).

2.7.5 Calculation of the activation energy for the 1st reaction intermediate

The activation energy (E_a) of the 1st reaction intermediate was determined as follows: The ternary POR-PChlide-NADPH complex with 30 µM POR, 5 µM PChlide and 200 µM NADPH concentrations in measuring buffer with 60% glycerol was incubated in the dark and maintained at various temperatures between 160 and 200 K. At each selected temperature the sample was irradiated at λ_{exc}= 625 nm for different time intervals in order to determine the initial reaction rate (v_0). From the initial rate, v_0, the rate constant k was estimated at the various temperatures and ln k then plotted against the absolute temperature. The activation energy was calculated from these plots by using the Arrhenius equation (Eq. 4):

$$\ln(k) = const. + \frac{-E_a}{RT} \qquad \text{Eq. 4}$$

where E_a is the activation energy, k is the rate constant, R is the gas constant and T is the absolute temperature.

2.7.6 Analysis of the reaction intermediates

The evidence that the absorbance changes in the low temperature spectra really represent the spectral characteristics of independent intermediates was provided using the algorithm given in the software package ReactLab™ KINETICS (Jplus Consulting). For this purpose, the absorbances between 650 and 710 nm were extracted from the spectra recorded at temperatures in the range from 180 to 290 K and submitted to the software after the offset in the spectra was removed. A single value decomposition (SVD) was followed in order to estimate the number of components in the data sets, which are required in the expected reaction model. In conjunction with the results of SVD analysis exploratory factor analysis, which predicts model-free spectral shapes and concentration profiles of the independent reaction components, was carried out in addition. Hence, the combination of SVD and EFA analysis resulted in the estimation of the spectra of the independent reaction components including their concentration profiles as function of the temperature.

2.7.7 Low temperature fluorescence spectroscopy

The time-resolved fluorescence decays at low temperatures were measured using a titanium:sapphire laser system (Tsunami, Newport Spectra-Physics GmbH). The repetition rate of the laser was reduced to 1 kHz by a pulse selector (Model 3980, Newport Spectra-Physics GmbH) and the fundamental beam of the oscillator was frequency doubled and thus spectrally tuned to 440 nm for the generation of the excitation pulse. The fluorescence signals were collected under a 90° angle using a streak camera (Hamamatsu HPD-TA) in combination with an imaging monochromator (Chromex 250IS) covering a spectral window of 100 nm. The resulting image from the streak camera was collected in photon-counting mode. The fluorescence was scanned in two time windows of 20 ns and 50 ns, respectively.
For the measurement of the ternary POR/mutant protein-PChlide-NADPH complexes, 60 µM POR/mutant protein in measuring buffer (50 mM Tris/HCl, 0.3 M NaCl, 0.1 % Triton-X-100, 7 mM DTT, 60% glycerol at pH 7.6) was mixed with 7 µM PChlide and 400 µM NADPH in the dark. After complex formation the samples were handled as in case of the low temperature absorption measurements (2.7.4). Placed into the nitrogen bath cryostat the samples were cooled to 150 K and after thermal equilibration the fluorescence decay measurements were initiated.

2.7.8 Fluorescence decay time – data analysis

The two-dimensional data matrices (wavelength in rows, time in columns), obtained by the streak-camera, were processed as follows: several individual columns were integrated to give 32 decay traces (between 590 and 730 nm). Each of the 32 traces was then normalized and background corrected. Scilab software was used to perform a global fit with one or two decay constants to describe sequentially occurring reactions, for both time-windows at the same time. The implemented fit procedure works numerically and includes a convolution integral (Eq. 5)

$$I(t) = \int R(t - t')S(t)dt' \qquad \text{Eq. 5}$$

R(t) = instrumental response
S(t) = sample response

where the detector response was modelled by a Gaussian function and the response from the sample by an exponential with a decay time τ (Eq. 6).

$$S(t) = I(0) \sum_{i}^{n} a \cdot e^{-\frac{t}{\tau_i}} \qquad \text{Eq. 6}$$

I= fluorescence intensity
t = time
a = amplitude
τ = decay time

Prior to the fit and base on the Gaussian response, the pulse arrival time was set to 0 ns. Terms for laser scatter were included if necessary.

3. Results

3.1 Purification of PChlide and POR A and B wild type enzymes

The extraction of PChlide from plant material and its purification was a standard routine and NMR analysis of the obtained pigment is reported in the PhD Thesis of Dr. Fey[94]. A UV-Vis spectrum is recorded in order to confirm the quality and the purity of each batch of produced and extracted PChlide. In Figure 3.1 A the typical absorption spectrum of PChlide in methanol at the end of the purification steps is reported. The spectral evolution as well as the absorption peaks agree very well with the spectral characteristics reported for PChlide in different organic solvents[20,23,25,95]. The purified PChlide sample does not contain protopheophorbide, the de-metallated analogue of PChlide, which is easily formed as unwanted by-product during isolation.

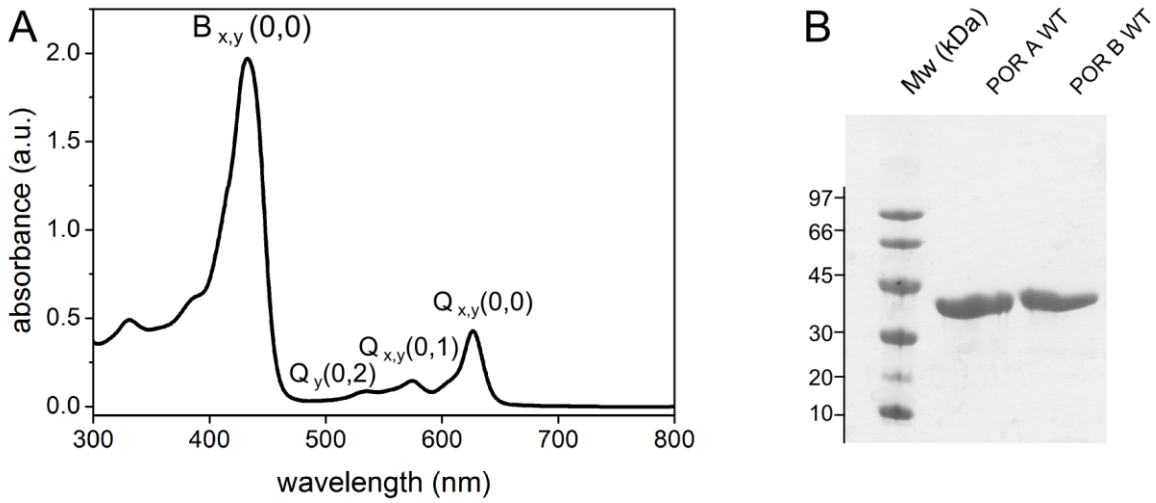

Figure 3.1: Characterization of the purified components of the ternary POR complex. **(A)** UV-Vis spectrum of PChlide in methanol after extraction and purification. The assignment of the absorption bands on the basis of the "four-orbital" model of Gouterman is also indicated[18] **(B)** SDS PAGE (12.5%) of the purified POR A and POR B wild type proteins.

The quality of the overexpressed and purified POR enzymes was controlled by SDS polyacrylamide gel electrophoresis. Figure 3.1 B represents a characteristic electropherogram of the POR A and POR B wild type enzymes, which were run along with a low molecular weight marker. Comparison between the electrophoretic mobility of the POR bands and the molecular weight of the standard led to the assignment of a molecular mass of 37 kDa and

37.5 kDa to POR A and B, respectively. The purity of POR wild types was confirmed by the presence of only one band at the expected molecular weight.

3.2 Characterization of the POR A and B wild type enzymes

3.2.1 Enzyme kinetic parameters of POR A and B

The enzyme kinetic parameters of the POR A and B wild type enzymes were measured by following the decrease in the concentration of PChlide and the increase in the concentration of Chlide, respectively (Figure 3.2). In a typical experiment, the absorption spectra were monitored for a definite PChlide concentration as a function of the irradiation time. From the initial slope of the progress curve reflecting the decrease/increase in the PChlide/Chlide concentration in dependence on the irradiation time, the initial reaction rate, v_0, was determined under steady-state conditions. Based on the requirements of the Michaelis-Menten kinetics the PChlide concentration was varied in an appropriate range while the POR concentration was kept constant. The initial reaction rates thus obtained for the individual PChlide concentrations were plotted against the PChlide concentration resulting in a rectangular hyperbolic curve (Figure 3.3).

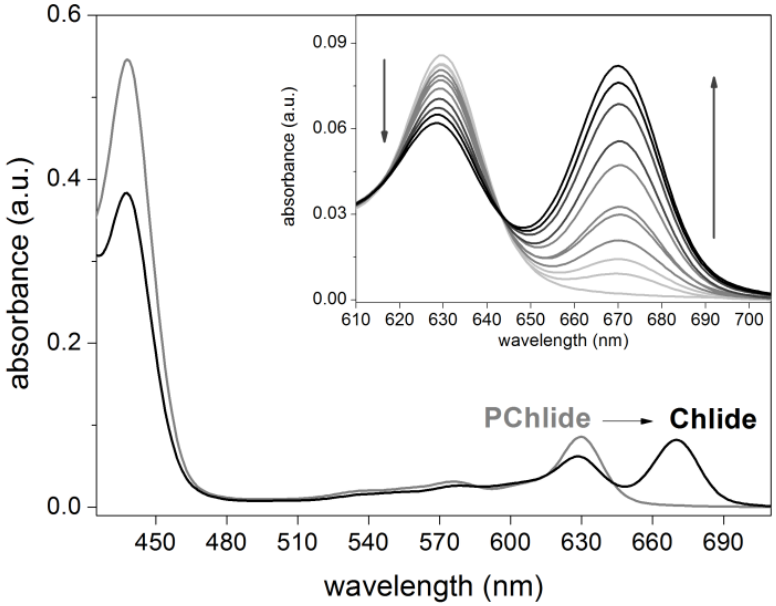

Figure 3.2: UV-Vis spectrum of PChlide and catalytically produced Chlide at room temperature (293 K) in measuring buffer. In the insert: disappearing of the 630 nm PChlide band and appearing of the 670 nm Chlide band along the reaction catalysed by POR in the presence of NADPH under continuum light illumination at different time points.

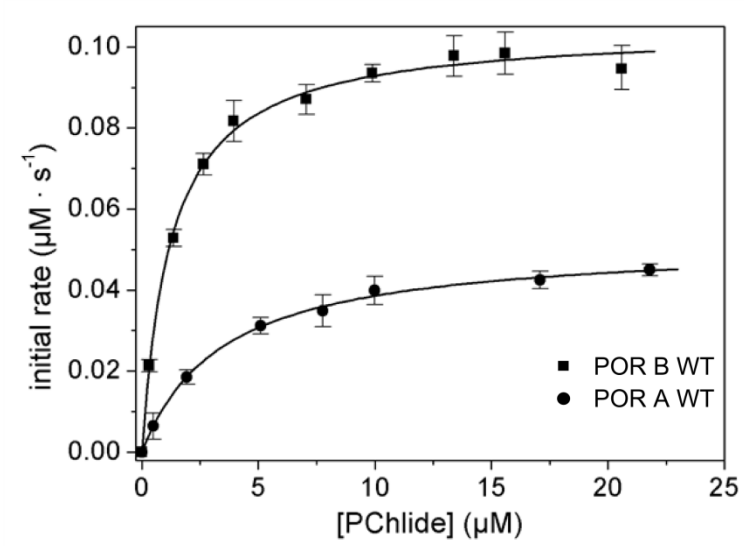

Figure 3.3: Dependence of the initial rate (v_o) of the POR-catalyzed reaction on the PChlide concentration ([PChlide]). The plots are shown for POR A (●) and POR B (■).The Michaelis-Menten constant, K_M, and the maximum reaction rate (V_{max}) were estimated from the v_0 versus [PChlide] plots by a nonlinear curve fitting procedure using the Michaelis-Menten equation (Eq. 1) as fit function in Matlab.

The fit of these hyperbolae to the Michaelis-Menten equation (Eq. 1) yielded values of K_M = (3.44 ± 0.3) µM for POR A and K_M = (1.25 ± 0.05) µM for POR B. From the same fit, values of V_{max} = 0.05 µM·s^{-1} were derived for POR A and V_{max} = 0.1 µM·s^{-1} for POR B (Figure 3.3). These results indicate that POR B has a higher affinity for PChlide and a higher maximum reaction rate, V_{max}, when it is saturated by the substrate. In order to compare the catalytic efficiencies of POR A and POR B also the turnover number, k_{cat}, and the specificity constant, k_{cat}/K_M, were used. The turnover number k_{cat}, which is equivalent to the numbers of substrate molecules converted to product by the enzyme in a given unit of time, was determined from the maximum velocity,V_{max}, (Eq. 2) and further used for the determination

Table 3.1: Comparison of the kinetic parameters between POR A and POR B. The estimates are the average of four independent measurements.

	K_M (µM)	V_{max} (µM·s^{-1})	k_{cat} (s^{-1})	k_{cat}/K_M (s^{-1}·M^{-1})
POR A	3.4 ± 0.3	0.050 ± 0.005	$5.5\cdot10^{-3} \pm 5.5\cdot10^{-4}$	$1.6\cdot10^{3} \pm 1.6\cdot10^{2}$
POR B	1.25 ± 0.07	0.100 ± 0.002	$1.2\cdot10^{-2} \pm 1.5\cdot10^{-3}$	$9.3\cdot10^{3} \pm 9.3\cdot10^{2}$

of the specificity constant k_{cat}/K_M. In Table 3.1 the kinetic constants thus obtained for the two isoenzymes, POR A and POR B are summarised for direct comparison.

As can be seen k_{cat} is about two times higher for POR B than for POR A indicating a considerably enhanced rate for the conversion of PChlide. In addition, the specificity

constant, k_{cat}/K_M is 6-fold higher for POR B than POR A implicating that POR B is the more efficient enzyme in the photoconversion of PChlide into Chlide.

3.2.2 Reaction intermediates in the catalytic cycle of POR A and B

In the ternary POR-PChlide-NADPH complexes the absorbance maximum of the porphyrin Q-band of PChlide undergoes a red shift by about 10 nm from 630 nm to 640 nm (Figure 3.4 A-B). This effect is clearly seen at 180 K both for POR A and POR B. At room temperature the absorbance shift also occurs in the case of POR B but in the case of POR A it is manifested in a broadening of the absorbance band. Such a red shift in the Q-band absorption is well known from the POR enzymes of cyanobacteria. It is suggested to represent the formation of the finally photoactive state as consequence of conformational rearrangements upon binding of PChlide and NADPH within the catalytic site[67,70,96,97]. The photoactive state is designated as S_{640} in the context of the low temperature absorbance measurements.

After photoexcitation of S_{640} at 180 K, the initial light-induced step of the POR A and POR B ternary complexes involves the formation of a first intermediate with an absorbance maximum at 677 nm (A_{677}). Due to its spectral characteristics A_{677} can be attributed to Chlide, the final reaction product, which however remains still bound in the POR-Chlide-$NADP^+$complex[78]. On the contrary to what is observed for the POR enzyme from *Synechocystis* (PORss) (Figure 3.4 C), no intermediate preceding A_{677} could be observed even at temperatures below 180 K. In *Synechocystis* POR a broad band at 698 nm appeared immediately after irradiation, which belongs to the first reaction intermediate, A_{698}. At higher temperature (214 K) A_{698} is converted into an intermediate with an absorption maximum at 677 nm, A_{677} (Figure 3.4 C). Based on studies of *Synechocystis* POR reported by the Heyes group it is very likely that A_{698} represents the first photoproduct, in which PChlide has received the hydride (H^-) from NADPH and forms an intermolecular charge transfer state with $NADP^+$ [67]. The H^+ transfer then occurs in the subsequent dark reaction which produces A_{677}. A_{677} generated by *Synechocystis* POR obviously corresponds to the A_{677} species seen as primary photoproduct in POR A and POR B.

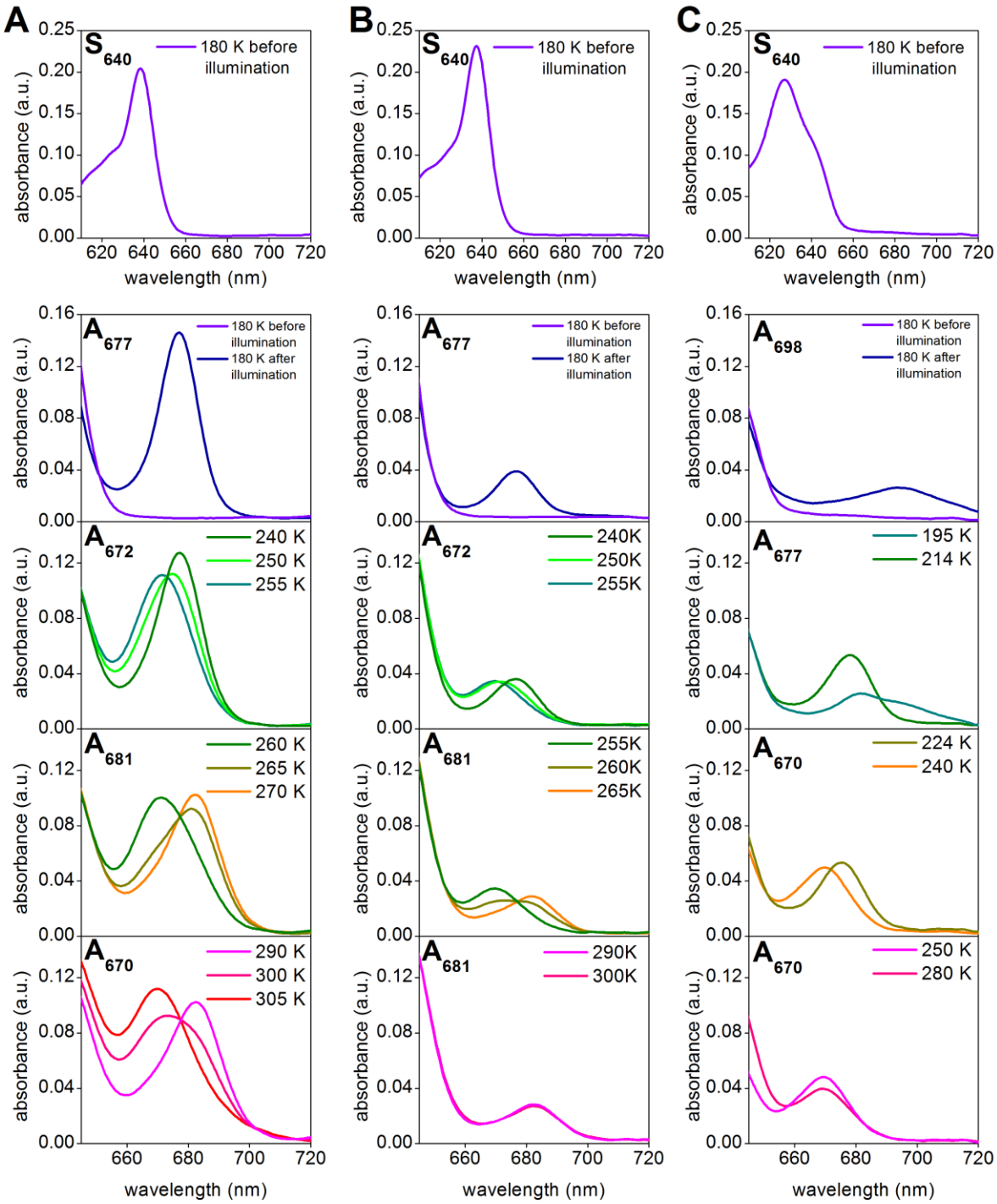

Figure 3.4: Intermediates in the reaction cycle of POR A and POR B as well as POR from *Synechocystis* as detected by low temperature absorbance spectroscopy. The ternary complexes were frozen at 180 K, irradiated by actinic light at λ_{exc} = 632 nm and then the temperature was raised in the range between 180 and 305 K step by step. The absorbance spectra were monitored at temperatures indicated in the insets. The spectra are grouped in vertical rows. **(A)** POR A WT from barley, **(B)** POR B WT from barley, **(C)** PORss from *Synechocystis*.

As the temperature profile reveals, in both POR A and POR B the first intermediate remains existent up to 240 K. Above this temperature the A_{677} band disappears accompanied by the simultaneous appearance of a new absorption band at 672 nm, which can be related to another intermediate, A_{672}, with an absorption maximum at 672 nm. In the temperature range between 255 and 270 K, A_{672} is converted into a product, A_{681}, peaking at 681 nm. At higher temperatures only A_{681} formed by POR A undergoes a further transformation yielding a species with a blue-shifted absorption band at 670 nm, which represents the absorbance of free, unbound Chlide. Hence, this reaction step involves the release of free Chlide, the final product of the enzymatic reaction. The corresponding reaction does not occur in POR B. In POR B the reaction stops at the formation of A_{681} and no Chlide is released in the time period of the measurement. There remains an explanation for the dark reactions involving the $A_{677} \rightarrow A_{672}$ and $A_{672} \rightarrow A_{681}$ conversions. The molecular nature of these processes can be deduced from low temperature binding studies of Chlide to POR in the presence and absence of NADPH and $NADP^+$ [78]. The absorbance shifts, characteristic of the different dark reaction stages, are very similar to those identified in the binding experiments. Thus, the dark reaction $A_{677} \rightarrow A_{672}$ can be attributed to the release of $NADP^+$ and the reaction $A_{677} \rightarrow A_{672}$ to the rebinding of the cofactor NADPH. Furthermore, it is evident that the dark reactions take place above the glass transition temperature. This suggests that they involve the rearrangement of protein domains/sites near or at the catalytic centre to modulate the product binding interactions and to release the cofactor and the product. On the contrary the first photochemical step resulting in the formation of the A_{677} species at 180 K seems to require only local interactions over a short distance without the necessity of large-scale motions.

In *Synechocystis* POR creation of A_{677} is followed by the direct release of Chlide from POR at temperatures above the glass transition. This process is reflected by the transformation of A_{677} into A_{670}, which matches the absorption features of free, unbound Chlide. Intermediate dark reaction steps as they occur in the ternary POR A and POR B complexes cannot be discerned in *Synechocystis* POR.

The comparison between the ternary complexes of *Synechocystis* POR and of the higher plant POR enzymes reveals a remarkably different intermediate pattern, whereas the sequence of the dark reactions as well as the spectral characteristics of the trapped intermediates in POR A and B does not differ significantly from each other

For the verification of the reaction cycle in the POR A and POR B ternary complexes the low temperature absorption spectra were also subjected to an SVD analysis. The results confirm that three different reaction intermediates are required to accurately model the experimental data sets for both POR A and POR B between 180 and 290 K. Moreover, the spectral analysis using exploratory factor analysis (EFA) also identifies three intermediate species, which fully match the intermediates extracted from the absorption spectra (Figure 3.5 A, C). The temperature profiles resulting as well from EFA show a difference in the

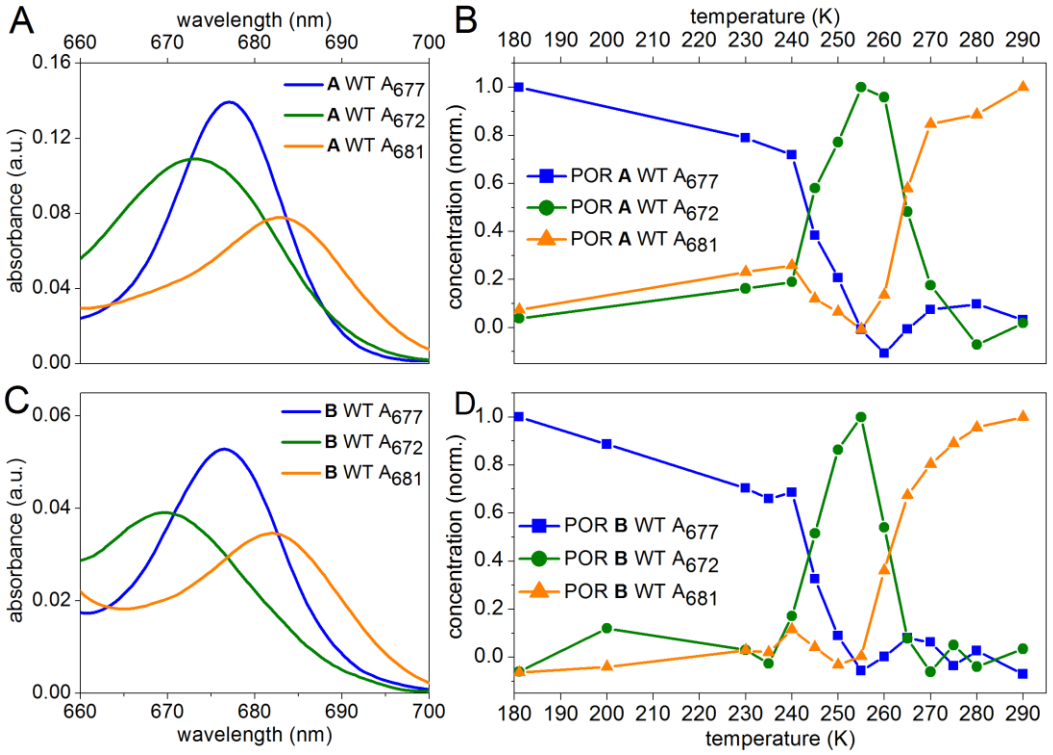

Figure 3.5: Spectroscopic characteristics of the intermediates in the reaction cycle of POR A and POR B as obtained from exploratory factor analysis. **(A)** – **(C)** Absorbance spectra of the intermediates approached for the reaction pathway of POR A WT and POR B WT, respectively. **(B)** – **(D)** Temperature dependence of the intermediates in the reaction path of POR A WT and POR B WT, respectively.

temperature dependence of the A_{672} and A_{681} species in POR A and POR B, respectively (Figures 3.5 B, D). The two species, which are associated with the liberation of $NADP^+$ and rebinding of NADPH, are shifted by about 5 K to a lower temperature in POR B as compared to POR A.

The low temperature absorption spectra (Figure 3.4 A, B) reveal that the yield of the first photoproduct, A_{677}, is significantly higher in POR A as compared with POR B. Since the conditions at low temperature allow only a single catalytic turnover, the activation

energy for this light-induced step was determined. For this purpose the rate constants for the formation of A_{677} were estimated over a temperature range from 160 - 200 K both for POR A and POR B. The data were then plotted in an Arrhenius graph (ln(k) *versus* 1/T) and fitted to the Arrhenius equation (Eq. 4). Activation energies (E_a) of (24.9 ± 2.1) kJ·mol^{-1} for POR A and (35.9 ± 1.8) kJ·mol^{-1} for POR B could be calculated implying a higher activation barrier that has to be crossed in POR B as compared with POR A to produce A_{672}.

.

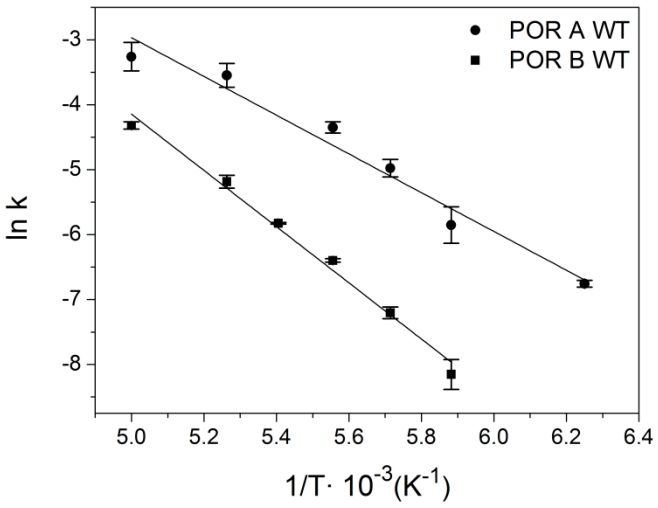

Figure 3.6: Arrhenius plots displaying the logarithm of the rate constant (ln(k)) for the initial photoreaction of the ternary POR complex to the first photoproduct, A_{677}, as function of the inverse temperature (1/T). From a fit of the data to the Arrhenius equation (Eq. 4) the activation energies (E_a) are calculated to be 24.9 ± 2.1 kJ·mol^{-1} for POR A and 35.9 ± 1.8 kJ·mol^{-1} for POR B. The plots are given for the reactions catalyzed by POR A (●) and POR B (■) in the temperature range from 160-200 K.

3.2.3 Primary processes in the reaction mechanism of PChlide in POR A and POR B

Using a cryostat to bring and maintain the samples at 150 K in combination with pulsed laser and a streak camera, two-dimensional data matrices (wavelength in rows, time in columns), were recorded. The results obtained at 150 K for free PChlide in measuring buffer, POR-PChlide and photoactive POR-PChlide-NADPH complexes including in each case both POR A and POR B are summarized in Figure 3.7. The emission spectra of PChlide in buffer and of the POR-PChlide complexes showed no differences. However, in case of the ternary POR-PChlide-NADPH complexes the emission maximum undergoes a 10 nm red shift (Δ 0.031 eV) in full analogy to the shift in the absorption spectra.

A global analysis was performed on the entire decay traces integrated in the wavelength range, recorded in each time window and fit to a single or multi exponential decay function. The decay traces and the results of the fits are shown in Figure 3.7 A and B for POR A WT and POR B WT, respectively. Two exponential components were necessary to fit the data. For PChlide in measuring buffer a short-lived component with τ_1 = 0.98 ± 0.02 ns and a long-lived one with τ_2 = 5.7 ± 0.2 ns were calculated (Table 3.2). The decay times are in agreement with already published data for PChlide measured at room temperature in a micellar Triton solution[98]. In the case of the POR-PChlide complexes the decay time of the short-lived component remains constant while the long-lived component increases to τ_2 = 6.2 ± 0.1 ns for POR A and τ_2 = 6.45 ± 0.02 ns for POR B. The increase in the decay time of the POR-PChlide complexes as compared to free PChlide is in accordance with results

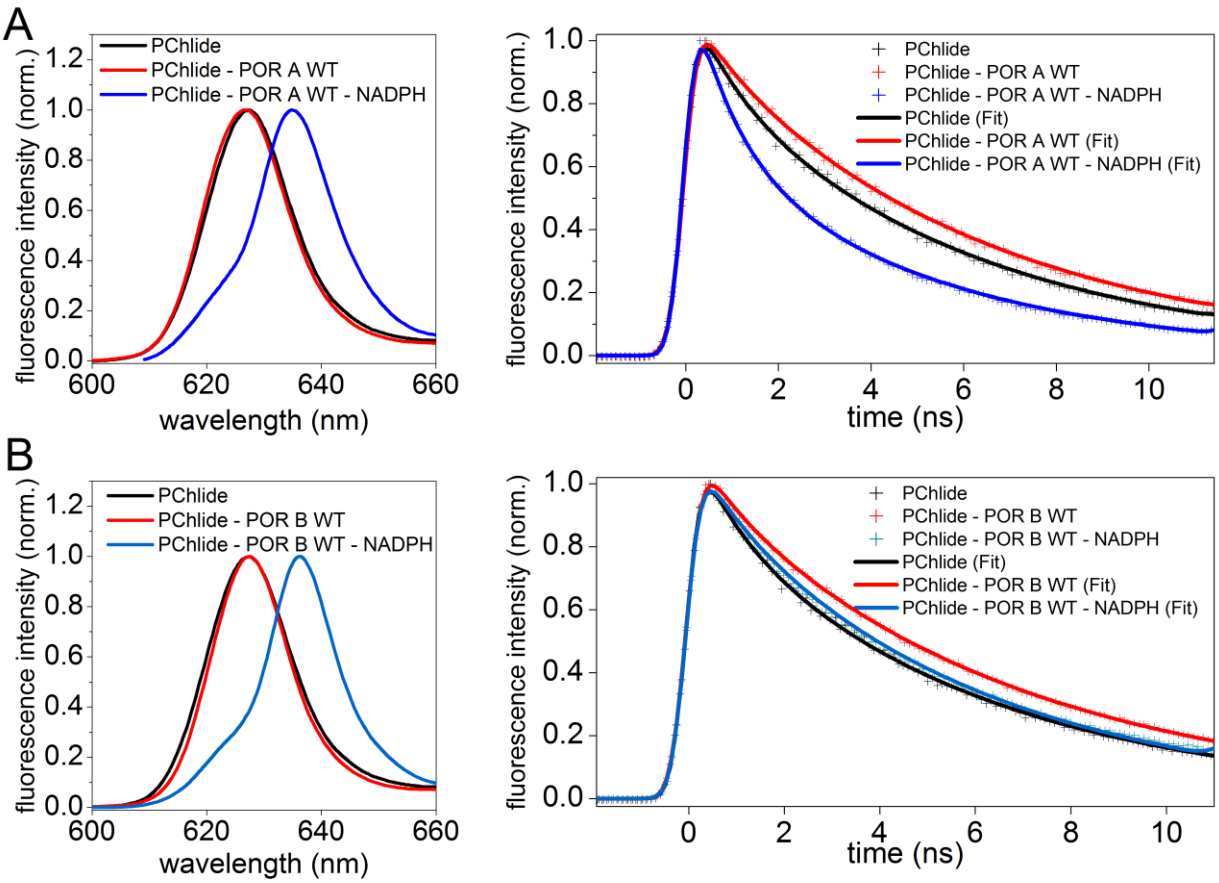

Figure 3.7: Fluorescence emission spectra and fluorescence decay kinetics of free unbound PChlide, PChlide-POR and PChlide-POR-NADPH complexes. The assignment of the spectra and decay traces to PChlide and the different POR complexes is given in the insets. For a clear differentiation between the decay traces only the first 11 ns of the 50 ns time windows are shown. The fluorescence spectra and decay kinetics were recorded at 150 K. The reaction mixture contained PChlide (7µM), POR enzyme (60 µM) and NADPH (400 µM) in measuring buffer. **(A)** POR A isoform, **(B)** POR B isoform.

reported by Hanf et al.[85] for respective POR A complexes studied at room-temperature. For the ternary POR-PChlide-NADPH complexes the fluorescence decay time is further varied. The decay time drops to τ_1 = 0.78 ± 0.23 ns and τ_2 = 5.04 ± 0.02 ns for the ternary POR A WT and to τ_1 = 0.97 ± 0.01 ns and τ_2 = 5.8 ± 0.3 ns for the POR B ternary complex. Although the regression analysis yielded two decay constants for all samples, only the decay time of the long-lived component undergoes a variation. Therefore, only the values related to τ_2 where taken into account in the following consideration.

Table 3.2: PChlide fluorescence decay times (τ) and the relative decay amplitudes (A) calculated by using a two-expoential model for the fit of the decay traces. The reaction mixture was composed of PChlide (7μM), POR enzyme (60 μM) and NADPH (400 μM) in measuring buffer containing 60% glycerol. The estimates are the average of at least two independent experiments.

Content of the reaction mixture	A_1	τ_1 (ns)	A_2	τ_2 (ns)
Isoform POR A				
PChlide	0.32 ± 0.03	0.98 ± 0.02	0.68 ± 0.03	5.7 ± 0.2
POR A WT - PChlide	0.36 ± 0.13	0.98 ± 0.01	0.64 ± 0.14	6.2 ± 0.1
NADPH - POR A WT - PChlide	0.54 ± 0.02	0.81 ± 0.15	0.46 ± 0.02	5.05 ± 0.01
Isoform POR B				
PChlide	0.32 ± 0.03	0.98 ± 0.02	0.68 ± 0.03	5.7 ± 0.2
POR B WT - PChlide	0.22 ± 0.02	0.97 ± 0.02	0.88 ± 0.02	6.46 ± 0.01
NADPH - POR B WT - PChlide	0.31 ± 0.06	0.97 ± 0.01	0.69 ± 0.06	5.8 ± 0.2

The fluorescence lifetime is traditionally considered to be a kinetic parameter and is determined as being inversely proportional to the sum of the rate constants for radiative processes k_r and non-radiative processes k_{nr} (Eq. 7)[99].

$$\tau = \frac{1}{k_{nr} + k_r} \qquad \text{Eq. 7}$$

The non-radiative pathway leading to the population of the triplet state has been reported to play an important role in the de-excitation processes of free PChlide in solution[23,25]. Further it was recently shown that in the POR-PChlide and pseudoternary POR-PChlide-$NADP^+$ complexes the non-radiative rates are decreased by ~30 and 40%, respectively, as compared with free PChlide. In parallel the fluorescence decay time is

lengthened from 3.4 ns for free PChlide to 4.4 and 5.4 ns in the POR-PChlide and POR-PChlide-$NADP^+$ complexes[85]. As proposed by Hanf et al.[85], the observed increase in the fluorescence lifetime of POR-PChlide complexes corresponds to the decrease in the non-radiative rates and this decrease is most likely due to the reduced probability of the non-radiative decay into the triplet state. Thus, intersystem crossing into the triplet state characteristic for the porphyrin photophysics is strongly reduced in the POR enzymes as far as the POR-PChlide and pseudoternary POR complex are considered. Most probably the side chains of the amino acids forming the POR active site control the excited dynamics of PChlide and impair the population of the triplet state. This statement can also be used to explain the results obtained for the POR-PChlide complexes in this work.

However, as can be seen from Table 3.2, a decrease in the decay time of the long-lived component is found for the ternary POR-PChlide-NADPH complexes. The decrease is detected in the two isoforms, but it is more remarkable in POR A than in POR B. To explain this decline of the decay time as compared to the POR-PChlide complexes two models can be used:

First, it has been shown that the reactive intramolecular charge transfer state, S_{ICT}, which is formed immediately after absorption of light and which precedes as a charge-separated intermediate the subsequent hydride and proton transfer reactions (see section 1.3.3) is stabilized in the ternary and pseudoternary POR complexes due to local interactions of PChlide with specific protein sites at the catalytic centre[84,85]. Hence, taken the reaction scheme derived for the initial decay processes in free PChlide in solution (Figure 1.3) it is possible that the relative energy of S_{ICT} and probably also of the preceding S_x state is lowered to a level, which opens the de-excitation channel along the reactive path for S_1-excited molecules. That means that in the ternary POR complexes direct deactivation of the S_1-excited state population towards the reactive route becomes available (Figure 4.2). As indicated by the very low fluorescence quantum yield and the rapid formation of the first reaction intermediates, S_X and S_{ICT}[84,85], the flow of S_1-excited state molecules into the reactive channel plays an important role. Thus, the switching-on of the reactive path and the efficient competition with the non-reactive one can easily explain the decrease in the fluorescence decay time of the photoactive ternary POR complexes as compared to the POR-PChlide complexes. As will be discussed below (chapter 3.6.1) the study on the POR mutant forms will further confirm this reaction model.

Second, it cannot be fully excluded that the energy gap law also provides a contribution to the decreased fluorescence decay times. According to this law the non-radiative decay rate of a metal–ligand complex increases exponentially as the energy gap or emission energy decreases[100,101] The 10-nm red shift in the fluorescence spectrum of the ternary POR complexes indicates a decrease in the emission energy, which has as consequence that the value of k_{nr} increases. Based on Eq. 7 the increase in k_{nr} goes along with a decrease in the fluorescence decay time. Thus, the decreased decay time of the ternary POR complexes could in part be due to an increase in the non-radiative decay rate.

3.3 POR B - Calculation of a 3-D (three dimensional) structural model

3.3.1 Modelling of the 3-D structure of POR B wild type apoprotein

Due to the current lack of a crystal structure for any of the POR enzymes and thus due to the lack of structural information, which can help to understand the nature of the molecular processes and reaction dynamics involved in the catalytic mechanism, a structural model was calculated for the POR B enzyme. For this purpose up-to-date *in silico* homology modeling techniques as they are made available by a series of structure-modeling web servers were used including adequate tools for docking the cofactor and substrate in the POR B model. POR B was chosen among the POR enzymes because it is the main enzyme of the light-controlled chlorophyll biosynthesis in plants.

To check the quality of the 3-D models obtained from the different on-line services they were submitted to the QMEAN server (Qualitative Model Energy Analysis), which estimates the quality of the calculated models. QMEAN is a composite scoring function which is able to derive both global (i.e. for the entire structure) and local (i.e. per residue) error estimates. The QMEAN service provides the:

- QMEAN score[102]: a global score of the whole model reflecting the predicted model reliability ranging from 0 to 1.
- QMEAN Z-score[103]: provides an estimate of the absolute quality of a model (global error estimation) by relating the model to reference structures resolved by X-ray crystallography.

- residue error value: is visualized in a 3D structure model with a colour gradient from blue (more reliable regions with an estimated error of <1 Å) to red (potentially unreliable regions with an estimated error >3.5 Å
- residue error plot: shows the estimated residue errors along the whole sequence (in Å)

The QMEAN score of all models, coming into question as possible structural candidate, are listed in Table 3.3 A. As evident, the I-TASSER algorithm produced 5 alternative models but all of them reached a very low score. This also applies for the structural models derived from the SWISS-MODEL services. The corresponding models have similar low QMEAN scores as the I-TASSER structures. From the models predicted only two have a comparatively high score. They are obtained from the M4T (0.60) and HHpredB (0.55) services.

In order to achieve a better differentiation between the two high-scored models, also the other QMEAN parameters were taken into consideration (Figure 3.3 B and C). As can be seen from the comparison with a non-redundant set of PDB structures, the QMEAN score for the M4T model (indicated by the red "X") is completely included in the allowed area (black and grey), whereas the QMEAN score of the HHpredB model is positioned slightly outside this area.

The analysis of the residue error value shows that for the two models the predicted structure of the protein core is more reliable (blue structural elements) than the structure calculated for the protein domains facing the surface region (red structural elements). Considering the residue error plot, which indicates the local model quality, the M4T model exhibits a comparatively high error level (> 15 Å) starting at about the position of the 240th amino acid. In contrast, the HHpredB model only shows a problematic region at the beginning of the N-terminal sequence. However, this sequence section corresponds to the signal peptide which is used by plant POR B to direct the precursor enzyme from the cytoplasm, where it is synthesized, into the chloroplast, where the transit peptide is cleaved off thus producing the active enzyme. Apart from this sequence segment the estimated error plot indicates a qualitatively good approach of the POR B 3-D structure by the HHpred model.

Table 3.3: Quality estimation of the POR B models predicted by the SWISS-MODEL, I-TASSER, M4T and HHpredB on-line services. **(A)** Comparison of the QMEAN values. **(B-C)** Z-score plot, residue error model and residue error plot for the 3-D models calculated by the M4T (B) and HHpredB (C) server.

A **QMEAN Score of POR B WT models produced by different on-line services**

Swiss Prot	I - TASSER					M4T	HHpredB
	1	2	3	4	5		
0.48	0.45	0.38	0.47	0.46	0.47	0.60	0.55

B **POR B WT | M4T QMEAN results**

Estimated absolute quality | Residue error - model | Residue error plot

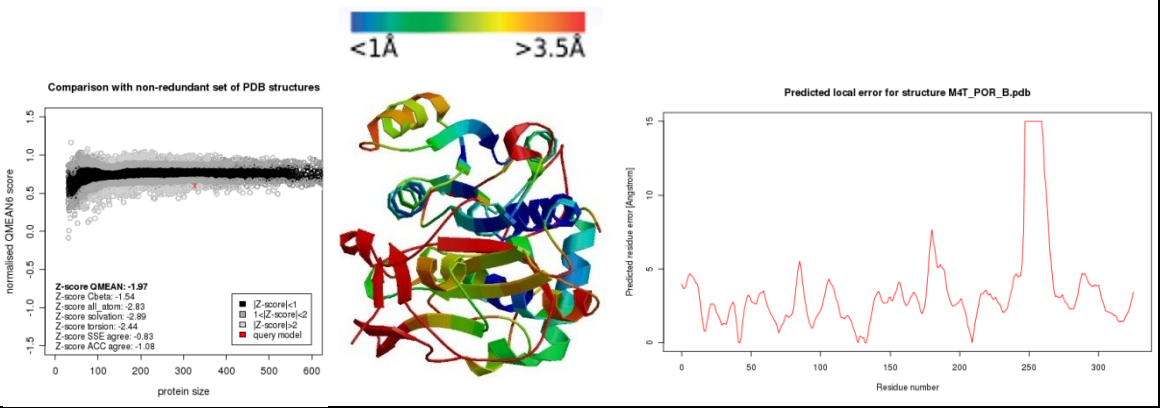

C **POR B WT | HHpredB QMEAN results**

Estimated absolute quality | Residue error - model | Residue error plot

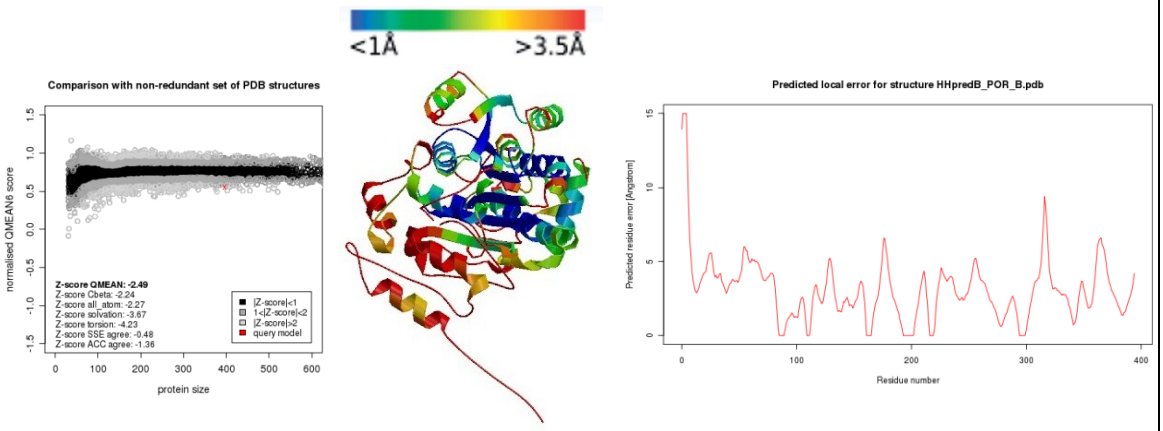

Thus, based on the good local quality prediction, the HHpred model is chosen as an adequate structural model for the POR B protein moiety and further used for the docking of the cofactor and substrate. The POR B model calculated by HHpredB service was processed with YASARA software. In Figure 3.8 A the 3D model of POR B is shown. The overall structural model exhibits the typical Rossmann fold structure with 7 parallel beta strands (in red) in the protein core surrounded by 6 alpha helices (in blue). Two central helix bundles form the outer wall of a cleft that can accommodate the substrate. An additional segment of

~30 amino acids unique to POR but not to other SDR enzymes is inserted as extra loop just before the conserved YxxxK motif, which corresponds to the substrate binding site. Taken these structural features the predicted POR B model is quite similar to previous models[45]

3.3.2 Docking of NADPH and PChlide in the catalytic pocket

For the docking of the NADPH cofactor and the PChlide substrate into the new POR B model structure the YASARA software was used, which allows the visualization of the 3-D model structure, the docking procedure and the energy minimization processes.

The docking of NADPH was performed as described in chapter 2.1.2. Figure 3.8 B shows the predicted POR B structure including the docked coenzyme NADPH. To judge whether the YASARA AutoDock software well approached the position of NADPH within POR B, the calculated structure of the POR B-NADPH complex was superimposed with the crystal structure of the enzyme porcine testicular carbonyl reductase. Porcine testicular carbonyl reductase also belongs to the class of SDR enzymes and its structure is available in the PDB data bank as co-crystal with bound NADPH.

The superposition (Figure 3.9) clearly shows that the core region of the two NADPH complexes agrees very well. This also applies to the arrangement of the bound NADPH in

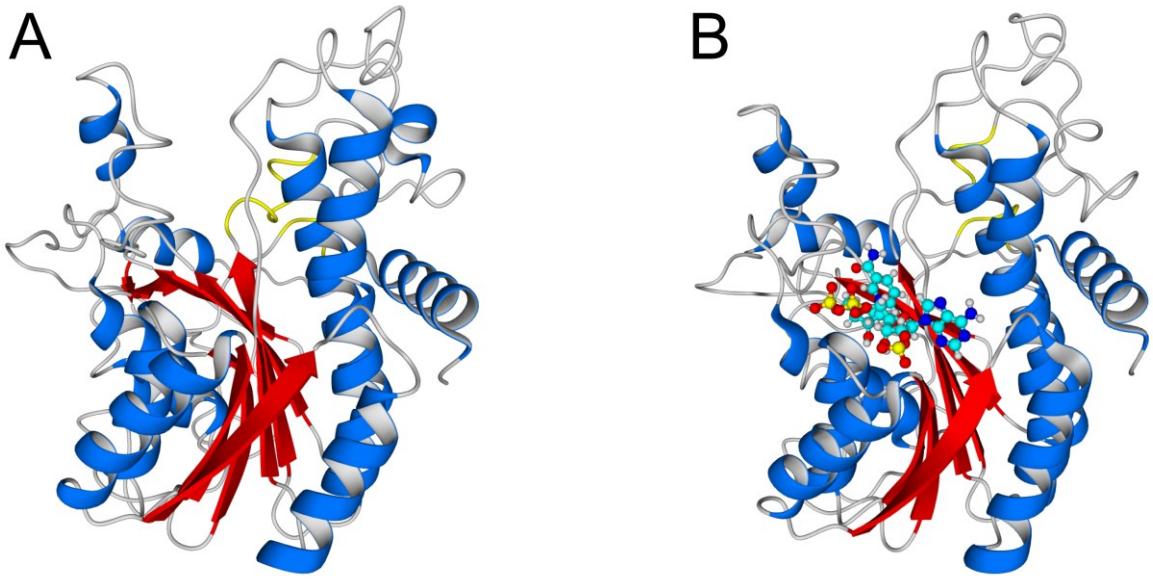

Figure 3.8: POR B 3-D model structure predicted by the HHpredB service. The typical Rossman fold with the characteristic twisted ß-sheets (red) in the centre flanked by α-helices (blue) can be seen. **(A)** Model of the apoprotein of POR B. **(B)** POR B model with NADPH docked into the 3-D structure.

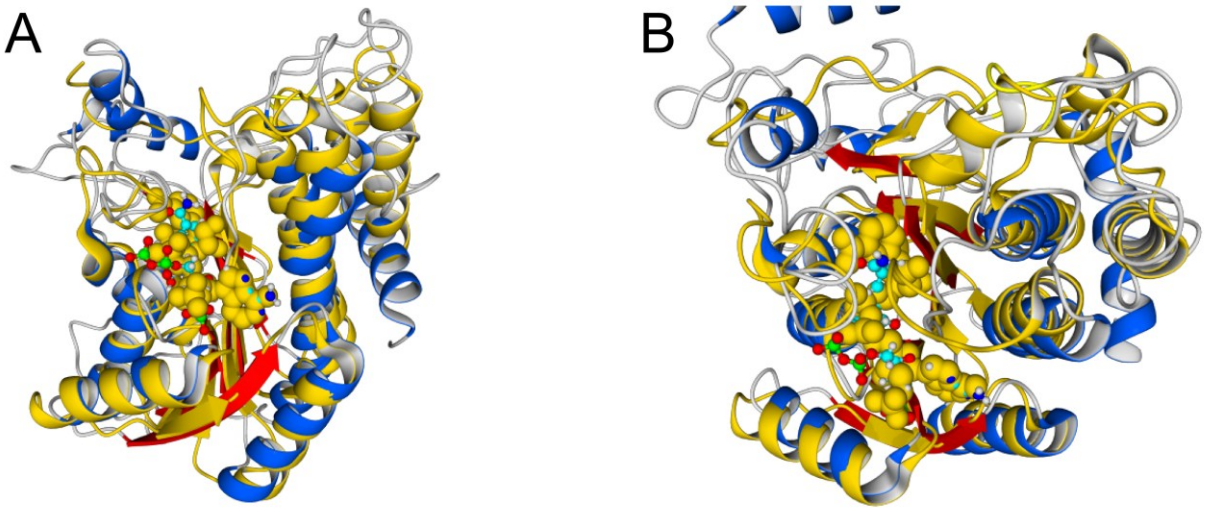

Figure 3.9: Superposition of the POR B-NADPH complex with the enzyme porcine testicular carbonyl reductase cocrystallized with NADPH. The POR B-NADPH complex is shown in blue (helices) and red (β-sheets), NADPH is laid-out in red, cyan and green balls. The porcine testicular carbonyl reductase complexed with NADPH is shown in yellow only. **(A)** front view. **(B)** top view.

the complex. As evident, the position of the docked NADPH in POR B highly matches the position of NADPH in the crystal structure of the porcine testicular carbonyl reductase. Thus, the AutoDock algorithm can be used for the reliable docking of the substrate, too.

The docking of the PChlide molecule into the active site provided several possible positions that fulfil the energetic and steric parameters given by the AutoDock algorithm and the force field used. Therefore, results, which did not match the following conditions, were discarded: (i) calculated position of PChlide in the center of the simulation cell; (ii) slight deformation of the protein structure; (iii) close proximity of the PChlide double bond at C(17)-C(18) to the nicotinamide ring of NADPH; (iv) low binding energy. In this way, two possible orientations of PChlide at the active site were found, which meet these requirements, the one with an binding energy of -27.3 $kJ \cdot mol^{-1}$, called "model 1" and the other one with a binding energy of –22.3 $kJ \cdot mol^{-1}$ called "model 2" from here on. With respect to the entire protein structure the localization of the PChlide substrate does not differ between the two models. Therefore, only the calculated structure of model 1 is presented in Figure 3.10. It can be seen that the docked NADPH and PChlide molecules are placed in the central part of the 3-D structure (Figure 3.10 A), where the typical Rossmann-fold generates a binding cleft for the accommodation of the cofactor and the substrate. Moreover it is apparent from the top view (Figure 3.10 B) that the nicotinamide ring of NADPH and the substrate are very close together, thus indicating the important role of the enzyme protein for the correct positioning

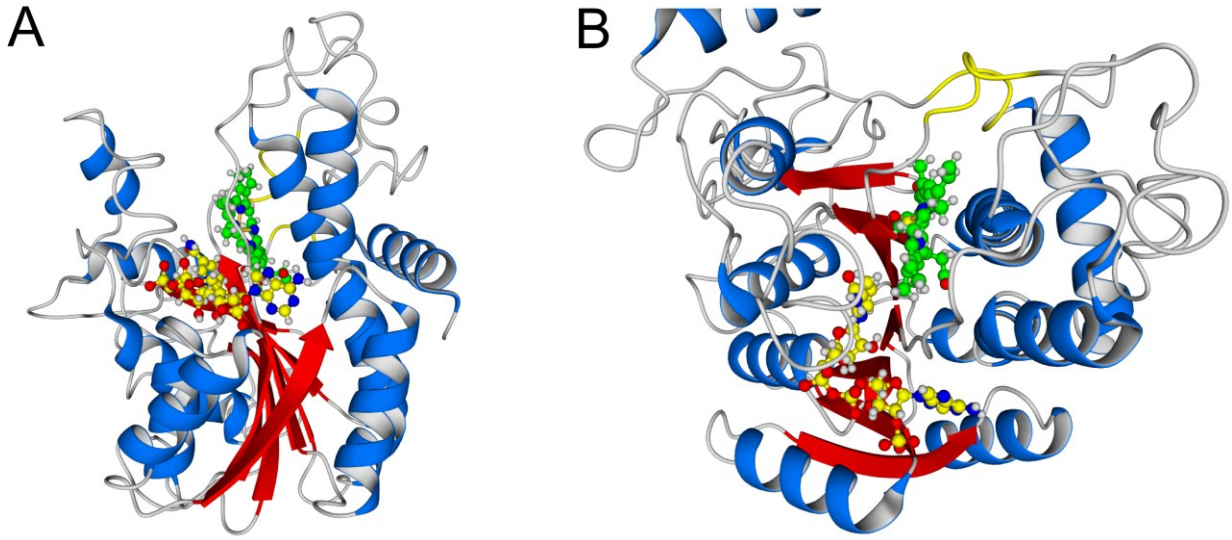

Figure 3.10: Predicted 3-D structure of the POR B ternary complex (model 1) obtained after the docking of PChlide and subsequent energy minimization. The coenzyme, NADPH, and the substrate, PChlide, are shown as balls and sticks. The carbons of NADPH are in yellow, the carbons of PChlide are in green; nitrogen atoms are in blue, oxygen atoms in red and hydrogen atoms in white. **(A)** front view. **(B)** top view.
of the substrate and cofactor at the active site.

3.3.3 Topology of the catalytic centre in POR B wild type

The prediction of the 3-D structure of POR B allows the identification of individual amino acid residues, which are in close proximity at the catalytic site to interact with PChlide and which, therefore, should play an important role in catalysis. In a second step, the potential role of these residues can be examined by introducing point mutations at the respective positions and studying their effect on the catalytic activity and reaction mechanism. Following this strategy, there is, however, a problem with the calculated 3-D structural model in so far as two models can be created. The two models do not differ with respect to the global position of PChlide in the homology model but they differ particularly with regard to the orientation of the PChlide molecule in the binding cleft.

In model 1, ring A and B of the porphyrin macrocycle (Figure 1.2 A) points towards the surface of the POR enzyme, whereas the propionic acid side chain at ring D and the isocyclic fifth ring are placed near to the bottom of the binding cleft (Figure 3.11). A closer inspection shows that PChlide is localized in between the α–helix including the YxxxK catalytic motif and the NADPH cofactor. Furthermore, the C(17)-C(18) double bond, which is reduced in the POR-catalysed reaction, is perfectly aligned between the active Tyr-212 and NADPH. In Figure 3.11 A the side chains of the five amino acids constituting together the

catalytic centre (YKDSK) are displayed. Both the catalytic Tyr-212 and Lys-216 are positioned towards the PChlide substrate, whereas Lys-213 appears to be slightly displaced from the active site Tyr-212 and Lys-216, but it still lies adjacent to PChlide. On the contrary, Asp-214 and Ser-215 are arranged at the back of the active helix and have neither contact sites to the cofactor nor to the substrate. Instead, they are involved in interactions with other protein sites within the 3-D structure.

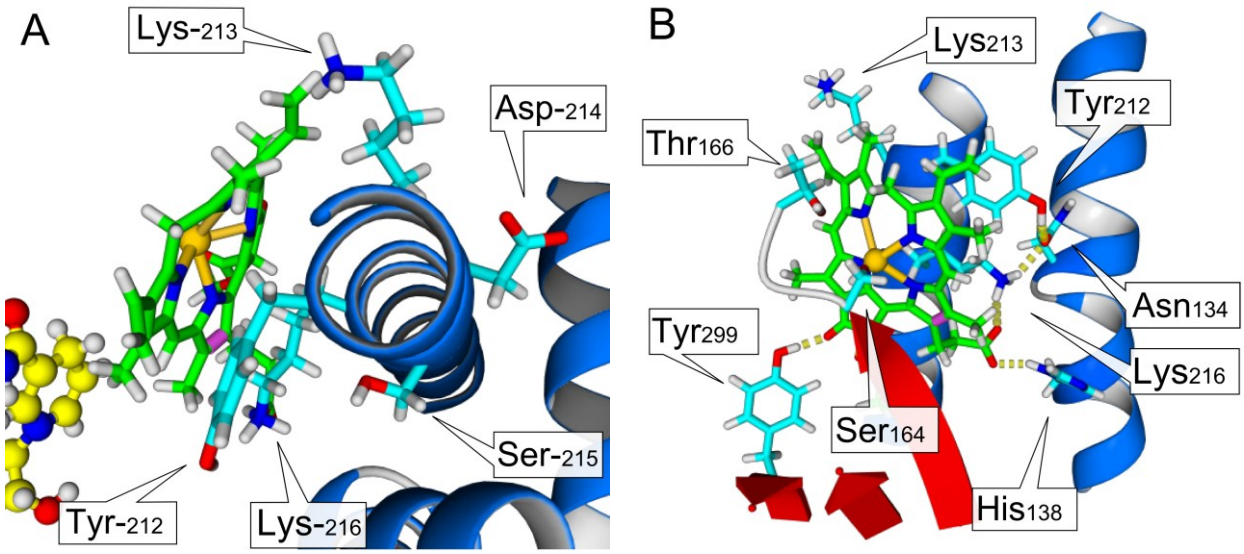

Figure 3.11: Close-up view of the catalytic site in the ternary POR B complex based on the calculations derived for "model 1". **(A)** Amino acids constituting the active site (top view). **(B)** Amino acids predicted to take part in the H-bond network (dashed yellow lines) between the POR B protein moiety and PChlide. The carbons of NADPH are in yellow, the carbons of PChlide are in green; nitrogen atoms are in blue, oxygen atoms in red and hydrogen atoms in white. The C(17)-C(18) double bond of PChlide, which is reduced in POR catalysis, is highlighted in violet.

Figure 3.11 B depicts that some of the amino acid side chains are located to each other in a hydrogen bonding distance. Thus, a network of hydrogen bonds can be built-up between Tyr-212, Asn-134 and Lys-216, whereas Lys-216 is also in hydrogen-bonding contact with the propionic acid side chain of PChlide at ring D. This side chain is additionally hydrogen-bonded by His-138. Even though the hydrogen bond, which emanates from Tyr-212 could be an artefact due to a remarkable steric repositioning of this Tyr during the energy minimization step, there remains the finding that the hydrogen bond network created between Asn-134, Lys-216, His-138 and the propionic acid side chain brings the active helix and the neighboured one in contact with each other and, in addition, is also important for the optimal positioning of PChlide. Another two structural features are of interest in model 1 (Figure 3.11.B). That is the formation of a hydrogen bond between Tyr-299 and the isocyclic

fifth ring at ring C on the one hand and on the other hand the position of Ser-164 near to the central Mg^{2+} of the PChlide molecule. Based on the spatial distance Ser-164 is perfectly placed to form a ligand to the Mg^{2+} ion of PChlide, which means, that a pentacoordinated magnesium complex is to be expected in the ternary POR B complex.

In model 2 (Figure 3.12) PChlide has rotated by 180° around an imaginary axis that goes through the C(10) – C(20) methine (methylylidene) bridges (Figure 1.2 A). In this

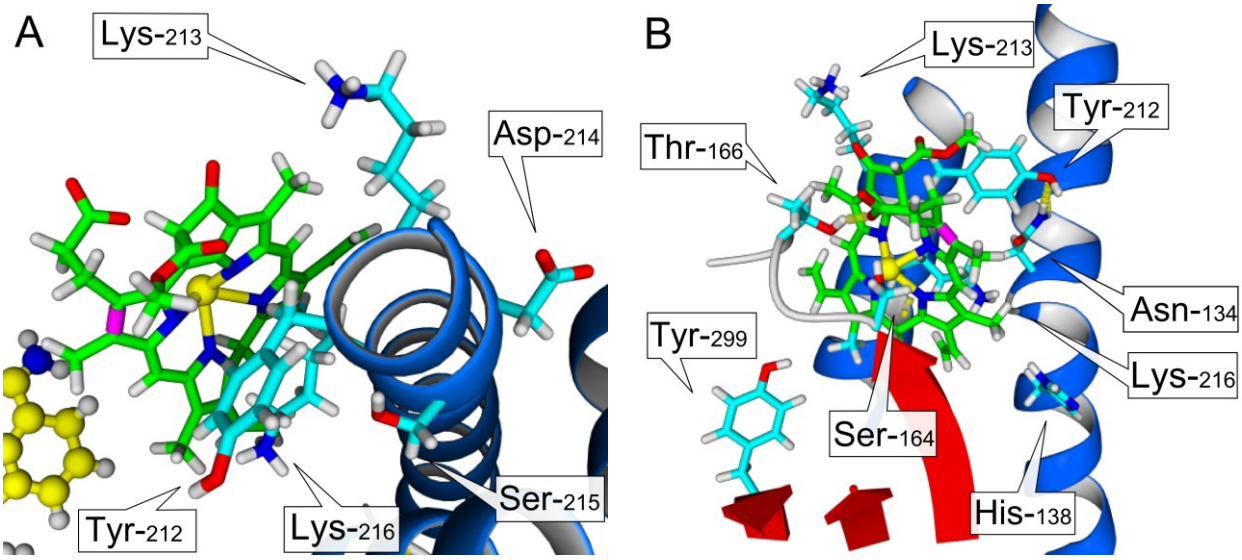

Figure 3.12: Close-up view of the catalytic site in the ternary POR B complex based on the calculations derived for model 2. **(A)** Amino acids constituting the active site (top view). **(B)** Amino acids predicted to take part in H-bonding interactions (dashed yellow lines) between the POR B protein moiety and PChlide. The carbons of NADPH are in yellow, the carbons of PChlide are in green; nitrogen atoms are in blue, oxygen atoms in red and hydrogen atoms in white. The C(17)-C(18) double bond of PChlide, which is reduced in POR catalysis, is highlighted in violet.

model the double bond also remains in proximity (4.4 Å) to the NADPH cofactor but the propionic acid side chain and the isocyclic fifth ring are exposed to the protein surface, whereas the more hydrophobic part of the PChlide structure is orientated towards the bottom of the substrate binding cleft (Figure 3.12).

Due to the rotation around the C(10) – C(20) axis Ser-164, Asn-138 and Try-212 keep the same orientation to PChlide as calculated for model 1. However, the propionic acid side chain can potentially form a hydrogen bond with Thr-166, while Lys-213 as component of the catalytic centre is orientated towards the isocyclic fifth ring, suggesting that an interaction between the C(13')=O carbonyl group and the ε-amino group of the lysine side chain might exist. Tyr-299, Lys-216 and His-138 remain in close proximity to the PChlide substrate in this conformation as well but the ability to form a hydrogen network as in model 1 has been lost.

Even though the two models appear to have their own legitimacy on the basis of the goodness-of-fit-criteria used, several reasons are in favour of model 1 as the best candidate for representing the adequate 3-D structure of the ternary POR B complex. (i) The study of chemically modified substrate analogues of PChlide provides strong evidence that rings C, D and E are deeply buried in the substrate binding pocket[29,104]. It is highly unlikely that in particular ring D with the propionic acid side chain protrudes from the POR surface as predicted for model 2. In contrast to the situation at rings C, D and E, rings A and B should most probably stick out of the of the active center and make no essential contact with the POR protein sites, which is again in accordance with model 1. (ii) Model 1 calculates a lower free energy of the POR B structure with -27.3 $kJ \cdot mol^{-1}$ as compared to –22.3 $kJ \cdot mol^{-1}$ for the structure in model 2; (iii) With respect to the orientation of the PChlide rings C, D and E in the substrate binding pocket, model 1 is in agreement with POR structures that have been recently predicted for enzymes from cyanobacteria and *Arabidopsis*[7,43,72,105] by using both manually-guided and *in silico* docking algorithms; (iv) Model 1 predicts an effective hydrogen bonding network between Asn-134, Lys-216, His-138 and PChlide that highlights the importance of the correct alignment of PChlide in the active site. (v) Model 1 clearly shows the interaction between the C(13')=O carbonyl group at ring E of PChlide and Tyr-299 via hydrogen bonding. Such an interaction, which facilitates the formation of an enolate structure at ring E, has already long been supposed[104] and considered as structural feature that could allow the formation of the intramolecular charge transfer state, S_{ICT}, that in turn creates a polarized and highly reactive C(17)-C(18) double bond.[26]

3.4 Site-directed mutagenesis of POR A and POR B wild type

3.4.1 Concept of site-directed mutagenesis

The site-directed mutagenesis experiments pursued two objectives: (i) the calculated 3-D model structure of POR B predicting in particular the active site architecture should be verified by an appropriate choice of amino acid substitutions; (ii) for the two plant POR A and POR B isoenzymes the role of all of the active site residues within the YK_1DSK_2 motif should be understood in more detail with respect to their mutual impact on substrate binding and the reaction mechanism/dynamics. Previous studies mainly focussed on the catalytically active Tyr (Y) as proton donator and the closely enough positioned Lys (K_2),

which is suggested to lower the pKa of the Tyr-OH group[7,90]. Moreover, the majority of studies include POR enzymes from cyanobacteria[43,72,84,87,90], which have established light-dependent chlorophyll biosynthesis at an evolutionary much earlier stage.

As usual for site-directed mutagenesis studies variants of the wild-type POR A and POR B enzymes were created by substituting a definite amino acid by another one with opposite properties that contradict the supposed hypothesis. In parallel, variants were generated that confirm the hypothesis in that the lost function was restored by the exchange of the wild-type amino acid with one of similar properties.

Thus, to validate the new structural model of POR B, amino acid residues, which can potentially interact with the PChlide substrate or are in close proximity to the PChlide binding site were altered by site-directed mutagenesis. They include Ser-164, His-138,Lys-216 and Tyr-299 (see Figure 3.11 B). Ser-164 is presumed to facilitate a coordinative bond to the central magnesium of the porphyrin structure, which led to the substitution of Ser by Ala and Thr. In this context it is worth mentioning that the position of Ser-164 is *a priori* occupied by Thr in the cyanobacterial POR enzymes (Figure 3.13). His-138 appears to be in contact via electrostatic interactions with the positively charged propionic acid side chain attached at ring C. Therefore, His-138 was replaced by Phe and Tyr. Lys-216 that turns out to be part of a hydrogen bonding network was exchanged by Arg and Gln. Because Lys-216 is part of the POR active site, the mutations at this position are also presented further in this chapter, in respect to the proposed function in the catalysis. Furthermore, Tyr-299, which, on the basis of the model, is proposed to participate in hydrogen bonding to the C(13')=O group at the isocyclic fifth ring, was exchanged by Phe and His. For a brief overview, the individual point mutations introduced are summarized in Table 3.4.

The key amino acids at the active site are formed by the YxxxK motif. The full sequence of this motif is YK_1DSK_2 (Figure 3.13) indicating a highly polar character of the active site. Across the POR A and POR B enzymes from barley as well as the enzymes from *Synechocystis*[106] and *Thermosynechococcus*[43] *(*Figure 3.13) the active site is highly conserved. To study the concerted role of all active site residues in the catalytic mechanism a series of mutated variants were constructed for both POR A and POR B. Because of the high homology between the POR A and POR B wild-type sequences (see below) it can be assumed that the active site architecture of POR A is very similar to that predicted for POR B. Therefore, analogous substitutions were introduced both into POR A and POR B. In this

Table 3.4: Summary of the individual point mutations introduced into the POR A and POR B wild-type enzymes. The effect of the amino acid exchange is briefly described.

	mutation		features of the substitution	code
POR B				
3D model validation	Ser164	Ala	loss of the coordinative bond to Mg^{2+}	S164A
		Thr	restoring the coordination with Mg^{2+}	S164T
	His 138	Phe	disruption of the electrostatic/hydrogen-bonding interaction to the propionic acid side chain	H138F
		Tyr	maintaining of the H-bonding and polar feature of the substituted amino acid	H138Y
	Lys216	Gln	loss of the positively charged side chain but maintenance of the polar, hydrogen bonding property	K216Q
		Arg	maintaining of the polar, positively charged side chain, keeping-up of the H-bonding property	K216R
	Tyr-299	Phe	disruption of the H-bond to C(13')=O	Y299F
		His	maintaining of the interaction to C(13')=O via H-bonding	Y299H
Active site investigation	Tyr212	Phe	impairment of the H^+-transfer	Y212F
		His	keeping-up the H^+-transfer	Y212H
	Lys213	Gln	loss of a positive charge	K213Q
		Arg	restoration of a positive charge	K213R
	Asp214	Met	impairment of the H-bonding	D214M
		Ala	impairment of the H-bonding	D214A
		Glu	maintenance of the H-bonding activity and keeping-up the negative charge at the side chain	D214E
		Asn	maintenance of the H-bonding activity by a polar, uncharged amino acid side chain	D214N
	Ser215	Gly	impairment of the H-bonding	S215G
		Ala	impairment of the H-bonding	S215A
		Thr	maintaining of the H-bonding	S215T
	Lys216	Arg	restoring of cation-π-electron interactions	K216R
		Gln	loss of cation-π-electron interactions	K216Q

	mutation		code
POR A			
Active site investigation	Tyr215	Phe	Y215F
		His	Y215H
	Lys216	Gln	K216Q
		Arg	K216R
	Asp217	Ala	D217A
		Glu	D217E
		Asn	D217N
	Ser218	Gly	S218G
		Ala	S218A
		Thr	S218T
	Lys217	Arg	K219R
		Gln	K219Q

way it has also been hoped to identify the active site amino acids, which are responsible for the differences in the catalytic efficiency of POR A and POR B (see Chapter 3.2).

Based on the function ascribed to the catalytically essential Tyr as H^+ donator, Tyr-212 of POR A and Tyr-215 of POB B, respectively, were substituted by Phe (Y215F, Y212F). Phe lacks the phenolic –OH group but is otherwise structurally similar to Tyr. In addition, Tyr was replaced by His (H215H, Y212H), which, analogous to Tyr, has also a deprotonable side chain. Hence, the Tyr → His exchange is expected to restore the POR activity.

Because the central residues within the YK_1DSK_2 motif, i.e. another Lys, Asp and Ser, have polar and, in part, positively or negatively charged side chains, they were replaced by residues, which uphold the polarity while the charge is maintained/lost and, thereby also have an impact on the hydrogen bonding pattern. Accordingly, Lys-216 in POR A and the corresponding Lys-213 in POR B were exchanged with Arg and Gln (K216R/Q, K213R/Q). The two mutant forms retain the polar properties and with respect to the Arg substitution also the positive charge. Asp-217 in POR A and Asp-214 in POR B were substituted by Ala (D217A, D214A) and Met in case of POR B (D214M), it was expected to gain insight into the role of steric effects at this active site position. In addition Asp→Asn and Asp→Glu mutant forms (D217N/E, D214N/E) were produced. Whereas the two substitutions conserve again the polar properties, the replacement by Glu also maintains the negative charge.

The Ser in the YK_1DSK_2 motif was changed by either Gly, Ala or Thr (S218G/A/T in case of POR A and S215G/A/T in case of POR B) with Thr keeping up the polar character but differing from Ser by a secondary –OH group.

Finally, the Lys, that is essential for catalysis because of its capability to reduce the pK_a of the Tyr-OH group, corresponds to Lys-219 and Lys-216 in POR A and POR B, respectively. Due the supposed function, this Lys was substituted with Gln (K219Q, K216Q) and Arg (K219R, K216R). Lys→Arg mutants should retain the catalytic activity for the following reason. Cation-π-electron interactions, which can be made responsible for the reduction in the pKa value of the Tyr-OH group, are still possible with Arg instead of Lys. On the contrary the Lys→Gln replacement excludes cation-π-electron interactions with the result that the respective mutants should lose the catalytic activity.

For a brief summary, the point mutations, which were constructed to modify the active site residues, are listed in Table 3.4. Further, Figure 3.13 shows the sequence alignment and

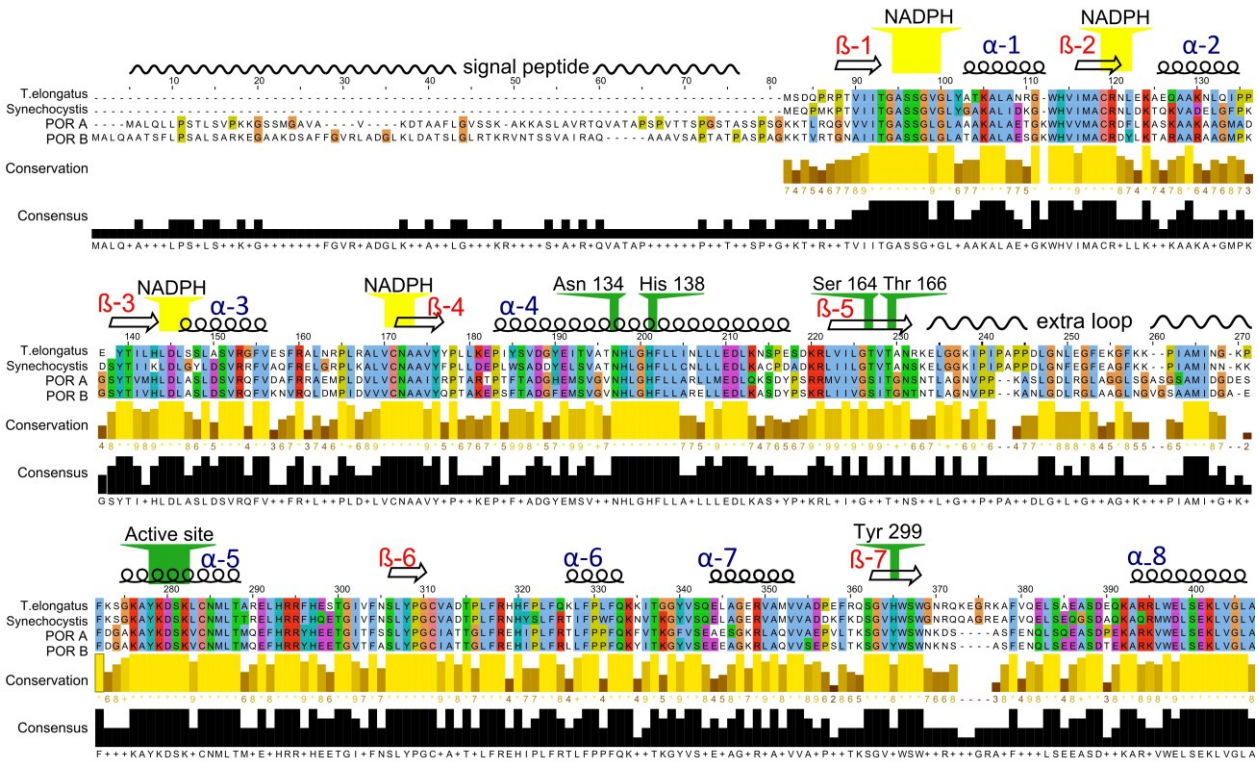

Figure 3.13: Sequence alignment and conservation pattern among the POR A and POR B isoenzymes from barley (Hordeum vulgare L.) and the cyanobacterial enzymes from *Thermosynechococcus elongatus* and *Synechocystis* sp. PCC 6803. The amino acid sequence of POR B from barley is aligned with the sequences of the other 3 POR enzymes. Numbering refers to the full length POR A and POR B sequences containing the transit peptide necessary for plastid import. The secondary structure indicated in the first raw also refers to the predicted model structure of POR B. The conservation grade is given by yellow bars of different intensity and the consensus sequence by black bars. The NADPH and PChlide binding sites are pointed out in the corresponding sequences region. The amino acids that were replaced in the mutational study are indicated by green arrows.

conservation pattern of the two POR B and POR A isoenzymes together with labels, which indicate all amino acids that were selected for site-directed mutagenesis within the scope of this work. The alignment includes two POR enzymes from cyanobacteria, namely *Synechocystis* sp. and *Thermosynechococcus elongates*, too. The reason for this is that the discussion of the results obtained from the mutation study refers to these two POR enzymes because cyanobacteria are considered as evolutionary ancestors of all organisms that conduct light-dependent chlorophyll synthesis. In consequence their POR enzymes are suggested to represent the evolutionary ancestral form of the plant enzymes[36]. As can be seen in Figure 3.13 the four POR enzymes show remarkably conserved amino acid conservation. More than 50% identical residues are shared among the four enzymes. As also evident, the highly conserved sequence regions are to be found in domains with characteristic secondary

structural features. More variable parts of the sequence exist in the loop or β-turn regions, which connect the α-helices and β-sheet structures including the so-called extra-loop between the β-5 sheet and α-5 helix as well. Consistent with the function, the greatest amount of variation is located in the N-terminal region of the POR A and POR B enzymes, which contains the sequence of the transit peptide necessary for plastid import. The alignment clearly shows that the ternary structure brings in close proximities residues which are extremely distanced and they could be hardly pointed out only by looking at the primary sequences.

3.4.2 Experimental design for the study of the mutant forms

As described in more detail in Materials and Methods (2.4.2) the site-directed mutant forms were generated by an *in vitro* mutagenesis approach using the Qickchange™ mutagenesis kit. To control the transformation of the mutated POR genes into competent *E. coli* cells a PCR reaction was carried out. The length of the amplified DNA fragments was checked by gel electrophoresis in agarose gels (Figure 3.14 A) and the appearance of a DNA band at ~600 pb was used as evidence for the successful transformation process. To further confirm the presence of the correct codon substitution and to exclude other alterations all mutated DNAs were subjected to DNA sequencing. The correctly mutated DNA variants were then overexpressed in *E. coli* and the enzymes purified as described in (chapter 2.6).

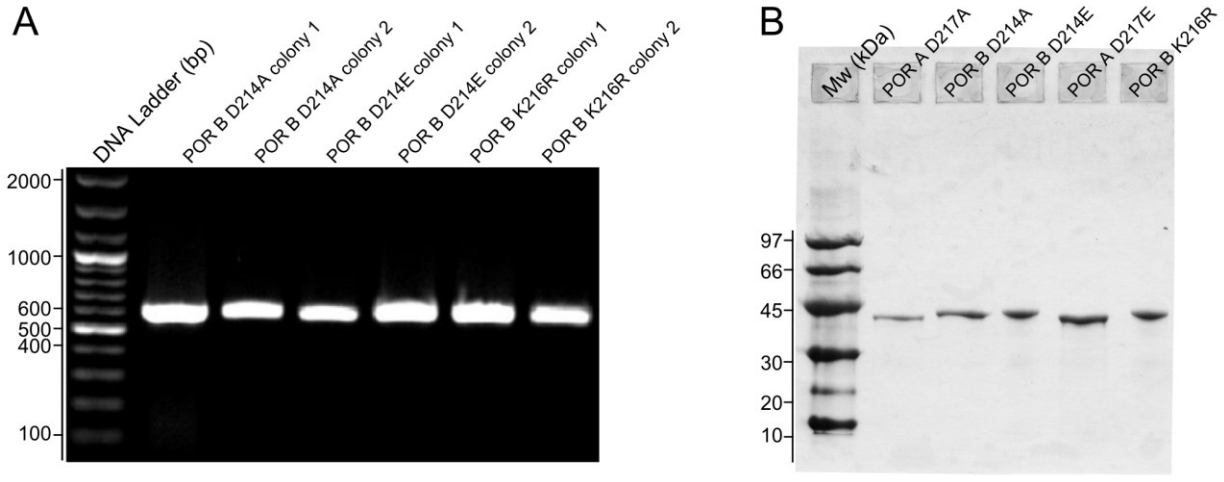

Figure 3.14 : Representative electropherograms of colony PCR products and finally purified POR enzyme variants. **(A)** Electropherogram of amplified POR genes representing 3 different point mutations in POR B as example. The figure is modified according to N. Archipowa master thesis [112]. **(B)** Electropherogram of purified POR A and B mutant forms. The point mutations for D217A and D217E in POR A and D214A, D214E and K216R in POR B are shown as examples.

The purity of the mutated enzyme proteins was verified by a final SDS gel electrophoresis. Based on the sensitivity of the staining with Coomassie Brilliant Blue R-250 the variant enzymes were ~95% pure and migrated as a single well separated band in the SDS PAGE (Figure 3.14 B).

For the analysis of the POR mutants and their effect on enzyme catalysis, first, the catalytic activity was evaluated from the steady state kinetics as relative activity at room temperature. Details of this procedure are given in Materials and Methods under 2.7.3. Second, for a more detailed evaluation of the mutation, the POR reaction cycle was inspected by trapping transient reaction intermediates at low temperatures as described under 2.7.4. Finally, the effect on the primary photochemistry was addressed by determining the lifetime of the S_1-excited state in the variant ternary complexes at cryogenic temperature, to avoid the progress of the reaction, as pointed out in chapter 2.7.7.

3.4.3 Point mutations in POR B for the validation of the active site architecture in the 3-D model structure

Table 3.5 shows the relative activity of the POR B mutant forms created with the aim to support the predicted active site structure in POR B. Table 3.5 also includes the turn over numbers, k_{cat}, in cases where the remaining activity made the determination possible. As can be seen the POR activity is fully inhibited in the His-138 and Lys-216 variants. This result is in accordance with the POR B model structure that indicates interactions between these two polar, positively charged amino acid side chains and the carboxyl group of the propionic acid attached at ring C of the PChlide macrocycle (Figure 3.11 B). In addition, the POR B activity is also nearly abolished in the S164A mutant, which only retains 1% of the wild type activity. On the contrary, the S164T substitution leads to a restoration of the POR mutant activity up to 95%, obviously due to the –OH side chain in Thr. Thus, the S164A/T POR B variants suggest that S164 is important for interaction with PChlide, most likely, as predicted by the structural model via a coordinative bond to the central Mg^{2+} (Figure 3.11 B). Also the Tyr-299 mutants affect the enzyme activity retaining 52% (Y299F) and 16% (Y299H) of the wild type activity. Even though the enzyme activity is not fully blocked it appears that also Tyr-299 has a major role in POR catalysis, which, in all probability, is mediated by the predicted hydrogen bonding interaction between the Tyr-OH and the isocyclic fifth ring in

	Code	v_0 ($\mu M \cdot min^{-1}$)	k_{cat} (s^{-1})	A_{rel} (%)
POR B				
validation of the 3-D model	**WT**	3.82	$1.2 \cdot 10^{-2}$	**100**
	S164A	0.03	-	**1**
	S164T	3.66	$9.2 \cdot 10^{-3}$	**95**
	H138F	-	-	-
	H138Y	-	-	-
	K216Q	-	-	-
	K216R	-	-	-
	Y299F	2.00	$4.0 \cdot 10^{-3}$	**52**
	Y299H	0.64	$2.7 \cdot 10^{-3}$	**16**

Table 3.5: Initial velocity (v_0), turnover number (k_{cat}) and relative activity (A_{rel}) for wild type (WT) and mutant forms of POR B determined under steady-state conditions at room temperature. The POR activity was triggered by excitation at 633 nm (λ_{exc} = 633 nm) using 10 µM wild type/ mutant POR B in the presence of 7 µM PChlide and 100 µM NADPH in measuring buffer. For the determination of k_{cat}, PChlide concentrations at substrate saturation (20 µM) were added.

the PChlide structure (Figure 3.17 B). In all mutant forms listed in Table 3.5 the loss in activity correlates well with the loss in the turnover numbers as far as a reliable determination of these values was allowed.

With respect to the photochemistry in the mutant forms, Figures 3.15 shows the absorption spectra of reaction intermediates, which could be trapped at low temperatures, and Figure 3.16 the fluorescence spectra and fluorescence decay traces observed at 150 K. As can be taken from the low temperature absorption spectra, the S164A mutant generates the S_{640} species. S_{640} is also observed in wild type POR B (Chapter 3.2.2) as first species immediately after freezing at 180 K but before the onset of irradiation. It is shown to represent the red-shifted absorbance of enzyme-bound PChlide in the ternary photoactive POR complex. However, for the S164A mutant form the S_{640} absorption band clearly reveals a significant shoulder at the blue side near to 630 nm, suggesting the presence of unbound PChlide, too (Figure 3.15 A) Following irradiation only the intermediates A_{677} and A_{672} can be detected (Figure 3.15 B). The A_{672} band has a very low intensity and the absorption is in part overridden by the main Q-band of the PChlide absorption, which is why the A_{672} intermediate is only represented by a small shoulder at around 672 nm. Based on the EFA analysis, A_{672} is generated at evidently higher temperatures (270 K) than in the wild type POR B.

In full agreement with the S_{640} absorbance spectrum, also the fluorescence spectrum at 150 K indicates a red-shifted fluorescence arising from enzyme-bound PChlide, and, in

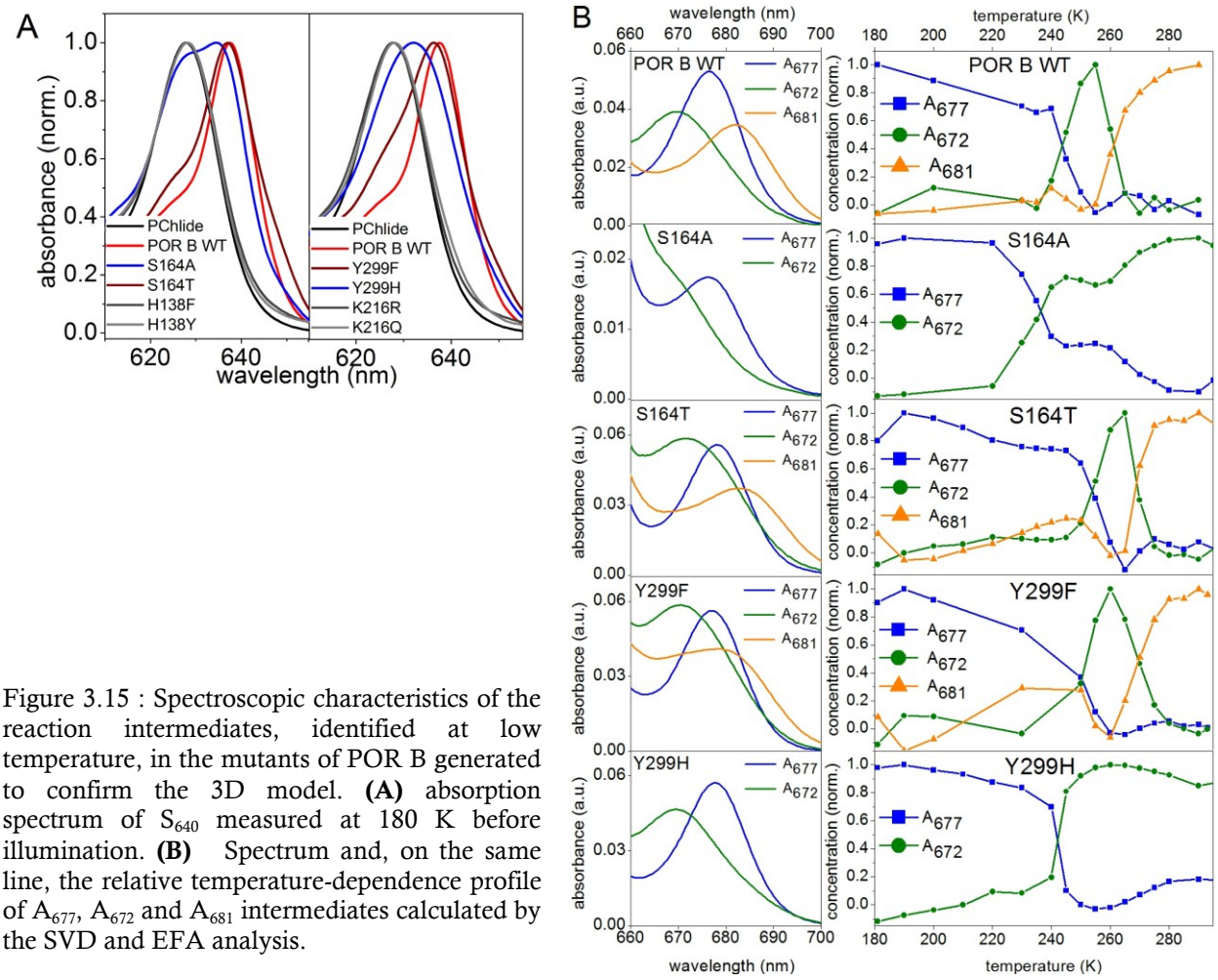

Figure 3.15 : Spectroscopic characteristics of the reaction intermediates, identified at low temperature, in the mutants of POR B generated to confirm the 3D model. **(A)** absorption spectrum of S_{640} measured at 180 K before illumination. **(B)** Spectrum and, on the same line, the relative temperature-dependence profile of A_{677}, A_{672} and A_{681} intermediates calculated by the SVD and EFA analysis.

addition, a shoulder at the blue edge (Figure 3.16 A). A global fit to the temporal evolution of the spectrally integrated fluorescence requires two exponential components (see supplement, Table 7.1), from which, in analogy to the wild type POR B, only the longer-lived component is taken into account in the following considerations. For the S164A mutant the fluorescence lifetime thus obtained is $\tau_{2\ S164A}$ = 6.4 ns. To check furthermore whether the fluorescence decay represents a combination of two different PChlide species, i.e. unbound and enzyme-bound PChlide, the emission was dissected into two spectral regions, the one extending over the blue wing from 610 to 630 nm and the other one extending over the red wing from 633 to 650 nm of the emission spectrum. As consequence two fluorescence components were resolved with $\tau_{2\ S164A\ blue}$ = 5.9 ns for the blue spectral region and $\tau_{2\ S164A\ red}$ = 6.5 ns for the red spectral region. In Figure 3.16 these decay times are compared with the values obtained for free PChlide in buffer, for the wild type POR-PChlide complex as well as the ternary POR-PChlide-NADPH complex. As can be clearly seen, the

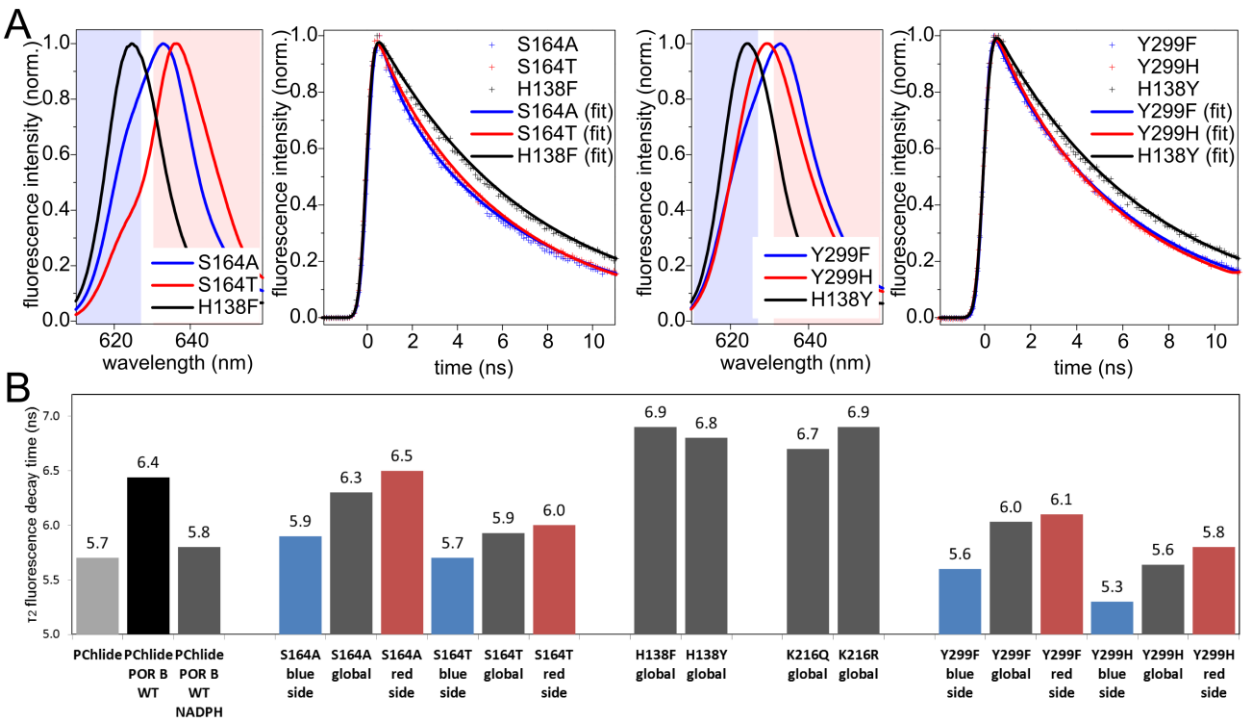

Figure 3.16: Low temperature fluorescence spectra and fluorescence decay traces of wild type POR B in comparison with mutant POR B forms. The mutant POR B forms include the variants that support the predicted POR B model structure. **(A)** Fluorescence spectra and decay traces recorded at 150 K. The shadowed areas in the fluorescence spectra indicate the spectral regions that were included in the data analysis of the blue (610-630 nm) and red wings (633-650 nm) of the fluorescence bands. **(B)** Fluorescence decay times estimated by a global fit procedure using the integrated fluorescence over the whole emission region (black/grey columns) and the emission regions separated into the blue (blue columns) and red spectral region (red columns) of the fluorescence band.

5.9 ns lifetime corresponds to the 5.7-ns decay time of free, unbound PChlide very well, also with respect to the spectral position of the evaluated fluorescence region. Therefore it is very likely that 5.9 ns lifetime in the S164A variant is related to the unbound PChlide fraction. Further, the 6.5 ns decay of the S164A mutant matches the 6.4 ns decay of the wild type POR-PChlide complex, but in contrast to the latter complex the emission is red-shifted in the mutant. Taking this red-shift, actually a shortened decay time is to be expected according to the energy gap law (see chapter 3.2.3), which, however, is not compatible with the experimentally measured decay time. Nonetheless, the longer 6.5 ns fluorescence decay can be well understood when the branched reaction model is considered, which is derived for the excited-state reactions in the POR B wild type (Chapter 3.2.3). Based on this model the direct depopulation of the S_1-excited state molecules along the reactive path becomes possible given the decrease in the relative energy of the S_X and S_{ICT} state. Hence, a very likely reason for the increase in the fluorescence decay time of the mutant as compared to the wild type is a strongly reduced probability for the depopulation of the S_1-excited state along the

reactive path. Finally, this means that the photochemistry is impaired by the replacement of Ser164 with Ala, obviously due to the loss of the coordinative bond to the central Mg^{2+}, which seems to stabilize the substrate within the ternary POR B complex.

Unlike the S164A mutant, the S164T mutations restore nearly completely the wild-type level of POR activity, which is also mirrored in the photochemistry. The S_{640} species reveals about the same spectral characteristics as the wild type form including the formation of all three reaction intermediates, A_{677}, A_{672}, and A_{681}, which, in addition, appear and go over into the next intermediate form with a very similar temperature profile as the wild type POR B (Figure 3.15). The fluorescence spectrum and the fluorescence decay time of the S164T mutant, both detected at 150 K, also show strong parallels to the wild type enzyme. Thus, there is only a very small edge at the blue flank of the emission spectrum suggesting the presence of only a small fraction of unbound PChlide with $\tau_{2\ S164T\ blue}$ = 5.7 ns while the red-shifted main peak reflects the correctly bound and positioned PChlide in the active site with a fluorescence decay time of $\tau_{2\ S164T\ red}$ = 6.0 ns. Even if this decay time is slightly lengthened as compared to the wild type value of τ_2 = 5.8 ns it exhibits the general features ascribed to the catalytically active PChlide in the wild type enzyme.

In the H138F and H138Y mutants the enzymatic activity is completely eradicated. Accordingly, the S_{640} species indicating enzyme-bound PChlide cannot be observed in the low temperature absorbance spectra. Rather, the absorption spectrum of the two mutants corresponds to that of unbound PChlide (Figure 3.15 A). In consequence, no reaction intermediates are to be trapped at low temperatures. The decay times determined from the temporal evolution of the spectrally integrated fluorescence between 610 and 650 nm was estimated to be τ_2= 6.9 ns and τ_2=6.8 ns, respectively, for the H138F and H138Y mutants (Figure 3.16). For the reason of (i) the comparatively long fluorescence decay times as compared to unbound PChlide and (ii) the absence of either a red shifted absorbance or fluorescence indicative of correct PChlide binding in the wild-type enzyme, the two fluorescence components are associated with PChlide fractions that are unspecifically bound in the substrate binding cleft and not arranged in an optimal geometry that is absolutely necessary for enzyme catalysis.

Similar results as in case of the H138F and H138Y mutants were obtained when Lys-216 is replaced by glutamine and arginine, respectively. Both the K216Q and K216R mutant form show a lack of any enzyme activity, the absence of any red shift in the low temperature

absorption (Figure 3.15 A) and fluorescence spectrum (Figure 3.16) and similar increased fluorescence decay times with values of τ_2= 6.7 ns and τ_2=6.9 ns for K216Q and K216R, respectively. This result supports the notion that Lys-216 provides key interactions with the carboxyl group of the propionic acid side chain in analogy to the predicted active site structure.

Mutations of Tyr-299 by replacing Tyr through Phe and His led to variants which only show a partial reduction in activity compared with the wild-type enzyme. There is a close correspondence between the reduced activity and the spectra of the S_{640} species at 180 K. For the Y299F mutant the S_{640} spectrum exhibits a nearly complete red shift and analogous reaction intermediates, which occur in the wild type enzyme, are also found for Y299F variant (Figure 3.15 A). The only slight differences compared with the wild type exist in the transformation of the intermediates $A_{672} \rightarrow A_{681}$, which takes place at a higher temperature

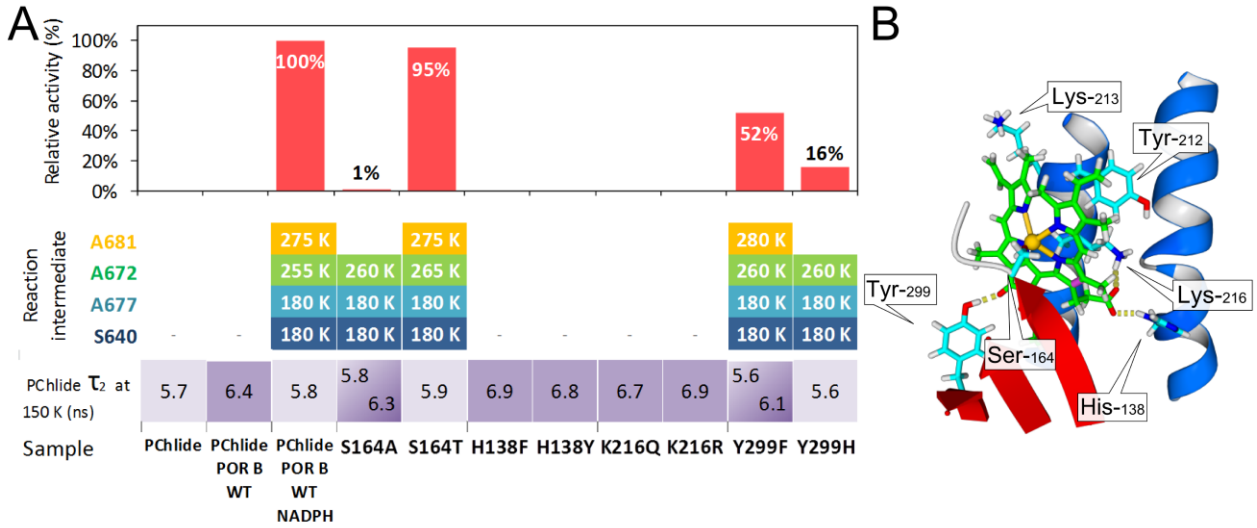

Figure 3.17: Summary of all the mutants generated and analysed to validate the proposed 3D model. **(A)** measurements carried out on the mutants and wild type (given as reference) of POR B, which includes: relative activity at room temperature (%); name and temperature at which the reaction intermediates were found in the low temperature absorption spectroscopy; fluorescence lifetimes (τ_2) of PChlide measured at 150 K in different ternary complexes. When two decay times are reported, they represent the value of fitting of the blue side (top left) and the red side (bottom right) of the emission band. **(B)** Graphical representation of the 3D model 1; PChlide's carbons are in green and the catalytic Tyr-212 and Lys-213 are also shown (carbons are cyan, oxygen red and hydrogen white.

(270 K), and in the absorption of the A_{681} intermediate, which is obviously composed of contributions from both A_{672} and A_{681} (Figure 3.15 B). The analysis of the fluorescence decay at the blue and red edge of the emission band yielded decay constants of $\tau_{2\ Y299F\ blue}$ = 5.6 ns and $\tau_{2\ Y299F\ red}$ = 6.1 ns, respectively. The 5.6 ns decay time is to be ascribed to contributions from free, unbound PChlide, whereas the 6.1 ns-decay time reveals that the flow of the S_1-

excited state population into the reactive path is scarcely restricted as compared to the wild type, resulting in only a slight increase in this decay time. The Y299H mutant form, instead, shows only a very small fraction of bound PChlide in the absorption spectrum of the S_{640} species (Figure 3.15 A). Following actinic irradiation, only the A_{677} and the subsequent A_{672} intermediates were to be detected at 240 K. Even at higher temperatures no further intermediates have been produced (Figure 3.15 B). The fit to the fluorescence decay curve resulted in decay times of $\tau_{2\ Y299F\ blue}$ = 5.3 ns for the analysis of the blue and $\tau_{2\ Y299F\ red}$ = 5.8 ns, for the red side of the fluorescence band (Figure 3.16. B). Thus, most of the PChlide remains unbound in this mutant but that small fraction, that is bound, is subjected to the wild type photochemistry. Hence, both the Y299F and Y299H mutants suggest that Tyr-299 is mainly involved in the correct binding of PChlide and is of minor importance for the photoreduction of PChlide. The low enzyme activity of the Y299H variant thereby likely reflects the loss of interactions via the predicted hydrogen bond due to steric reasons and/or the formation of fake hydrogen bonds exerted by the imidazole group of His.

Figure 3.17 represents a summary for the effect of all POR B mutants, discussed above, on the enzymatic activity, the reaction mechanism and the photochemistry assessed by the fluorescence decay times of the ternary enzyme complexes.

3.4.4 Amino acid substitutions in the active center of POR A and POR B and their implications for the catalytic mechanism.

Table 3.6 reports the relative activity of the mutation on the catalytic Tyr showing a remaining activity of 1% and 2.5% for POR A Y215F and POR B Y212F, respectively. This provides the evidence that in absence of the Tyr hydroxyl group, the catalysis is drastically affected but it can still be performed with a very low efficiency. The Tyr → Phe mutants (in POR A and B) showed no difference with the WTs with respect to the formation of the S_{640} (Figure 3.18 A and B) but the A_{677} was not formed at 180 K and the ternary complex had to be illuminated at higher temperature (205 K) to obtain the characteristic band of the first intermediate (Figure 3.19 A and B). This result indicates that the absence of the –OH group affects the temperature at which the H^+/H^- transfer occurs. Moreover, those two mutants performed the $A_{677} \rightarrow A_{672}$ exchange in the early glass transition phase without presenting any further intermediate. The fluorescence emission spectra at 150 K, reported in Figure 3.20, confirmed for POR B Y212F the complete formation of the shift at 640 nm. The global

decay time was calculated to τ_2 = 6.6 ns (Figure 3.20). Analogously to the case of the S164A, the emission is red-shifted and the lifetime slightly increases, as compared to PChlide-POR B complex, instead of decrease, as observed in the wild type form (Figure 3.20 B). Since this mutant dramatically affects the reaction, the same reasoning, as for S164A, can be taken into consideration. This strengthens the interpretation that a reduced probability of PChlide deactivation into the reactive pathway is responsible for the impaired light activation step. The corresponding mutation in the POR A isoform showed bright emission peak, therefore the blue and red side were fitted, providing values of $\tau_{2\ Y215F\ blue}$= 6.0 ns and $\tau_{2\ Y215F\ red}$ = 6.3 ns respectively (Figure 3.21 B). In this mutant, the different decay time might indicate that an incomplete binding is coupled with alteration of the flow into the reactive path.

POR A Y215H and POR B Y212H, which maintain proton donation feature, showed no

Table 3.6 : Initial velocity (v_0), turnover number (k_{cat}) and relative activity (A_{rel}) for wild type (WT) and mutant forms of POR B and POR A determined under steady-state conditions at room temperature. The POR activity was triggered by excitation at 633 nm (λ_{exc} = 633 nm) using 10 µM wild type/ mutant POR in the presence of 7 µM PChlide and 100 µM NADPH in measuring buffer. For the determination of k_{cat}, PChlide concentrations at substrate saturation (20 µM) were added.

	Code	v_0 ($\mu M \cdot min^{-1}$)	k_{cat} (s^{-1})	A_{rel} (%)		Code	v_0 ($\mu M \cdot min^{-1}$)	k_{cat} (s^{-1})	A_{rel} (%)
POR A					**POR B**				
Active site's amino acid	WT	0.7	$5.5 \cdot 10^{-3}$	**100**	Active site's amino acid	WT	3.82	$1.2 \cdot 10^{-2}$	**100**
	Y215F	0.005	-	**1**		Y212F	0.79		**2.5**
	Y215H	-	-	-		Y212H	-	-	-
	K216R	-	-	-		K213R	< 0.01	-	-
	K216Q	-	-	-		K213Q	-	-	-
						D214M	-	-	-
	D217A	-	-	-		D214A	0.02	-	**1**
	D217E	0.05	-	**8**		D214E	0.73	$2.3 \cdot 10^{-3}$	**20**
	D217N	0.21	$5.4 \cdot 10^{-4}$	**30**		D214N	2.25	$8.7 \cdot 10^{-3}$	**60**
	S218G	0.02	-	**2**		S215G	0.91	$1.5 \cdot 10^{-3}$	**24**
	S218A	0.02	-	**3**		S215A	0.14	$3.8 \cdot 10^{-3}$	**18**
	S218T	0.28	$1.7 \cdot 10^{-3}$	**40**		S215T	1.85	$4.6 \cdot 10^{-3}$	**48**
	K219R	-	-	-		K216R	-	-	-
	K219Q	-	-	-		K216Q	-	-	-

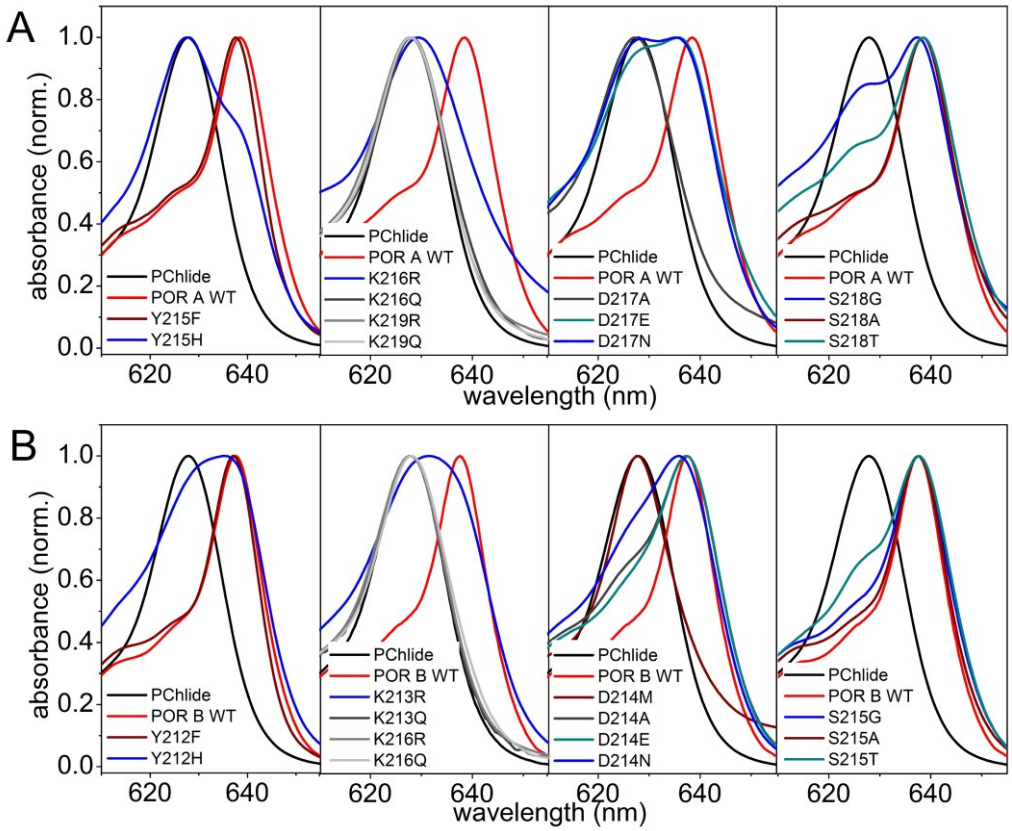

Figure 3.18: Absorption spectra of the S_{640} species measured at 180 K before the onset of irradiation **(A)** Mutants in the active site of POR A. **(B)** Mutants in the active site of POR B. The spectra are normalized for better comparison

activity at room temperature (Table 3.6). The low temperature absorption experiment showed that at 180 K the S_{640} specie appeared in POR A Y215H as shoulder on the red flank of the absorption peak and in POR B Y212H as a double peak with a maximum at 630 and 640 nm (Figure 3.18). After illumination, as shown in Figure 3.19 A and B, both mutants could form the intermediate A_{677} at 180 K, while at temperature, ~ 260 – 250 K, the $A_{677} \rightarrow A_{672}$ transition occurred. In Tyr → His variants no A_{681} intermediate was detected. These results reinforce the role of a polar residue in restoring the formation of the first intermediate at the same temperature, as in the case of the WTs. Nevertheless, a variation of the steric effect in this position also has an influence on the correct alignment of the substrate in the active site (S_{640}) and on the coenzyme turnover. These results are also supported by the low temperature fluorescence. The emission red shifts of the Y → H mutants were less pronounced compared to the Y → F variants, in POR B (Figure 3.20 A) and POR A (Figure 3.21 A). In POR B Y212H the decay time of the blue and red side of the spectral region were analysed but resulted similar to the globally fitted value (τ_2 = 6.4 ns) which is comparable

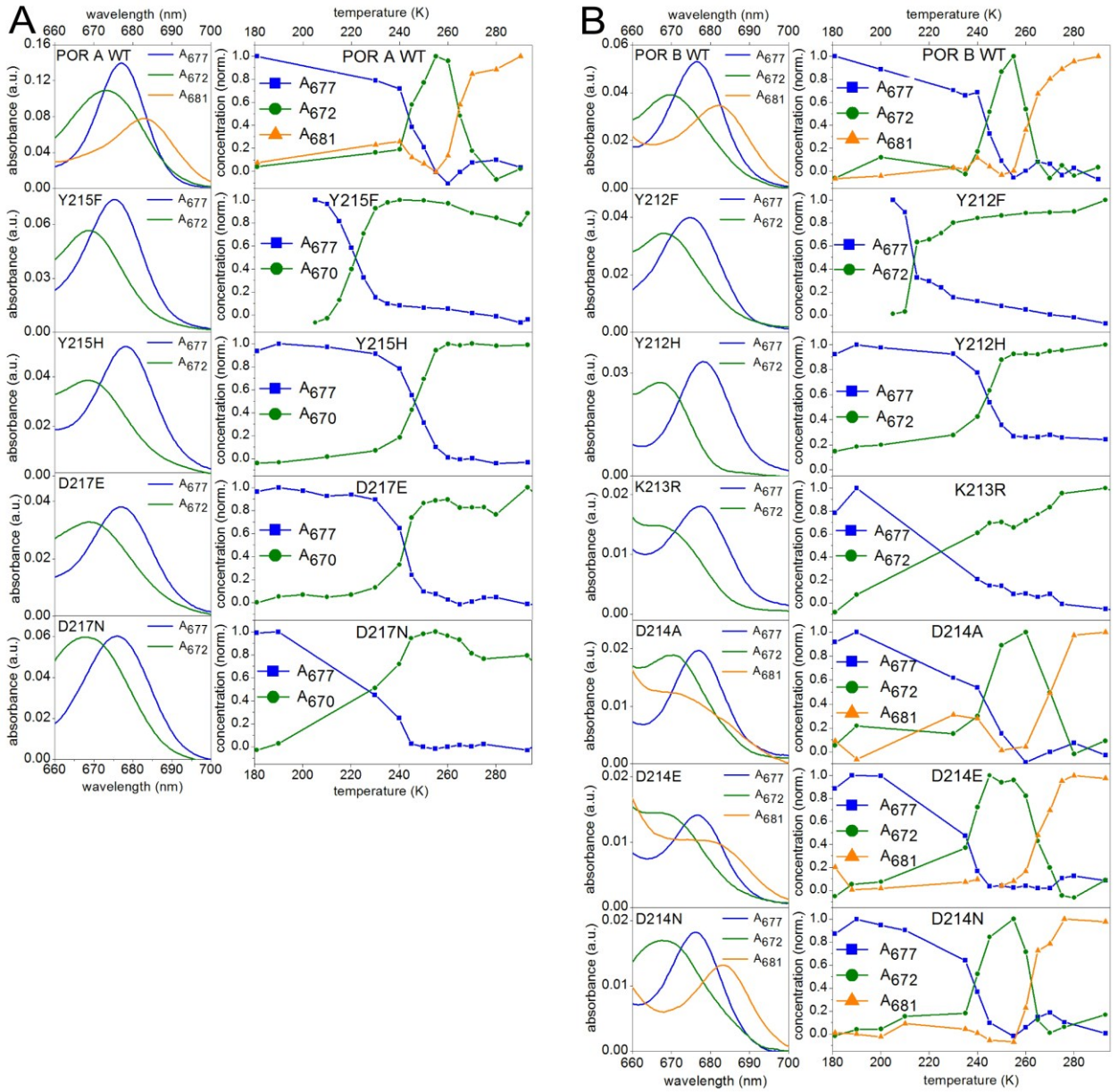

Figure 3.19: Spectra of the reaction intermediates trapped for the distinct POR forms (Tyr, Lys and Asp mutants) at different temperatures (left column) and the relative temperature-dependence profile of the intermediates A_{677}, A_{672} and A_{681} as calculated by SVD and EFA analysis (right columns) **(A)** Mutants in POR A isoforms. **(B)** Mutants in POR B isoform.

with the lifetime obtained in the PChlide-POR B complex. Also in the POR A Y215H the lifetime resulted to be comparable with the PChlide-POR A complex (τ_2 = 6.7 ns) suggesting that the different steric effect of the His compared to the Tyr disturb the proper alignment between the three reaction components. Because the red shift is still measurable in both absorption and emission measurements, it cannot be excluded that a small population of PChlide could be properly bound in the active site and therefore be converted in to A_{672}

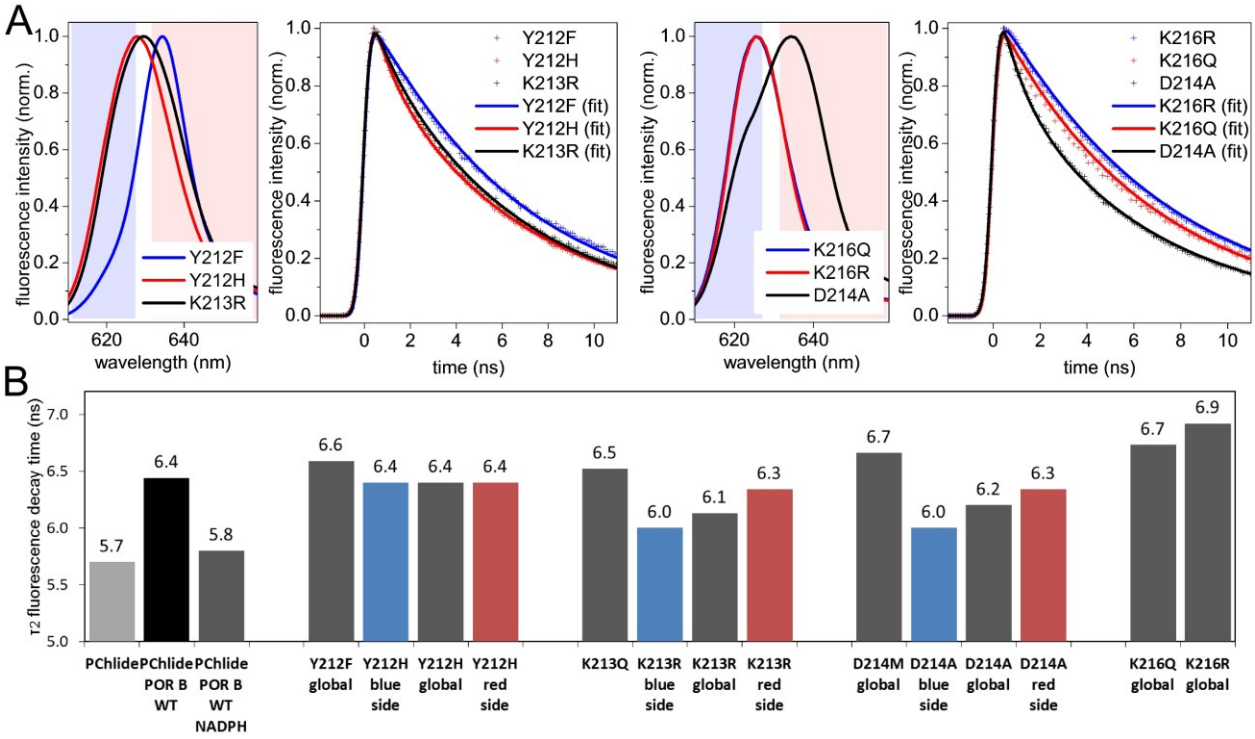

Figure 3.20: Low temperature fluorescence spectra and fluorescence decay traces of wild type POR B in comparison with mutant POR B forms. The mutant POR B forms include the variants in the active site. **(A)** Fluorescence spectra and decay traces recorded at 150 K. The shadowed areas in the fluorescence spectra indicate the spectral regions that were included in the data analysis of the blue (610-630 nm) and red wings (633-650 nm) of the fluorescence bands. **(B)** Fluorescence decay times estimated by a global fit procedure using the integrated fluorescence over the whole emission region (black/grey columns) and the emission regions separated into the blue (blue columns) and red spectral region (red columns) of the fluorescence band.

reaction intermediate at 180 K. However, the low enzyme-substrate complex formed in the room temperature measurement, can explain why the formation of Chlide was not observed.

The mutations on the first Lys, next to the catalytic Tyr, had a dramatic effect on the catalysis. While POR B K213Q, POR A K216Q, and POR A K216R completely abolish the reaction, POR B K216R produced Chlide at room temperature. This amount was close to the lower detection limit of the experiment, therefore no relative activity could be calculated (Table 3.6). These findings were further confirmed by the low temperature absorption measurements. At 180 K the spectrum of PChlide measured in the K → Q, in POR A and POR B mutants, showed no difference with the spectrum of PChlide in buffer. Instead, as shown in Figure 3.18, POR B K213R and POR B K216R resulted in having a partial shift to 640 nm, more pronounced in the POR B mutant than in POR A. This reflects the ability of POR B K213R, but not POR A K216R, to form the first two intermediates at 180 K (Figure 3.19) demonstrating that the presence of a positive charged side chain in position 213 is

required to promote the correct positioning of PChlide in the active site and thus the formation of A_{677}. The absence of A_{681} also implies that the coenzyme turnover is affected. The fluorescence measurements at 150 K of POR B K216Q (Figure 3.20 A), POR A K216Q and POR A K216R (Figure 3.21 A), showed no emission shift and an increased lifetime of PChlide, compared with the decay time of the substrate in the buffer. The increase is more pronounced in the K → Q mutants (τ_2= 6.4 ns in POR A and τ_2= 6.5 ns in POR B variant) than in the POR A K216R (τ_2= 6.2 ns) suggesting that the POR-PChlide-NADPH geometrical alignment was disrupted. In contrast, POR B K213R showed a broadening of the emission spectrum with a global decay time of τ_2= 6.1 ns (Figure 3.20). The fitting of the decay traces on the blue and the red side resulted $\tau_{2\ K213R\ blue}$= 6.0 ns and $\tau_{2\ K213R\ red}$ = 6.3 ns suggesting that the positive charge of the arginine could disturb the binding ($\tau_{2\ K213R\ blue}$= 6.0 ns), restore the compromised substrate alignment (red shift) and also reducing the flow of the

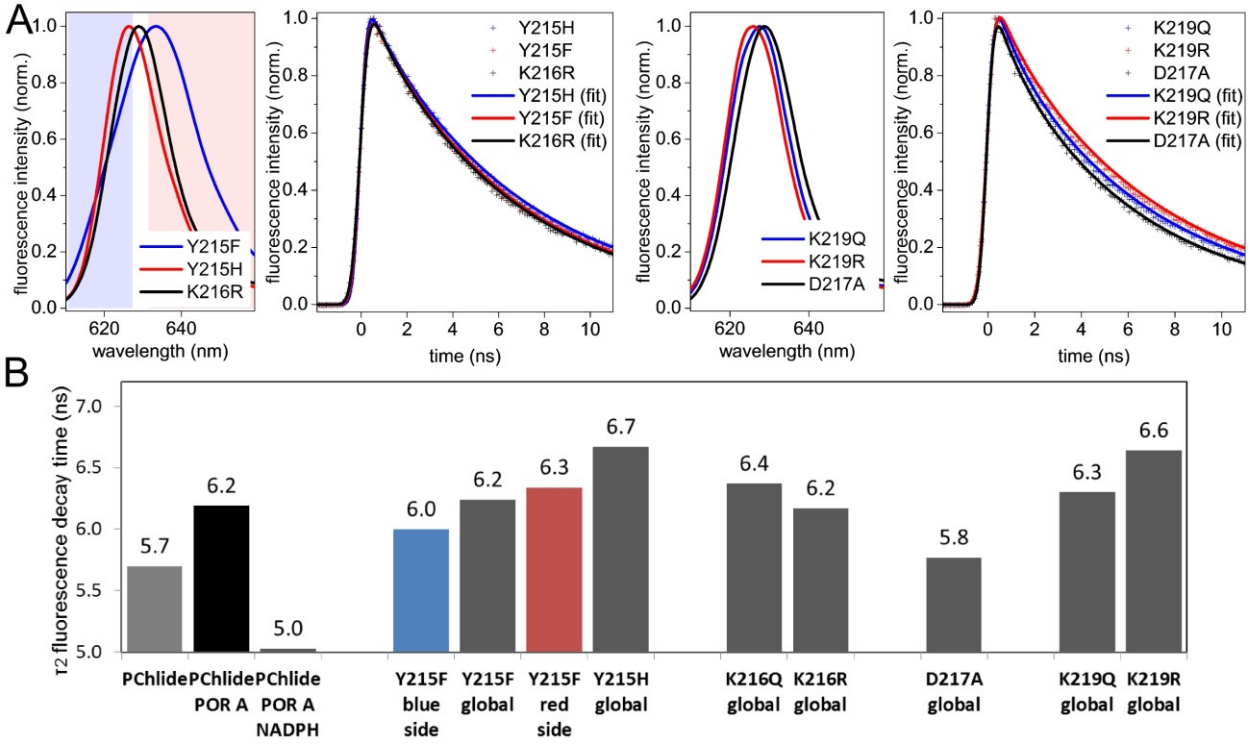

Figure 3.21: Low temperature fluorescence spectra and fluorescence decay traces of wild type POR A in comparison with mutant POR forms. The mutant POR A forms include the active site. **(A)** Fluorescence spectra and decay traces recorded at 150 K. The shadowed areas in the fluorescence spectra indicate the spectral regions that were included in the data analysis of the blue (610-630 nm) and red wings (633-650 nm) of the fluorescence bands. **(B)** Fluorescence decay times estimated by a global fit procedure using the integrated fluorescence over the whole emission region (black/grey columns) and the emission regions separated into the blue (blue columns) and red spectral region (red columns) of the fluorescence band.

exited molecule into the reactive path ($\tau_{2\ K213R\ red}$ = 6.3 ns).

The kinetic parameters of the mutants produced in the aspartate position in POR A and POR B are reported in Table 3.6. POR A D217A complete impairs the reaction, while D217E and D217N retained 8 % and 30 % of the relative activity, respectively. A similar trend but with an increased relative activity was observed in the three mutants produced in these positions in the sequence of POR B. No activity was found in D214M, 1 % was measured for D214A, 20 % in D214E and 60% in case of D214N (Table 3.6). At 180 K, POR A D217A as well as POR B D214M mutants reported no spectral shift (Figure 3.18). The low temperature fluorescence showed that in POR A D217A, PChlide has a decay time of τ_2= 5.8 ns (Figure 3.21 B) comparable to the value of PChlide in buffer, confirming that in this mutant the lack of activity is linked with a loss of PChlide binding. Oppositely, in POR B D214M the substrate decays with a time constant of τ_2= 6.7 ns (Figure 3.20), similarly to the PChlide-POR complex, indicating that the mutation affects the alignment of the substrate in the active site.

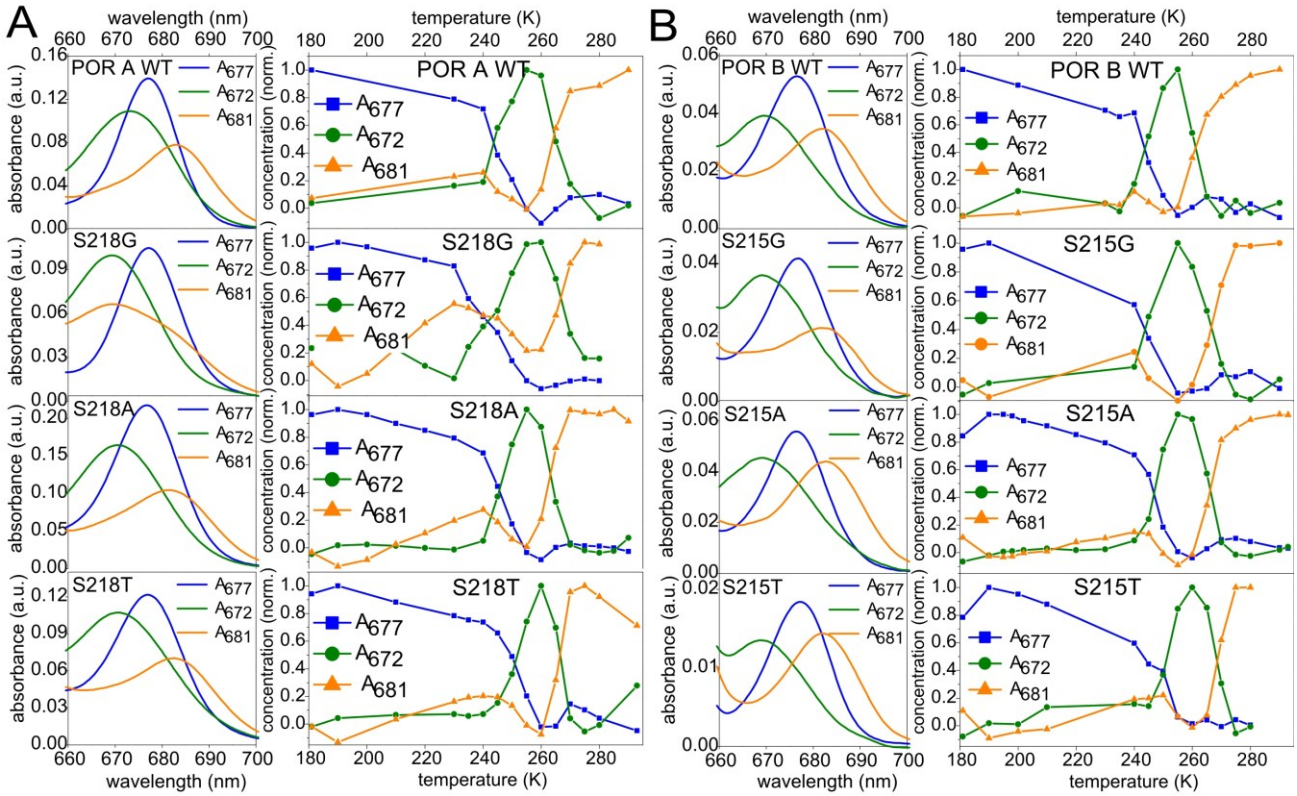

Figure 3.22: Spectra of the reaction intermediates trapped for the distinct POR Ser mutants at different temperatures (left column) and the relative temperature-dependence profile of the intermediates A_{677}, A_{672} and A_{681} as calculated by SVD and EFA analysis (right columns). **(A)** Mutants in POR A isoform. **(B)** Mutants in POR B isoform.

The POR A mutants, D217E and D217N, reported a double 630 - 640 nm peak at 180 K (Figure 3.18 A) and only the first two intermediates, A_{677} and A_{672} were detected (Figure 3.19 A). In the corresponding mutants in POR B, the absorption shift in PChlide spectrum was almost complete (Figure 3.18 B). As reported in Figure 3.19 B, the mutants POR B D214A, POR B D214E and POR B D214N produced, after illumination, the three intermediates. A_{677} and A_{672} were observed to possess a similar spectral shape with the corresponding intermediate in the wild type. In contrast, A_{681} in D214A and in D214E resulted as an incomplete transition from the A_{672}. This evidence suggests that the NADPH re-bound is still feasible, but it escapes a complete detection probably because higher temperatures are necessary, over the range of the experiment, to observe the complete formation of A_{672}. Further confirmation of this finding came from the analysis of the temperature profile. The peak of A_{672} was broader than the same in POR B WT, meaning that the releasing of $NADP^+$ also required broader temperature range to be completed. It is interesting to notice how, within the three mutations (D-A → D-E → D-N), a trend could be found. The formation of a correct A_{681} spectral shape correlate with a decreasing of the temperature at which the $A_{672} \rightarrow A_{681}$ occurred and which corresponded to an increased relative activity (1 % → 20 % → 60 %).

Because D214A reported an extremely low activity and an incomplete absorption shift to 640 nm, the fluorescence of PChlide at low temperature was measured when this mutant is present in the reaction mixture (Figure 3.20). At 150 K, the red shift in the emission spectrum was not complete and a shoulder appeared in the blue side. The global analysis of the decay time reported a value of $\tau_{2\ D214A} = 6.2$ ns. Fitting the blue and the red side resulted in $\tau_{2\ D214A\ blue} = 6.0$ ns and $\tau_{2\ D214A\ red} = 6.3$ ns, suggesting that the PChlide binding is affected as well as the flow into the reactive path. However, a part of the PChlide population resulted correctly bound and the formation of Chlide observed.

The mutants produced in the Serine position also shown a decrease in the retained activity, compared with the WTs. In POR A S218A, S218G and S218T a relative activities of 3 %, 2 %, and 40 %, respectively, were measured (Table 3.6). The corresponding mutations in POR B sequence have a similar trend but with an increased A_{rel}. S215A, S215G and S215T reported a relative activity of 18 %, 24 % and 48 % compared with the WT. The mutations on the Ser demonstrate that even in this position the presence of a polar amino acid is capable of retaining a higher activity compared with mutants which carried

hydrophobic side chains. For the mutant forms that allowed a reliable determination of the maximum velocity, the turnover numbers (k_{cat}) were additionally determined and well correlated with the loss in the relative enzyme activity (A_{rel}).

The mutation on the active site Ser in POR A and POR B shows, at low temperatures, a less pronounced difference with respect to the WTs and between the two isoforms. As reported in Figure 3.18, the S_{640} resulted incomplete in the POR A Ser mutants while complete absorption spectra could be observed in the POR B Ser mutants. After the illumination, all mutants of this group performed the reduction of the substrate and the coenzyme exchange steps (Figure 3.22). In particular, the S → A and the S → T substitutions, in both POR A and POR B, presented similar intermediates absorption bands and temperature-dependent profiles comparable with the respective WTs. Only the A_{672} → A_{681} transition was observed at higher temperature, as compared with the WTs. (Figure 3.22). In contrast, POR A S218G and POR B S215G showed an incomplete formation of the A_{681} spectral band which indicates a less efficient NADPH re-binding. In general, the catalytic Ser, compared with the other amino acid of the active site, has less influence in terms of performing the correct steps along the reaction, while, at least in POR A, it also has a role in maintaining the correct alignment between the reaction components.

The Lys-219 in POR A and Lys-216 in POR B are the last amino acids composing the catalytic site. In the POR B 3-D model Lys-216 is also indicated as part of the network that links the propionic acid with the protein structure. Since the role of Lys-216 could support the 3D model, the results are already presented in the chapter 3.6.1. However, the corresponding mutations in POR A had comparable effects. The mutants POR A K219Q and POR A K219R did not show any activity at room temperature (Table 3.6). At low temperature, no red shift was recorded, neither in the absorption (Figure 3.18) nor in the emission spectra (Figure 3.21). The lifetime of PChlide, measured in the ternary complex with these two mutants, increased to τ_2=6.3 ns and τ_2= 6.6 ns for K219Q and K219R, respectively. This indicates that the substrate is bound in the active site, but the correct alignment between the three reaction components is affected, as it is also shown for the POR B mutants.

Figure 3.23 represents a summary for the effect of all POR A and POR B mutants, discussed above, on the enzymatic activity, the reaction mechanism and the photochemistry assessed by the fluorescence decay times of the ternary enzyme complexes.

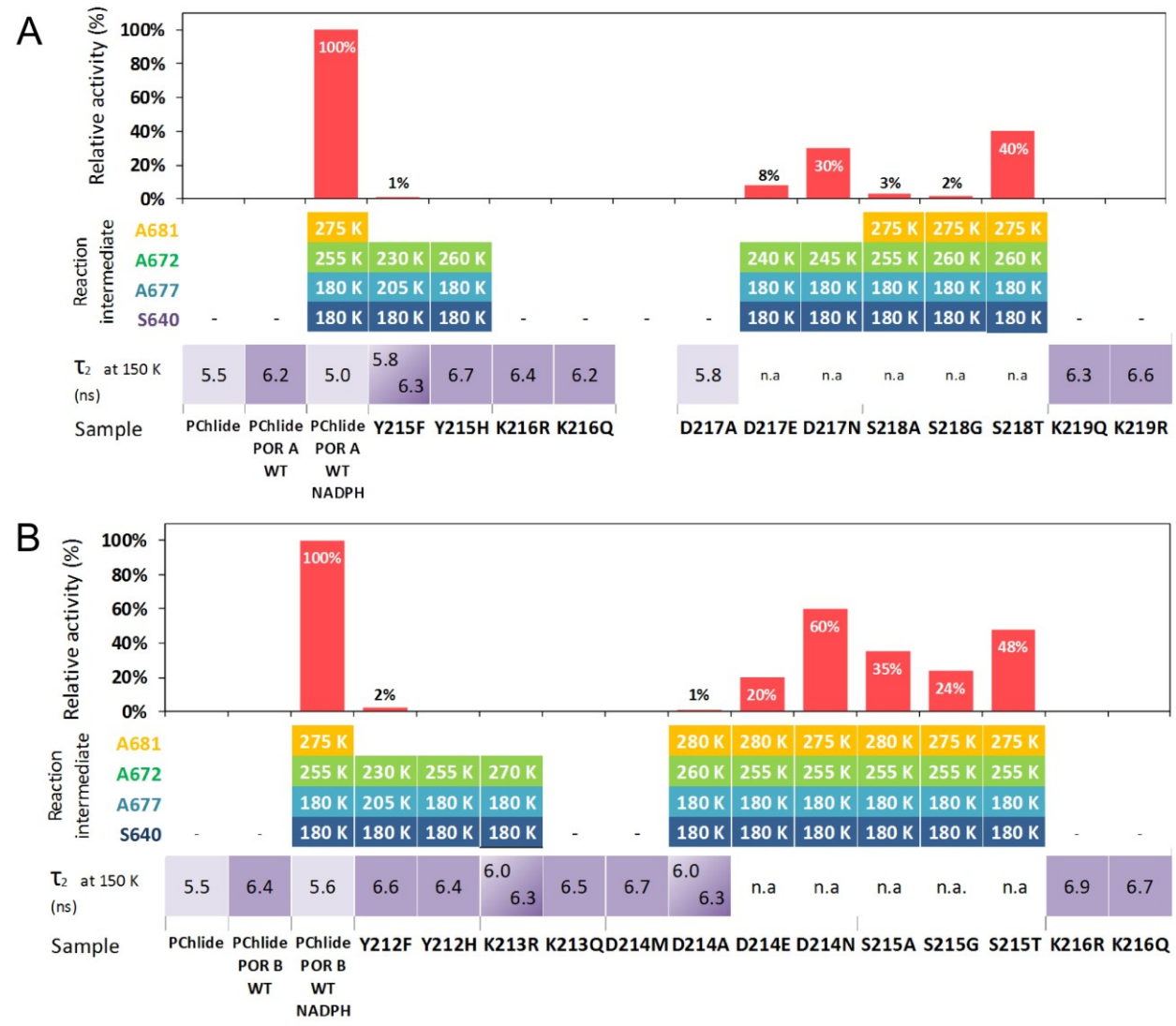

Figure 3.23: Overview on the catalytic activity, spectral characteristics of the low temperature intermediates and fluorescence decay times for all mutants constructed to investigate the active site. Upper part: steady-state enzyme activities given as relative values in comparison to the wild type POR B activity. Middle part: Reaction intermediates trapped at low temperatures including the temperatures at which they arise from the preceding form. Lower part: fluorescence decay times (τ_2) obtained at 150 K. The results of the fits when the emission range is separated into a blue and red one are indicated as follows: decay time at the blue wing - top, left and at the red wing - bottom, right. **(A)** Wild type and mutants in POR A isoform. **(B)** Wild type and mutants in POR B isoform. **(C)** Graphical representation of the 3-D model structure for POR B based on model 1; the carbon atoms of PChlide are in green; the catalytically important Tyr-212 and Lys-213 residues are included, whereas the carbon atoms are in cyan, oxygen atoms in red and hydrogen atoms in white.

4. Discussion

4.1 Comparison between POR A and POR B wild type and their biological function

Within this work, in order to fill the lack of knowledge about POR enzymes from plants, the photocatalysis of POR A and B from *H. vulgare L.* was characterized employing different spectroscopic techniques both, at room and at low temperature. The reactive ternary complex (POR-PChlide-NADPH) was recreated *in vitro*, using heterologously expressed protein, enabling detailed studies on the reaction mechanism without disturbances by aggregated POR complexes and associated problems due to pigment-pigment interactions. From the steady-state kinetics at room temperature K_M was calculated, resulting in a lower value for POR B (1.25 ± 0.07 μM) compared to POR A (3.44 ± 0.3 μM). The lower K_M indicates a higher (~ 3-fold) affinity for PChlide in POR B than POR A. The turnover number k_{cat} and the specificity constant k_{cat}/K_M, commonly used to compare catalytic efficiencies of different enzymes, further confirm the trend. They are 2- and about 6-fold, respectively, larger for POR B than POR A. The higher catalytic efficiency of POR B supports previous findings which provide evidence for a 2-fold higher quantum efficiency of POR B compared to POR A[53]. In contrast with this finding, a recent publication on reconstituted enzyme complexes of POR A, POR B and POR C from *A. thaliana* reported that, under the specific experimental conditions, POR A and POR B, did not differ in their catalytic activity[105]. This disagreement between *Arabidopsis* and barley POR might be explained by the following reasons: (i) the paper reported the formation of aggregated PChlide-POR-NADPH complexes, while within the scope of this work the reaction mixture contains a surfactant above the critical micellar concentration to prevent the formation of such complexes and to avoid PChlide-PChlide interactions and/or energy transfer processes between PChlide and Chlide; (ii) the lineages that led to *Arabidopsis* (eudicots) and *Hordeum* (monocots) separated already about 200 million years ago[107]. Moreover, POR A and B from barley appear to trace back to ancient gene duplication within grasses (see appendix Figure 7.2). Because of these evolutionary divergences, differences between barley and *Arabidopsis* isoforms are not unexpected. Rather, they are most likely due to the different organisms, from which the isozymes originate.

The low temperature absorption measurements of POR A and B WT offered the opportunity to trap reaction intermediates in POR catalysis and, thus, to get a deeper insight into the reaction mechanism. When compared with each other, a similar set of reaction intermediates can be identified in POR A and POR B after actinic irradiation. They include the formation of the POR-Chlide-$NADP^+$ complex (A_{677}) followed by the release of $NADP^+$ from the enzyme (A_{672}) and its replacement by NADPH (A_{680}). In the examined temperature range (180-300 K), the final reaction reflected by desorption of the Chlide product from the enzyme takes only place in the case of POR A. In POR B the release of Chlide obviously requires higher temperatures to be accomplished. The reason for this effect is that POR B most likely has a higher affinity to the Chlide product, similar to the higher substrate affinity of POR B versus POR A.

Apart from the final step the reaction sequence is identical for both POR A and POR B isoenzymes. Nevertheless, slight differences occur. (i) The one difference is the activation energy for the first light induced reaction $S_{640} \rightarrow A_{677}$, i.e. the conversion of PChlide in the POR-PChlide-NADPH complex into Chlide. With 24.9 ± 2.1 $kJ \cdot mol^{-1}$ the activation energy is lower for POR A than POR B with 35.9 ± 1.8 $kJ \cdot mol^{-1}$. This explains well the higher amount of the first reaction intermediate, A_{677}, produced in POR A as compared to POR B. (ii) The other difference refers to the second dark reaction, $A_{672} \rightarrow A_{681}$. As evidenced by SVD and EFA analysis, this reaction is shifted to lower temperatures in POR B compared to POR A. Since the reaction only occurs above the glass-transition temperature, where protein dynamics plays a prominent role, the temperature shift suggests higher protein flexibility in POR B than POR A. The conversion $A_{672} \rightarrow A_{681}$ is coupled to the replacement of $NADP^+$ by NADPH, which means that this exchange is facilitated by the increased protein flexibility of POR B within the NADPH binding site.

The reaction cycle for cyanobacterial POR from *Synechocystis* was already published in literature and perfectly fits with the results obtained for *Synechocystis* POR in this work.[77] Interestingly, when the *Synechocystis* enzyme is compared with POR A and POR B, then the complete red-shift in the absorption of species S_{640}, characteristic of the plant enzymes, is only manifested in a shoulder, whereas after the actinic irradiation a broad band at 698 nm isformed and ascribed to the first reaction intermediate, A_{698}. A_{698} is further converted into an intermediate with a maximum absorption at 677 nm, A_{677}. The latter two intermediates represent the reaction product resulting from the H^- and subsequent H^+ transfer[97]. A_{677}

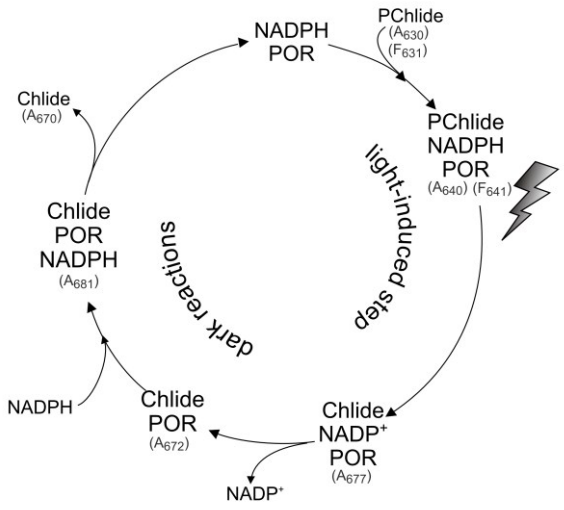

Figure 4.1: Catalytic reaction cycle of POR A and B from barley (*Hordeum vulgare* L.) based on the results from low temperature absorption spectroscopy. The primary light-induced reaction is suggested to involve a coupled hydride/proton transfer yielding enzyme-bound Chlide as primary reaction product. Intermediates indicating a sequential H^-/H^+ transfer are not to be identified. The absorption maximum of the individual intermediates is given in subscripts.

obviously corresponds to the A_{677} intermediate detected in POR A and POR B, whereas no preceding intermediate, similar to A_{698}, is to be identified in the case of the two plant PORs. This means that either the activation barrier separating A_{698} from A_{677} is too small in the two plant enzymes so that an intermediate similar to A_{698} cannot be trapped at low temperatures or that enzyme-bound Chlide is directly produced in a first reaction step immediately after light excitation. Accordingly, the initial photoreaction should involve a concerted H^-/H^+ transfer in contrast to the sequential mechanism realized in S*ynechocystis* POR. This finding agrees with recent studies, which have shown that the H^-/H^+ transfer is faster in eukaryotic than prokaryotic POR enzymes suggesting that the active site architecture has been optimized in eukaryotic PORs[108,109]. Further, in cyanobacterial PORs the H^+ transfer is coupled to the solvent dynamics in order to achieve an optimal proton donor-acceptor distance. However, in plant PORs this H^+ transfer is independent of a solvent-coupled dynamics and only requires localized motions at the active site. It is therefore conceivable that, as consequence of evolution, the optimization of the H^+ transfer step has led to an active site architecture, which enables a concerted H^-/H^+ transfer reaction in plant POR enzymes. According to the results of this work, the catalytic reaction cycle of POR A and B from barley is presented in Figure 4.1.

Taken together, the findings of the steady-state kinetics and the analysis of the low temperature intermediate spectra clearly show that, based on K_M, POR B has a higher (~3x)

binding affinity for PChlide and a higher (~2x) turnover number, k_{cat}. It follows that the catalytic efficiency of POR B versus POR A is significantly higher. The photoactive ternary POR-PChlide-NADPH complexes and the reaction intermediates identified at low temperatures are spectroscopically identical for the two isoforms. This analogy also includes the reaction sequence in the appearance of the individual intermediates. Hence, the higher catalytic efficiency of POR B cannot be attributed to differences in the catalytic mechanism. However, the second dark reaction, which goes along with the release of $NADP^+$ and rebinding of NADPH is shifted to lower temperatures in POR B compared to POR A, implying for POR B a higher conformational flexibility of protein sites within the catalytic pocket. In multiple turnover reactions as opposed to the single turn over reaction in the low temperature experiments this higher protein flexibility plays an important role and by facilitating the $NADP^+$/NADPH replacement it obviously exerts a positive effect on the catalytic efficiency. In this respect, results are of interest, which reveal that enzyme dynamics also controls the binding of PChlide to POR from the thermophilic cyanobacteria *Thermosynechococcus elongatus*[110]. It thus appears that enzyme dynamics is an integral part in the catalytic function of POR. Therefore, the higher catalytic efficiency of POR B compared to POR A is suggested to result from a higher binding affinity of PChlide to the enzyme and, most likely, from dynamic effects, which control conformational fluctuations of protein sites around the catalytic centre and finally lead to a higher turnover number.

Low-temperature fluorescence measurements at 150 K allowed, besides the characterization of the stationary emission spectra, also the evaluation of the photophysics/photochemistry of the S_1-excited state in the ternary POR-PChlide-NADPH complexes without disturbances caused by produced Chlide. The S_1-excited state lifetime was assessed on the basis of the fluorescence decay time. As to be expected from the low-temperature absorption spectra, the fluorescence spectra of the ternary POR A and POR B complexes also exhibit the red-shift in the emission characteristic for PChlide correctly configured at the active site. For the ns-fluorescence decay times values of $\tau_2 = 5.04 \pm 0.02$ ns for the POR A ternary complex and $\tau_2 = 5.8 \pm 0.3$ ns for the POR B ternary complex were obtained. Compared with unspecifically bound PChlide in the POR-PChlide complexes (identified as unspecifically bound because of the lack of the red shift in the fluorescence,) with $\tau_2 = 6.2 \pm 0.1$ ns for POR A and $\tau_2 = 6.45 \pm 0.02$ ns for POR B, the decay times are significantly shortened but similar to PChlide in buffer solution, for which, however, the

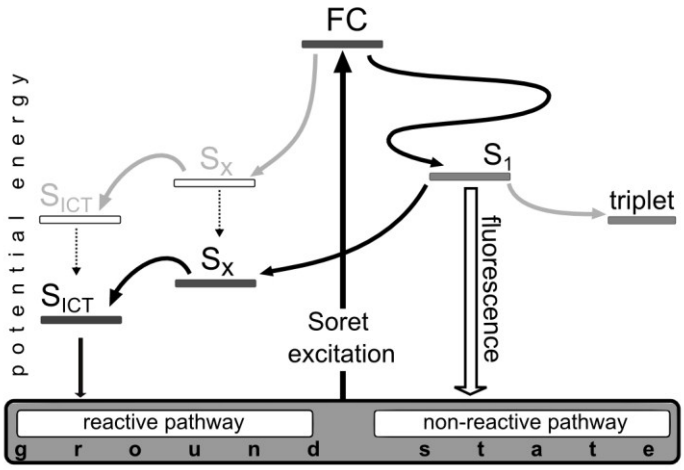

Figure 4.2: Scheme of the relaxation path of PChlide in solution as compared to that in the ternary complex after the excitation in the Frank-Codon (FC) state. The decrease of the decay time of the POR-PChlide-NADPH complex reflects a new deactivation route (black arrows) from the exited state S_1 to energetically stabilized S_x and S_{ICT} exited states.

fluorescence emission spectrally overlaps with that of unspecifically-bound PChlide in the ternary POR complexes. Between those results and the excited-state photophysics/ photochemistry of the ternary POR-PChlide-NADPH complexes the following relationship becomes evident.

Considering the well-accepted reaction scheme for the deexcitation processes in free PChlide and taking into account that the fluorescence decay times of the ternary POR complexes are reduced as compared to POR-PChlide complexes, this decrease can be understood by an increase in the rate constants for the nonradiative decays. Due to the very low fluorescence quantum yield[85] the effect of the radiative constant is to be neglected. However, in the ternary POR-PChlide-NADPH complexes the assumption of increased nonradiative decays, which go along the non-reactive channel via internal conversion back to the PChlide ground state as well as intersystem crossing into the triplet state, is not rational. Rather, the desactivation along the reactive path leading to the formation of the intramolecular charge transfer state, S_{ICT}, as precursor of the final PChlide reduction is gaining great importance. In the relaxation path suggested for free PChlide, the relaxation along the reactive path would not affect the decay time of the S_1-excited state. Nevertheless, the reactive path would become accessible in the ternary POR complexes if the relative energies of the S_X and /or S_{ICT} states are lowered below the S_1-excited state level due to the stabilization of these two states within the active site of the POR complexes (Figure 4.2). Recent work has really shown that the S_{ICT} state is stabilized by local interaction with protein

sites in the catalytic pocket.[85,84] Hence, a modified excited-state reaction path has been established in the ternary POR A and POR B complexes, in so far as the photochemical channel is opened for the S_1-excited state population. The competition between the efficient photochemical processes along the reactive path and the nonradiative processes along the non-reactive path thus explains the reduced decay times in the ternary complexes. From these findings it is obvious that interactions between PChlide and protein sites at the catalytically active centre obviously affect the energetics of the photochemistry and guarantee the high efficiency in catalysis.

4.2 Evaluation of the 3-D Model and the role of the active site amino acids

In order to provide a more in-depth rationale for the reaction mechanism of POR a large number of studies focused on the introduction of point mutations in the active site of predominantly cyanobacterial POR enzymes (see under chapter 1.3.4)[43,72,84,87,90]. By contrast, fewer findings regarding the replacement of active site residues and their impact on the catalytic function are reported for plant enzymes[28,88,89]. However, in general the evaluation of the structural features of POR, which are important for the photochemistry and catalysis, is still being hampered by the lack of a crystal structure. This situation led to the prediction of the 3-D structure using closely related SDR enzymes as structural template. So, the structures of *Synechocystis*[7] and *Thermosynechococcus*[72] POR, POR from barley (*Hordeum vulgare*)[45] and *Arabidopsis thaliana*[105] were calculated. The *Synechocystsis* model was the first one published. The structure was rebuilt on a template from the tyrosine-dependent oxidoreductase family but PChlide and NADPH were docked in the catalytic cleft manually and mainly guided by inspection[7]. The 3-D structure of the *Arabidosis* and barley POR enzymes were only calculated for the apoenzyme form[45,105]. Adequate state-of-the-art methods were used in the construction of the POR model for the *Thermosynechococcus* enzyme but POR from *Thermosynechococcus* and *Hordeum vulgare* originate from distinct cyanobacterial and eukaryotic lineages in the evolution so that it makes no sense to adapt the latter model for the evaluation of the reaction mechanism in the plant POR B isoenzyme.

Therefore, to identify the structural regions, which are important for the photochemistry and catalysis in POR B a homology model of the 3-D structure was derived using *in silico* homology modelling algorithms followed by the docking of the NADPH coenzyme and

PChlide substrate into the model (see under Chapter 2.1). As shown in Figure 3.10 the overall 3-D structure is represented by the typical Rossman-fold, which is made up from a central parallel β-sheet that in turn is surrounded by nine α-helices. The three-dimensional arrangement of the secondary structure elements including the extensions of the α–helices results in the formation of a cleft that accommodates the cofactor and substrate. The PChlide substrate is positioned deeply in the binding cleft and associated via several interactions with active site residues (Figure 3.11 and Figure 4.3). Based on the calculated model, His-138 and Lys-216 are close enough to the propionic acid side chain at the C(17) position of PChlide to

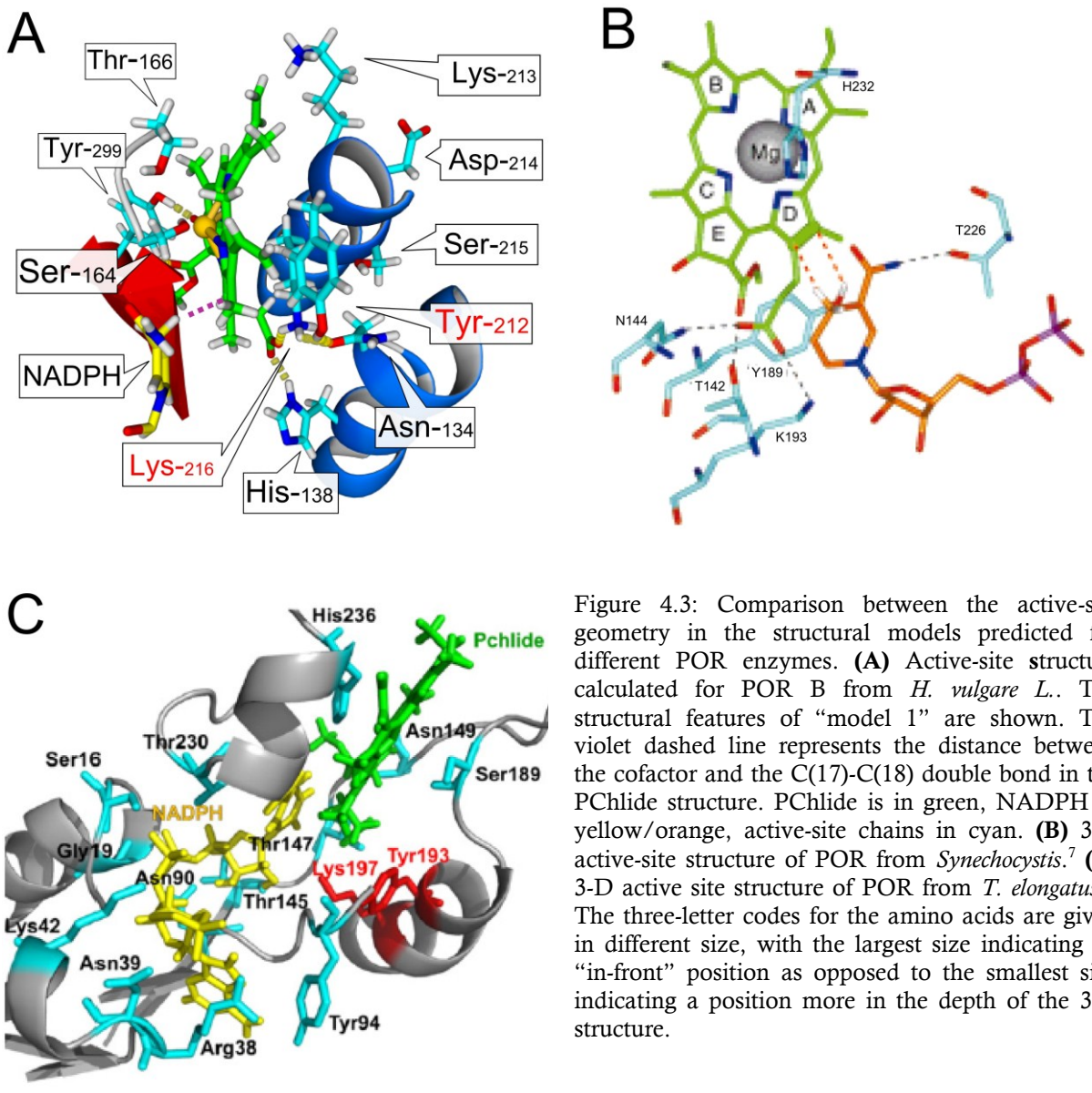

Figure 4.3: Comparison between the active-site geometry in the structural models predicted for different POR enzymes. **(A)** Active-site **s**tructure calculated for POR B from *H. vulgare L.*. The structural features of "model 1" are shown. The violet dashed line represents the distance between the cofactor and the C(17)-C(18) double bond in the PChlide structure. PChlide is in green, NADPH in yellow/orange, active-site chains in cyan. **(B)** 3-D active-site structure of POR from *Synechocystis*.[7] **(C)** 3-D active site structure of POR from *T. elongatus*.[43] The three-letter codes for the amino acids are given in different size, with the largest size indicating an "in-front" position as opposed to the smallest size indicating a position more in the depth of the 3-D structure.

undergo interactions via electrostatic and/or hydrogen bonding. Ser-164 is in contact with the central Mg^{2+} ion of PChlide obviously via formation of a coordinative bond. Tyr-299 is placed in close proximity to the C(13')=O group at the isocyclic fifth ring of the PChlide structure suggesting the formation of a hydrogen bond between the Tyr-OH and the C(13') carbonyl group and thus facilitating keto/enol tautomerism about this bond. Asn-134 is part of hydrogen bonding network extending between Tyr-212, Asn-134, Lys-216 up to the carboxyl group of the propionic acid side chain. In this role, Asn-134 is also important for the maintenance of the active-site architecture.

When compared with the homology models of the cyanobacterial POR enzymes[7,72] (Figure 4.3), striking differences are evident. In the POR B model the PChlide substrate is positioned deeper within the catalytic cleft and the catalytically active Tyr-212 and Lys-216 are arranged rather behind than beneath the PChlide substrate. However, the *Synechocystis* POR model also predicts interactions between the catalytically active Lys-193 and the propionic acid residue at C(17) of PChlide, whereas the geometry around this active site region is slightly different compared to the POR B model. In addition, Asp-144 has been suggested to be in contact with the propionic acid. In POR B this interaction is established by His-138, i.e. by a positively *versus* a negatively charged amino acid side chain. The *Synechocystis* POR model further suggests that His-232 is involved in PChlide binding by providing the ligands for chelating the central Mg^{2+} ion[7]. The *Thermosynechococcus* model does not confirm this chelation but instead shows that there is no possibility for the direct contact of His-236 (analogous to His-232 in the Synechocystis sequence) with Mg^{2+}. On the contrary, the POR B model predicts that, in an alternative to His, Ser-164 is well placed to form a coordinative bond to the central Mg^{2+} ion and to contribute to the correct positioning of PChlide at the active site.

The active site variants produced for the validation of the POR B model structure confirm the role ascribed to His-138, Ser-164, Lys-216 and Tyr-299 to a large extent.

Substitution of Ser-164 by Ala (S164A) leads to a nearly complete loss in the enzymatic activity, whereas ~90% of the wild type activity could be restored in the Thr mutant (S164T). As evidenced by the low temperature absorbance and fluorescence spectra, the dramatic activity decrease is due to a loss in the binding capability of PChlide at the active site. Moreover, the small fraction of enzyme-bound S164A that can be trapped at low temperature indicates that, based on a lengthened fluorescence decay time, also the

photochemistry is impaired in the mutant. Hence, apart from the role in substrate binding, Ser164 and its interaction with the central Mg^{2+} via coordinative bonding is also essential for the efficient photochemistry. This conclusion is strongly supported by the recovery of the activity in the S164T mutant and the analogous photochemistry compared to the non-mutated wild type enzyme. Very recently, it has been reported that in free, unbound PChlide the central Mg^{2+} has an impact on the charge separation in the intramolecular charge transfer state (S_{ICT})[111]. It is thus conceivable that also in the ternary POR B complex Ser-coordinated Mg^{2+} helps in creating the electron-deficient site across the C(17)=C(18) double bond of PChlide.

Moreover, the important role of Ser-164 is also evident in that it is replaced by Thr-145 in cyanobacteria POR from *Thermosynechococcus* (Figure 3.13). As it is generally accepted that cyanobacterial POR enzymes are the ancestor of plant POR[36] it is most likely that Ser/Thr is highly conserved at the active site because it is required to optimize the active site architecture and the primary photochemistry.

The substitution of His-138 results in a strong impairment of the catalytic activity. All mutant forms examined, H138F and H138Y, have a completely abolished catalytic activity. There is also no red shift neither in the low temperature absorbance or fluorescence spectra. However, the significantly lengthened fluorescence decay time between 6.8 and 6.9 ns is a strong indication of unspecifically bound PChlide, i.e., of PChlide, which is not bonded in the correct active site geometry. Even in the H138Y variant that again retains a polar side chain with the ability to form hydrogen bonds, the catalytic activity is completely lost. It thus appears that His138 provides key interactions with the carboxyl group of the propionic acid side chain at the C(17) position of PChlide. These interactions are obviously brought about by electrostatic bonding between the negatively charged carboxyl group and the positively charged side chain of His138. Consequently, as suggested by the POR B model structure His138 plays a potentially important role for the correct alignment of PChlide within the ternary POR complex.

Lys-216 turns out to be a component of the hydrogen bonding network extending over Tyr-212, Asn-134, Lys-216 and ending at the propionic acid side chain. The Lys-216 mutants, K216Q and K216R as highly conserved substitutions, show similar effects in the low temperature spectra as well as in the fluorescence decay times as the His-138 mutants. That means that also Lys-216 appears to be involved in the correct positioning of the

PChlide substrate via interactions with the propionic acid side chain. Unfortunately neither the replacement by a positively charged Arg nor a polar Gln leads to the recovery of the catalytic activity, which makes the identification of the interacting forces difficult. Rather, the result indicates that the position of Lys-216 is extremely sensitive to any variation in the active site architecture and that even minor changes in this structure have profound effects on the PChlide binding capability

In contrast to the mutant forms mentioned so far, the replacement of Tyr-299 by Phe and His in the Y299F and Y299H variants only results in a moderate loss of the catalytic activity. In the Y299F mutant the enzyme-bound PChlide fraction appears well aligned within the ternary POR B complex, which results in the formation of analog intermediates as in the wild type POR at low temperatures. Also, judged from the fluorescence decay time, the primary photochemistry is only very slightly, if at all, impaired in relation to the unmutated enzyme. This finding is unexpected. In contrast to the supposed function of the T

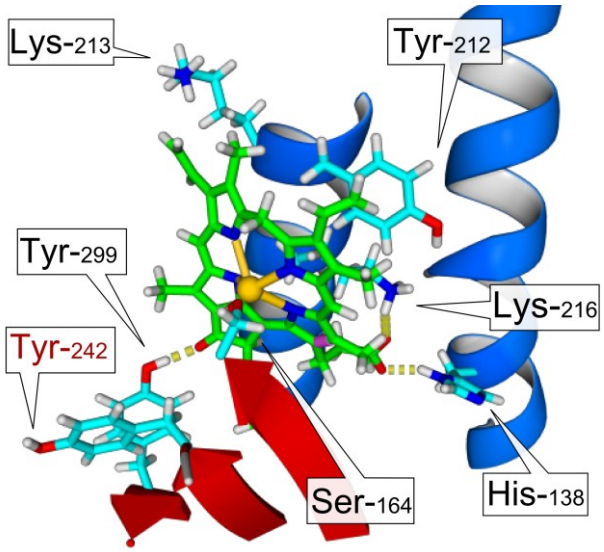

Figure 4.4: 3-D structural model of POR B from *Hordeum vulgare*. The position of the alternative Tyr-242, which can substitute Tyr-299 as surrogate proton donor is shown and highlighted in red.

yr-299 OH group in stabilizing PChlide binding via hydrogen bonding to the C(13')=O carbonyl group at the isocyclic fifth ring of PChlide (Figure 3.11, Figure 4.3), the Y299F mutant exhibits wild type-like catalysis. A plausible explanation for this effect is that another Tyr-OH makes the hydrogen bond available and fulfills a surrogate function in this respect. Indeed, another Tyr, Tyr-242 is located in close proximity to Tyr-299 so that it could

substitute the Tyr-299 OH group in creating the hydrogen bond. However, to achieve an adequate position of Tyr-242 relative to the isocyclic fifth ring it must undergo a rotation. As molecular dynamic simulations have shown, such a structural rearrangement can be easily adopted.

The replacement of Tyr-299 by His, carrying an aromatic imidazole group at the side chain, is expected to restore the catalytic activity. This prediction is contradicted by the catalytic activity of still 16%. Probably due to the involvement of the imidazole ring in the formation of fake hydrogen bonds, the Y299H mutant shows a significantly reduced affinity to the PChlide substrate. However, the ternary complex of the Y299H mutant, as far as it is created, undergoes the wild type-like photochemistry. This can be concluded once more again from the fluorescence decay time, which agrees with that of the wild type complex. Based on the maintenance of the primary photochemistry in the two mutants, it could be speculated that Tyr-299 plays a major role in PChlide binding rather than in impairing the photochemical processes. Nevertheless, more efforts are necessary to understand the importance of Tyr-299 and the C(13')=O carbonyl group of PChlide for POR catalysis.

The 3-D model was also exploited to understand the roles of the catalytically active Tyr-212 and Lys-216 residues as components of the active site **Y**xxx**K** motif in more detail. The role of Tyr as proton donor is confirmed by the results obtained for POR B. That is, as to be expected, the catalytic activity of the Y212F mutant resulting from the replacement of Tyr by Phe is reduced dramatically up to 2.5 % of the wild type activity but it is not completely abolished. This result agrees with that reported for POR from cyanobacteria[87]. In this case the remaining low POR activity is explained by the use of a surrogate proton source as it is often practiced when key proton donors are removed from an enzyme active site by site-directed mutagenesis[38,39,87]. As evident from the low temperature absorbance spectra, the reason for the major loss in activity is in an impaired photochemistry in the Y212F variant enzyme. Although the formation of species S_{640} indicates appropriately positioned PChlide, the first reaction intermediate, A_{677}, is only produced at significantly higher temperatures, namely at 205 K versus 180 K in the wild type enzyme. Accordingly the so-called "near attack" conformation[70] is maintained in the mutant but the proton transfer to PChlide is hindered most probably by an increased activation barrier. Further evidence for the impairment of the photochemistry is provided by the significantly lengthened fluorescence decay time of the ternary Y212F complex with 6.6 ns versus 5.6 ns in the wild type POR. It

clearly shows that the de-excitation along the reactive path leading to the generation of the intramolecular charge transfer state, S_{ICT}, is substantially compromised by the mutation. This is obviously due to a loss in excited-state interactions that stabilize the S_X and S_{ICT} states as important "reactive" intermediates in the excited-state chemistry of wild-type POR (Figure 4.2).

Although His could take over the role as proton donor, the enzymatic activity of the Y212H mutant has fully got lost. The low temperature absorption spectrum reveals that the main fraction of PChlide is rather unspecifically bound than in the "near attack" position necessary for catalysis. This suggests that Tyr-212 is also of importance for the proper alignment of PChlide towards NADPH within the active site structure. With respect to the structural model of POR B, Tyr-212 could not be optimally relaxed in the last energy minimization process leading to a position of the Tyr-OH, which is not close enough to the C(17)=C(18) double bond to be reduced in PChlide. Therefore, the validation of the role of Tyr-212 in photocatalysis and substrate binding is not readily possible. However, it is quite conceivable that the Tyr-212 side chain can execute rotational motions, as a result of which the Tyr-OH comes in closer contact to the C(17)=C(18) double bond of PChlide.

As already shown above, the catalytically active Lys-216 provides key interactions to the propionic acid attached at C(17) of PChlide. Direct evidence for a role in lowering the pK_a of the Tyr-OH can only be found for the replacement of Lys-216 by Gln. The K216Q mutant turns out to be fully inactive, because Gln cannot form cation-π-electron interactions that are responsible for the effect on the pK_a of the Tyr-OH. On the other hand, the substitution of Lys by Arg in the K216R mutant also results in a complete loss of the catalytic activity, even though Arg has a positively charged guanidinium group at the side chain and thus the potential to form cation-π-electron interactions. However, the strength of such dipole-dipole interactions is strongly dependent on the distance (r) between the two dipoles, i.e. the interaction energy is indirectly proportional to the power of five or six, respectively, of the distance. Therefore, only small steric constraints as exerted by the guanidinium group of Arg could affect the realization of the cation-π-electron interaction.

While the roles of the two catalytically active site residues, Tyr and Lys, in the YxxxK motif are well accepted for POR enzymes from cyanobacteria, this is the first direct evidence, which demonstrates the importance of the two residues for the correct binding of PChlide at the active site and for catalysis in POR B.

The importance of the remaining active site residues Lys-213, Asp-214 and Ser-215, which are positioned between the catalytically active Tyr and Lys in the **Y**KDS**K** motif, was assessed in particular under the aspect of their contribution to a highly polar surrounding at the catalytic site.

Replacement of Lys-213 by Gln and Arg shows that this amino acid is also crucial for the correct binding of PChlide at the active site as well as for proper POR catalysis. In the mutant forms, K213Q and K213R, the activity is almost completely eradicated with an extremely low remaining activity of >1% in the K213R variant. The loss in activity of the K213Q mutant corresponds to unspecifically bound PChlide being unable to undergo photocatalysis. This result is in agreement with binding studies carried out with the Microscale Thermophoresis technique (MST) indicating a 4-fold lower affinity of PChlide to the ternary K213R mutant complex compared with the wild type enzyme[112]. Regarding the K213R mutant, a small fraction of a final "poised" photoactive state can be trapped at low temperatures. Nevertheless, as can be concluded from the longer fluorescence decay time the Lys/Arg substitution significantly impairs the wild type photochemistry. It seems likely that a positively charged side chain as in Lys and Arg is required to promote the proper substrate binding and an effective photochemistry. In the 3-D model of POR B, Lys-213 is placed towards the PChlide substrate but no direct interactions with PChlide sites are predicted. However, it has to be considered that structural rearrangements take place when the catalytically active ternary POR complex is built-up. Within this reorganization process Lys-213 could move close enough to Tyr-212 and finally cooperate with the catalytically active Lys-216.

With respect to Asp-214 in the **Y**KDS**K** motif it is particular striking that this Asp is positioned at the opposite site of the α-helix, which carries the catalytically active Tyr-212 and Lys-216. Since there is no direct contact to the PChlide substrate the effects of the Asp-214 substitutions are only indirectly related to PChlide binding and enzyme catalysis. Replacement of Asp-214 by Met and Ala with nonpolar aliphatic side chains results in an almost complete loss of the catalytic activity as it is shown for the D214M and D214A mutations. Obviously, these substitutions modify the position of the α-helix thereby bringing about alterations in the position of the catalytically active Tyr-212 and Lys-216 and disrupting interactions, which normally maintain the effective contact between PChlide and the active site residues. In consequence, the substrate binding and the photochemistry, in

addition to the $NADP^+$/NADPH exchange are affected by the Asp substitutions with Met and Ala.

On the contrary, the replacement of Asp-214 by polar amino acids as in the D214N and D214E mutant forms leads to the recovery of the catalytic activity, which reaches values of 19% in the D214E and 59% in the D214N mutant compared with the wild type enzyme. Furthermore, analogue reaction intermediates as in case of the wild type enzyme are produced at low temperatures implying that the reaction mechanism is not impaired in the mutant forms. From the substitution pattern it is apparent that at the position of Asp-214 a polar amino acid with adequate steric demand is absolutely necessary to maintain the active site architecture and, in consequence, the catalytic activity.

Similar effects are to be concluded from the replacement of Ser-215 by Gly, Ala and Thr in the S215G, S215A and S215T mutant forms. Whereas the catalytic activity is moderately reduced to 24% and 35 % in the S215G and S215A variants, which lack a polar side chain, the catalytic activity is restored up to 48% in the S215T mutant. In the low temperature reaction sequence the same intermediates as in the wild type are to be identified.

If the results obtained for all mutant forms of the POR B enzyme are taken together, the mutants fall into two categories: The first category includes the mutants affecting the polar residues Lys-213, Asp-214 and Ser-215 within the **Y**KDS**K** motif. These residues are not in immediate contact with the PChlide substrate. Instead, they are positioned within the α-helix, flanking the catalytic cleft, opposite to the substrate binding region or at the lateral helix site, respectively. Their influence on the catalytic efficiency is, therefore, only indirect and most likely due to the creation of intricate hydrogen bonding network and/or appropriate electrostatic interactions, which in turn affect the active site geometry at the substrate/NADPH binding site. It thus appears that the interplay between these residues and the surrounding protein sites fine-tunes the catalytic properties of POR B. It is striking how only small steric perturbations or changes in the hydrogen bonding tendency have a profound effect on the photoreaction. The second category includes the catalytically active Tyr-212 and Lys-216 plus Ser-164 and His-138. The replacement of these residues by appropriate substitutions results in an almost total loss in activity with < 3% of the wild type activity. The reason for the activity loss is the impairment of the photochemistry and of the correct alignment of PChlide in the active enzyme-substrate-cofactor complex. These residues are predicted by the 3-D model to directly interact with the PChlide substrate

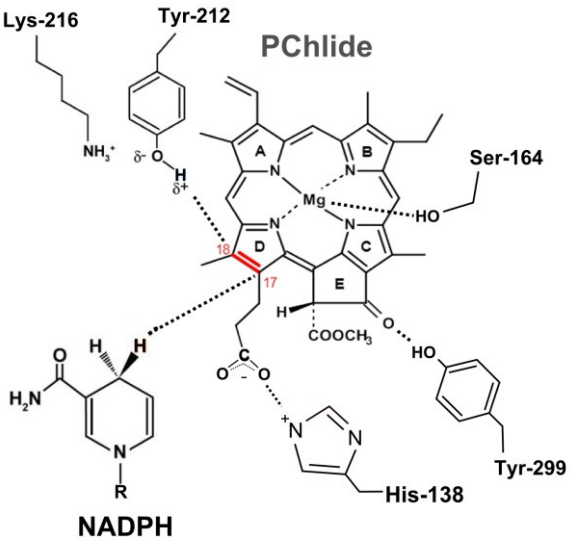

Figure 4.5: Active-site residues involved in the reduction of PChlide as predicted from the POR B model structure and evidenced by site-directed mutagenesis experiments. Lys-216 and Tyr-212 are involved in the alignment of the PChlide substrate in the ternary complex as well as in the proton transfer reaction to C(18) of PChlide. Ser-164 undergoes coordinative bonding to the central Mg^{2+}, thereby facilitating correct binding of PChlide in the photoactive ternary POR complex and contributing to the stabilization of "reactive" intermediates (S_X, S_{ICT}) by excited state interactions. Tyr-299 promotes the binding of PChlide throught the formation of H-bond with the C(13')=O carbonyl group. The His-138 interacts with the negatively charged propionic acid at C(17) of PChlide via electrostatic forces and thereby maintains a "near attack conformation" in the ternary POR-PChlide-NADPH complex.

involving several types of bonding. The predicted interactions between the PChlide substrate and the active site are confirmed by the point-mutation experiments. In conclusion of these results, Figure 4.5 shows the active site architecture of POR B as it follows from the calculation of the POR B structural model and the findings from site-directed mutagenesis. It is again interesting to note that only slight changes in the architecture of the catalytic pocket have a dramatic effect on the POR photochemistry. This highlights how precise interactions between the protein sites at the catalytic centre and the PChlide substrate are generated in order to drive the excited-state chemistry of PChlide along the reactive path yielding Chlide as final product and to guarantee an efficient catalysis.

The comparison of the POR A and POR B wild types reveals that the two enzymes use the same catalytic mechanism involving analogue reaction intermediates along the reaction cycle. However, POR B shows a higher binding affinity for PChlide and a higher catalytic efficiency. To address the question whether these different catalytic properties are associated with differences in the active site architecture, identical variant forms as in case of POR B were also produced for POR A. As could be shown, very similar results have been obtained

for the POR A mutant forms, when the amino acids localized around the active site, i.e., Tyr-215, Lys-216 and Lys-219 are compared. In POR A the replacement of these residues also has a profound effect on the photochemistry as well as on the appropriate positioning of the PChlide substrate within the active site. Discrepancies are manifested with respect to Asp-217 and Ser-218 in the **Y**KDS**K** motif. With respect to the same point mutation, there is a stronger decrease in the catalytic activity for the POR A than POR B variant forms. Moreover, at low temperatures, the D217E and D217N mutants of POR A do not produce the A_{681} intermediate, which usually happens above the glass- transition temperature where protein dynamics plays a prominent role. Even though no particular amino acid can be held responsible for these differences, it is tempting to suggest that there is restricted protein flexibility around the active site in POR A. In other words: It seems likely that a higher protein flexibility localized to the POR B active site can better balance single point mutations in its structure.

5. Conclusion

This work provides a more in depth rationale for the catalytic mechanism of the enzyme NADPH:protochlorophyllide oxidoreductase (POR), EC 1.3.1.33. POR catalyses an essential step in the synthesis of chlorophyll, which is the light-dependent reduction of protochlorophyllide (PChlide) in chlorophyllide (Chlide).

Of the two isoenzymes being active in higher plants, POR B as compared to POR A shows the higher catalytic efficiency. This is due to a higher binding affinity to PChlide and higher protein flexibility of protein sites positioned at the active centre. The two isoenzymes operate through the same reaction mechanism. The higher catalytic activity of POR B can be seen as evolutionary advantage, by which light-adapted mature plants are able to adjust chlorophyll biosynthesis to the environmental factor light and to avoid photosensitised oxidations in consequence of excess unbound PChlide and subsequent formation of reactive oxygen species (ROS).

Time-resolved fluorescence spectroscopy at low temperatures, at which no interference by formation of Chlide is to be expected, can be used to differentiate between free or unbound PChlide, unspecifically enzyme-bound PChlide and correctly positioned PChlide within the active ternary enzyme complex. The fluorescence decay times evaluated for the wild type POR enzymes in comparison with catalytically inactive mutant forms allow the conclusion that "reactive" intermediates in the excited-state chemistry of PChlide (S_X, S_{ICT}) are stabilized by excited-state interactions with protein sites at the active center. Due to these interactions the S_1-excited state population of the ternary complex can undergo direct deexcitation along the photoreactive path, which most likely prevents unwanted side reactions and leads to a higher efficiency of the primary photoprocesses.

The predicted 3-D model for the structure of POR B provides an insight into its active site architecture. The PChlide substrate is "held" at the active site in an optimal position by electrostatic/hydrogen bonding interactions between His-138/Lys-216 and the propionic acid chain at C(17) of PChlide, by coordinative bonding between Ser-215 and the central Mg^{2+} ion and by hydrogen bonding interactions between Tyr-299 and the C(13')=O carbonyl group attached at the isocyclic fifth ring of PChlide. This active site architecture finds its

confirmation in appropriate experiments using site-directed mutagenesis. Moreover, the mutagenesis experiments provide evidence that the active site of POR B is finely tuned to facilitate efficient photochemistry. Only small steric perturbations or changes in the hydrogen bonding network affect the efficiency of photochemistry dramatically.

6. Bibliography

1. Von Wettstein, D., Gough, S. & Kannangara, C. G. Chlorophyll Biosynthesis. *Plant Cell* **7,** 1039–1057 (1995).
2. Gupta, R. S., Mukhtar, T. & Singh, B. Evolutionary relationships among photosynthetic prokaryotes (Heliobacterium chlorum, Chloroflexus aurantiacus, cyanobacteria, Chlorobium tepidum and proteobacteria): Implications regarding the origin of photosynthesis. *Mol. Microbiol.* **32,** 893–906 (1999).
3. Robert E. Blankenship. *Molecular Mechanisms of Photosynthesis*. (Wiley-Blackwell, 2014).
4. Reinbothe, C. *et al.* Chlorophyll biosynthesis: spotlight on protochlorophyllide reduction. *Trends Plant Sci.* **15,** 614–24 (2010).
5. Brettel, K. & Byrdin, M. Reaction mechanisms of DNA photolyase. *Curr. Opin. Struct. Biol.* **20,** 693–701 (2010).
6. Masuda, T. & Fujita, Y. Regulation and evolution of chlorophyll metabolism. *Photochem. Photobiol. Sci.* **7,** 1131–1149 (2008).
7. Townley, H. E., Sessions, R. B., Clarke, A. R., Dafforn, T. R. & Trevor Griffiths, W. Protochlorophyllide oxidoreductase: A homology model examined by site-directed mutagenesis. *Proteins Struct. Funct. Genet.* **44,** 329–335 (2001).
8. Sarma, R. *et al.* Crystal structure of the L protein of Rhodobacter sphaeroides light-independent protochlorophyllide reductase with MgADP bound: a homologue of the nitrogenase Fe protein. *Biochemistry* **47,** 13004–15 (2008).
9. Brzezowski, P., Richter, A. S. & Grimm, B. Regulation and function of tetrapyrrole biosynthesis in plants and algae. *Biochim. Biophys. Acta* **1847,** 968–85 (2015).
10. Fujita, Yuichi Bauer, C. E. in *The Porphyrin Handbook* **13,** 109–156 (Elsevier, 2003).
11. Masuda, T. Recent overview of the Mg branch of the tetrapyrrole biosynthesis leading to chlorophylls. *Photosynth. Res.* **96,** 121–143 (2008).
12. Vavilin, D. V & Vermaas, W. F. J. Regulation of the tetrapyrrole biosynthetic pathway leading to heme and chlorophyll in plants and cyanobacteria. *Physiol. Plant.* **115,** 9–24 (2002).
13. Tanaka, A. & Tanaka, R. Chlorophyll metabolism. *Curr. Opin. Plant Biol.* **9,** 248–255 (2006).
14. Tanaka, R. & Tanaka, A. Tetrapyrrole Biosynthesis in Higher Plants. *Annu. Rev. Plant Biol.* **58,** 321–346 (2007).
15. Mochizuki, N. *et al.* The cell biology of tetrapyrroles: a life and death struggle. *Trends Plant Sci.* **15,** 488–498 (2010).
16. Yin, L. & Bauer, C. E. Controlling the delicate balance of tetrapyrrole biosynthesis. *Philos. Trans. R. Soc. B Biol. Sci.* **368,** (2013).
17. Grimm, B. Novel insights in the control of tetrapyrrole metabolism of higher plants. *Curr. Opin. Plant Biol.* **1,** 245–250 (1998).
18. Gouterman, M., Wagnière, G. H. & Snyder, L. C. Spectra of porphyrins: Part II. Four orbital model. *J. Mol. Spectrosc.* **11,** 108–127 (1963).
19. Gouterman, M. Spectra of porphyrins. *J. Mol. Spectrosc.* **6,** 138–163 (1961).
20. Dietzek, B., Kiefer, W., Hermann, G., Popp, J. & Schmitt, M. Solvent effects on the excited-state processes of protochlorophyllide: A femtosecond time-resolved absorption study. *J. Phys. Chem. B* **110,** 4399–4406 (2006).
21. Dietzek, B. *et al.* Dynamics of charge separation in the excited-state chemistry of protochlorophyllide. *Chem. Phys. Lett.* **492,** 157–163 (2010).

22. Scrutton, N. S., Groot, M. L. & Heyes, D. J. Excited state dynamics and catalytic mechanism of the light-driven enzyme protochlorophyllide oxidoreductase. *Phys. Chem. Chem. Phys.* **14,** 8818–24 (2012).

23. Sytina, O. A. *et al.* Protochlorophyllide Excited-State Dynamics in Organic Solvents Studied by Time-Resolved Visible and Mid-Infrared Spectroscopy. *J. Phys. Chem. B* **114,** 4335–4344 (2010).

24. Dietzek, B. *et al.* The excited-state chemistry of protochlorophyllide a: A time-resolved fluorescence study. *ChemPhysChem* **7,** 1727–1733 (2006).

25. Dietzek, B. *et al.* Protochlorophyllide a: A comprehensive photophysical picture. *ChemPhysChem* **10,** 144–150 (2009).

26. Colindres-Rojas, M. *et al.* Excited-state dynamics of protochlorophyllide revealed by subpicosecond infrared spectroscopy. *Biophys. J.* **100,** 260–7 (2011).

27. Dietzek, B. *et al.* The excited-state dynamics of magnesium octaethylporphyrin studied by femtosecond time-resolved four-wave-mixing. *Chem. Phys. Lett.* **415,** 94–99 (2005).

28. Wilks, H. M. & Timko, M. P. A light-dependent complementation system for analysis of NADPH:protochlorophyllide oxidoreductase: identification and mutagenesis of two conserved residues that are essential for enzyme activity. *Proc. Natl. Acad. Sci. U. S. A.* **92,** 724–8 (1995).

29. Beer, N. S. & Griffiths, W. T. Purification of the enzyme NADPH: protochlorophyllide oxidoreductase. *Biochem. J.* **195,** (1981).

30. Suzuki, J. Y. & Bauer, C. E. A prokaryotic origin for light-dependent chlorophyll biosynthesis of plants. *Proc. Natl. Acad. Sci. U. S. A.* **92,** 3749–53 (1995).

31. Chew, A. G. M. & Bryant, D. A. Chlorophyll biosynthesis in bacteria: the origins of structural and functional diversity. *Annu. Rev. Microbiol.* **61,** 113–29 (2007).

32. Reinbothe, S., Reinbothe, C., Apel, K. & Lebedev, N. Evolution of chlorophyll biosynthesis--the challenge to survive photooxidation. *Cell* **86,** 703–5 (1996).

33. Franck, F. Protochlorophyllide Reduction: Mechanisms and Evolution. *Photochem. Photobiol.* **78,** 543–557 (2003).

34. Yamamoto, H., Kurumiya, S., Ohashi, R. & Fujita, Y. Oxygen sensitivity of a nitrogenase-like protochlorophyllide reductase from the cyanobacterium Leptolyngbya boryana. *Plant Cell Physiol.* **50,** 1663–73 (2009).

35. Nomata, J., Kitashima, M., Inoue, K. & Fujita, Y. Nitrogenase Fe protein-like Fe-S cluster is conserved in L-protein (BchL) of dark-operative protochlorophyllide reductase from *Rhodobacter capsulatus*. *FEBS Lett.* **580,** 6151–6154 (2006).

36. Yang, J. & Cheng, Q. Origin and evolution of the light-dependent protochlorophyllide oxidoreductase (LPOR) genes. *Plant Biol. (Stuttg).* **6,** 537–44 (2004).

37. Baker, M. E. Protochlorophyllide reductase is homologous to human carbonyl reductase and pig 20 beta-hydroxysteroid dehydrogenase. *Biochem. J.* 605–7 (1994).

38. Joernvall, H. *et al.* Short-chain dehydrogenases/reductases (SDR). *Biochemistry* **34,** 6003–6013 (1995).

39. Rossmann, M., Liljas, C.I. and Banaszak, L. in *The Enzymes* (ed. Paul D. Boyer) 61– 102 (Academic Press, NY, 1975).

40. Lesk, A. M. NAD-binding domains of dehydrogenases. *Curr. Opin. Struct. Biol.* **5,** 775–83 (1995).

41. Benach, J., Atrian, S., Gonzàlez-Duarte, R. & Ladenstein, R. The catalytic reaction and inhibition mechanism of Drosophila alcohol dehydrogenase: observation of an enzyme-bound NAD-ketone adduct at 1.4 A resolution by X-ray crystallography. *J. Mol. Biol.* **289,** 335–55 (1999).

42. Filling, C. *et al.* Critical residues for structure and catalysis in short-chain dehydrogenases/reductases. *J. Biol. Chem.* **277,** 25677–84 (2002).

43. Menon, B. R. K., Hardman, S. J. O., Scrutton, N. S. & Heyes, D. J. Multiple active site residues are important for photochemical efficiency in the light-activated enzyme protochlorophyllide

oxidoreductase (POR). *J. Photochem. Photobiol. B Biol.* **161,** 236–243 (2016).

44. Gabruk, M. *et al.* Insight into the oligomeric structure of PORA from A. thaliana. *Biochim. Biophys. Acta - Proteins Proteomics* **1864,** 1757–1764 (2016).

45. Buhr, F. *et al.* Photoprotective role of NADPH:protochlorophyllide oxidoreductase A. *Proc. Natl. Acad. Sci. U. S. A.* **105,** 12629–12634 (2008).

46. Reinbothe, C., Buhr, F., Pollmann, S. & Reinbothe, S. In vitro reconstitution of light-harvesting POR-protochlorophyllide complex with protochlorophyllides a and b. *J. Biol. Chem.* **278,** 807–15 (2003).

47. Reinbothe, C., Lebedev, N. & Reinbothe, S. A protochlorophyllide light-harvesting complex involved in de-etiolation of higher plants. *Nature* **397,** 80–84 (1999).

48. Armstrong, G. A., Runge, S., Frick, G., Sperling, U. & Apel, K. Identification of NADPH:protochlorophyllide oxidoreductases A and B: a branched pathway for light-dependent chlorophyll biosynthesis in Arabidopsis thaliana. *Plant Physiol.* **108,** 1505–17 (1995).

49. Holtorf, H., Reinbothe, S., Reinbothe, C., Bereza, B. & Apel, K. Two routes of chlorophyllide synthesis that are differentially regulated by light in barley (Hordeum vulgare L.). *Proc. Natl. Acad. Sci. U. S. A.* **92,** 3254–8 (1995).

50. Reinbothe, S., Reinbothe, C., Lebedev, N. & Apel, K. PORA and PORB, Two Light-Dependent Protochlorophyllide-Reducing Enzymes of Angiosperm Chlorophyll Biosynthesis. *Plant Cell* **8,** 763–769 (1996).

51. Su, Q., Frick, G., Armstrong, G. & Apel, K. POR C of Arabidopsis thaliana: a third light- and NADPH-dependent protochlorophyllide oxidoreductase that is differentially regulated by light. *Plant Mol. Biol.* **47,** 805–813 (2001).

52. Pattanayak, G. K. & Tripathy, B. C. Catalytic Function of a Novel Protein Protochlorophyllide Oxidoreductase C of Arabidopsis thaliana. *Biochem. Biophys. Res. Commun.* **291,** 921–924 (2002).

53. Hanf, R. *et al.* Catalytic efficiency of a photoenzyme-An adaptation to natural light conditions. *ChemPhysChem* **13,** 2013–2015 (2012).

54. Aronsson, H., Sundqvist, C., Timko, M. P. & Dahlin, C. Characterisation of the assembly pathway of the pea NADPH:protochlorophyllide (Pchlide) oxidoreductase (POR), with emphasis on the role of its substrate, Pchlide. *Physiol. Plant.* **111,** 239–244 (2001).

55. Dahlin, C. *et al.* The role of protein surface charge in catalytic activity and chloroplast membrane association of the pea NADPH: protochlorophyllide oxidoreductase (POR) as revealed by alanine scanning mutagenesis. *Plant Mol. Biol.* **39,** 309–23 (1999).

56. Teakle, G. R. & Griffiths, W. T. Cloning, characterization and import studies on protochlorophyllide reductase from wheat (Triticum aestivum). *Biochem. J.* **296,** 225–30 (1993).

57. Reinbothe, S., Mache, R. & Reinbothe, C. A second, substrate-dependent site of protein import into chloroplasts. *Proc. Natl. Acad. Sci. U. S. A.* **97,** 9795–800 (2000).

58. Reinbothe, S., Quigley, F., Gray, J., Schemenewitz, A. & Reinbothe, C. Identification of plastid envelope proteins required for import of protochlorophyllide oxidoreductase A into the chloroplast of barley. *Proc. Natl. Acad. Sci. U. S. A.* **101,** 2197–202 (2004).

59. Schopfer, P. & Siegelman, H. W. Purification of protochlorophyllide holochrome. *Plant Physiol.* **43,** 990–6 (1968).

60. Bjorn, L. O. Action Spectra for Transformation and Fluorescence of Protochlorophyll Holochrome from Bean Leaves. *Physiol. Plant.* **22,** 1–17 (1969).

61. Nielsen, O. F. & Kahn, A. Kinetics and quantum yield of photoconversion of protochlorophyll(ide) to chlorophyll(ide) a. *Biochim. Biophys. Acta - Bioenerg.* **292,** 117–129 (1973).

62. Townley, H. E., Griffiths, W. T. & Nugent, J. P. A reappraisal of the mechanism of the photoenzyme protochlorophyllide reductase based on studies with the heterologously expressed protein. *FEBS Lett.* **422,** 19–22 (1998).

63. Belyaeva, O. B., Timofeev, K. N. & Litvin, F. F. The primary reactions in the protochlorophyll(ide) photoreduction as investigated by optical and ESR spectroscopy. *Photosynth. Res.* **15,** 247–256 (1988).

64. Ignatov, N. V., Belayeva, O. B. & Litvin, F. F. Low temperature phototransformations of protochlorophyll(ide) in etiolated leaves. *Photosynth. Res.* **38,** 117–124 (1993).

65. Griffiths, W. T. Reconstitution of chlorophyllide formation by isolated etioplast membranes. *Biochem. J.* **174,** 681–92 (1978).

66. Begley, T. P. & Young, H. Protochlorophyllide Reductase. 1. Determination of the Regiochemistry and the Stereochemistry of the Reduction of Protochlorophyllide to Chlorophyllide. *J. Am. Chem. Soc.* **111,** 3095–3096 (1989).

67. Heyes, D. J. *et al.* The first catalytic step of the light-driven enzyme protochlorophyllide oxidoreductase proceeds via a charge transfer complex. *J. Biol. Chem.* **281,** 26847–53 (2006).

68. Valera, V., Fung, M., Wessler, A. N. & Richards, W. R. Synthesis of 4R- and 4S-tritium labeled NADPH for the determination of the coenzyme stereospecificity of NADPH: Protochlorophyllide oxidoreductase. *Biochem. Biophys. Res. Commun.* **148,** 515–520 (1987).

69. Heyes, D. J., Sakuma, M., de Visser, S. P. & Scrutton, N. S. Nuclear quantum tunneling in the light-activated enzyme protochlorophyllide oxidoreductase. *J. Biol. Chem.* **284,** 3762–7 (2009).

70. Heyes, D. J. & Hunter, C. N. Making light work of enzyme catalysis: Protochlorophyllide oxidoreductase. *Trends in Biochemical Sciences* **30,** 642–649 (2005).

71. Lebedev, N. & Timko, M. P. Protochlorophyllide photoreduction. *Photosynth. Res.* **58,** 5–23

72. Menon, B. R. K., Davison, P. a, Hunter, C. N., Scrutton, N. S. & Heyes, D. J. Mutagenesis alters the catalytic mechanism of the light-driven enzyme protochlorophyllide oxidoreductase. *J. Biol. Chem.* **285,** 2113–9 (2010).

73. Griffiths, W. T., McHugh, T. & Blankenship, R. E. The light intensity dependence of protochlorophyllide photoconversion and its significance to the catalytic mechanism of protochlorophyllide reductase. *FEBS Lett.* **398,** 235–8 (1996).

74. Heyes, D. J., Ruban, A. V, Wilks, H. M. & Hunter, C. N. Enzymology below 200 K: the kinetics and thermodynamics of the photochemistry catalyzed by protochlorophyllide oxidoreductase. *Proc. Natl. Acad. Sci. U. S. A.* **99,** 11145–50 (2002).

75. Sytina, O. a *et al.* Enzyme activation and catalysis: characterisation of the vibrational modes of substrate and product in protochlorophyllide oxidoreductase. *Phys. Chem. Chem. Phys.* **13,** 2307–13 (2011).

76. Sytina, O. a, Heyes, D. J., Hunter, C. N. & Groot, M. L. Ultrafast catalytic processes and conformational changes in the light-driven enzyme protochlorophyllide oxidoreductase (POR). *Biochem. Soc. Trans.* **37,** 387–391 (2009).

77. Heyes, D. J., Ruban, A. V. & Hunter, C. N. Protochlorophyllide oxidoreductase: 'Dark' reactions of a light-driven enzyme. *Biochemistry* **42,** 523–528 (2003).

78. Heyes, D. J. & Hunter, C. N. Identification and characterization of the product release steps within the catalytic cycle of protochlorophyllide oxidoreductase. *Biochemistry* **43,** 8265–8271 (2004).

79. Heyes, D. J., Sakuma, M. & Scrutton, N. S. Solvent-Slaved protein motions accompany proton but not hydride tunneling in light-activated protochlorophyllide oxidoreductase. *Angew. Chemie - Int. Ed.* **48,** 3850–3853 (2009).

80. Hoeven, R., Hardman, S. J. O., Heyes, D. J. & Scrutton, N. S. Cross-Species Analysis of Protein Dynamics Associated with Hydride and Proton Transfer in the Catalytic Cycle of the Light-Driven Enzyme Protochlorophyllide Oxidoreductase. *Biochemistry* **55,** 903–913 (2016).

81. Heyes, D. J., Hunter, C. N., van Stokkum, I. H. M., van Grondelle, R. & Groot, M. L. Ultrafast enzymatic reaction dynamics in protochlorophyllide oxidoreductase. *Nat. Struct. Biol.* **10,** 491–2 (2003).

82. Sytina, O. a *et al.* Conformational changes in an ultrafast light-driven enzyme determine catalytic

activity. *Nature* **456,** 1001–4 (2008).

83. Heyes, D. J., Hardman, S. J. O., Mansell, D., Gardiner, J. M. & Scrutton, N. S. Mechanistic Reappraisal of Early Stage Photochemistry in the Light-Driven Enzyme Protochlorophyllide Oxidoreductase. *PLoS One* **7,** (2012).

84. Heyes, D. J. *et al.* Excited-State charge separation in the photochemical mechanism of the light-driven enzyme protochlorophyllide oxidoreductase. *Angew. Chemie - Int. Ed.* **54,** 1512–1515 (2015).

85. Hanf, R. *et al.* Protein-induced excited-state dynamics of protochlorophyllide. *J. Phys. Chem. A* **115,** 7873–7881 (2011).

86. Reinbothe, C., Lebedev, N. & Reinbothe, S. A protochlorophyllide light-harvesting complex involved in de-etiolation of higher plants. **397,** 80–84 (1999).

87. Menon, B. R. K., Waltho, J. P., Scrutton, N. S. & Heyes, D. J. Cryogenic and laser photoexcitation studies identify multiple roles for active site residues in the light-driven enzyme protochlorophyllide oxidoreductase. *J. Biol. Chem.* **284,** 18160–6 (2009).

88. Reinbothe, C. *et al.* In vitro-mutagenesis of NADPH:protochlorophyllide oxidoreductase B: two distinctive protochlorophyllide binding sites participate in enzyme catalysis and assembly. *Mol. Genet. Genomics* **275,** 540–52 (2006).

89. Lebedev, N., Karginova, O., McIvor, W. & Timko, M. P. Tyr275 and Lys279 stabilize NADPH within the catalytic site of NADPH:protochlorophyllide oxidoreductase and are involved in the formation of the enzyme photoactive state. *Biochemistry* **40,** 12562–12574 (2001).

90. Heyes, D. J. & Hunter, C. N. Site-directed mutagenesis of Tyr-189 and Lys-193 in NADPH: protochlorophyllide oxidoreductase from Synechocystis. *Biochem. Soc. Trans.* **30,** 601–604 (2002).

91. Morris, G. M. *et al.* AutoDock4 and AutoDockTools4: Automated docking with selective receptor flexibility. *J. Comput. Chem.* **30,** 2785–91 (2009).

92. Ghosh, D. *et al.* Porcine carbonyl reductase: Structural basis for a functional monomer in short chain dehydrogenases/reductases. *J. Biol. Chem.* **276,** 18457–18463 (2001).

93. Krieger, E., Darden, T., Nabuurs, S. B., Finkelstein, A. & Vriend, G. Making optimal use of empirical energy functions: force-field parameterization in crystal space. *Proteins* **57,** 678–83 (2004).

94. Fey, S. Enzymkatalyse in verschiedenen Formen der lichtabhaengigen NADPH:Protochlorophyllid-Oxidoreduktase. (Friedrich-Schiller-University Jena, 2011).

95. Hanf, R. *et al.* Probing the structure and Franck-Condon region of protochlorophyllide a through analysis of the Raman and resonance Raman spectra. *J. Raman Spectrosc.* **41,** 414–423 (2010).

96. Martin, G. E., Timko, M. P. & Wilks, H. M. Purification and kinetic analysis of pea (Pisum sativum L.) NADPH:protochlorophyllide oxidoreductase expressed as a fusion with maltose-binding protein in Escherichia coli. *Biochem. J.* **325,** 139–45 (1997).

97. Heyes, D. J., Ruban, A. V, Wilks, H. M. & Hunter, C. N. Enzymology below 200 K: the kinetics and thermodynamics of the photochemistry catalyzed by protochlorophyllide oxidoreductase. *Proc. Natl. Acad. Sci. U. S. A.* **99,** 11145–11150 (2002).

98. Myśliwa-Kurdziel, B., Solymosi, K., Kruk, J., Böddi, B. & Strzałka, K. Protochlorophyll complexes with similar steady-state fluorescence characteristics can differ in fluorescence lifetimes. A model study in Triton X-100. *J. Photochem. Photobiol. B Biol.* **86,** 262–271 (2007).

99. Berezin, M. Y. & Achilefu, S. Fluorescence lifetime measurements and biological imaging. *Chem. Rev.* **110,** 2641–2684 (2010).

100. Caspar, J. V. & Meyer, T. J. Application of the energy gap law to nonradiative, excited-state decay. *J. Phys. Chem.* **87,** 952–957 (1983).

101. Freed, K. F. & Jortner, J. Multiphonon Processes in the Nonradiative Decay of Large Molecules. *J. Chem. Phys.* **52,** 6272 (1970).

102. Benkert, P., Tosatto, S. C. E. & Schomburg, D. QMEAN: A comprehensive scoring function for model

quality assessment. *Proteins Struct. Funct. Bioinforma.* **71,** 261–277 (2008).

103. Benkert, P., Biasini, M. & Schwede, T. Toward the estimation of the absolute quality of individual protein structure models. *Bioinformatics* **27,** 343–350 (2011).

104. Klement, H., Helfrich, M., Oster, U., Schoch, S. & Rüdiger, W. Pigment-free NADPH:protochlorophyllide oxidoreductase from *Avena sativa* L. *Eur. J. Biochem.* **265,** 862–874 (1999).

105. Gabruk, M. *et al.* Photoactive protochlorophyllide-enzyme complexes reconstituted with PORA, PORB and PORC proteins of A. thaliana: Fluorescence and catalytic properties. *PLoS One* **10,** 1–18 (2015).

106. Dahlin, C., Sundqvist, C. & Timko, M. P. The in vitro assembly of the NADPH-protochlorophyllide oxidoreductase in pea chloroplasts. *Plant Mol. Biol.* **29,** 317–30 (1995).

107. Wolfe, K. H., Gouy, M., Yang, Y. W., Sharp, P. M. & Li, W. H. Date of the monocot-dicot divergence estimated from chloroplast DNA sequence data. *Proc. Natl. Acad. Sci. U. S. A.* **86,** 6201–5 (1989).

108. Heyes, D. J., Levy, C., Sakuma, M., Robertson, D. L. & Scrutton, N. S. A twin-track approach has optimised proton and hydride transfer by dynamically-coupled tunnelling during the evolution of protochlorophyllide oxidoreductase . **7,**

109. Hoeven, R., Hardman, S. J. O., Heyes, D. J. & Scrutton, N. S. Cross-species analysis of protein dynamics associated with hydride and proton transfer in the catalytic cycle of the light-driven enzyme protochlorophyllide oxidoreductase. *Biochemistry* **55,** 903–913 (2016).

110. Heyes, D. J., Menon, B. R. K., Sakuma, M. & Scrutton, N. S. Conformational events during ternary enzyme-substrate complex formation are rate limiting in the catalytic cycle of the light-driven enzyme protochlorophyllide oxidoreductase. *Biochemistry* **47,** 10991–10998 (2008).

111. Heyes, D. J. *et al.* Excited-State Properties of Protochlorophyllide Analogues and Implications for Light-Driven Synthesis of Chlorophyll. *J. Phys. Chem. B* **121,** 1312–1320 (2017).

112. Archipowa, N. NADPH:Protochlorophyllide Oxidoreductase - Analysis of the Substrate-Binding Pocket-. (Friedrich Schiller University Jena, 2013).

113. Kavanagh, K. L., Jörnvall, H., Persson, B. & Oppermann, U. Medium- and short-chain dehydrogenase/reductase gene and protein families: The SDR superfamily: Functional and structural diversity within a family of metabolic and regulatory enzymes. *Cell. Mol. Life Sci.* **65,** 3895–3906 (2008).

7. Appendix

Table 7.1: fluorescence decay time, and relative amplitude, of PChlide measured at 150 K alone in buffer, with POR enzyme and in ternary complex with POR A, POR B and the mutants. For each measurement the decay traces are integrated along the wavelength range to obtain a global fit (590 – 730 nm), a fit of the blue side of the main emission peak (610 – 630 nm) and a fit of the red side of the main emission peak (633 – 640 nm).

Content of the sample	a_1	τ_1 (ns)	a_2	τ_2 (ns)	a_1	τ_1 (ns)	a_2	τ_2 (ns)	a_1	τ_1 (ns)	a_2	τ_2 (ns)
POR B isoform	**Global fit**				**610 – 630 nm fit**				**633 – 640 nm fit**			
PChlide	0.3	0.98	0.7	**5.7**	0.5	0.97	0.5	5.7	0.2	0.97	0.8	5.8
PChlide - POR B	0.2	0.98	0.8	**6.4**	0.3	0.96	0.7	6.4	0.1	0.99	0.9	6.5
PChlide - POR B - NADPH	0.3	0.97	0.7	**5.8**	0.4	0.98	0.6	5.5	0.3	0.98	0.7	5.9
3D Model												
S164A	0.3	0.99	0.7	**6.3**	0.4	0.98	0.6	5.9	0.4	1.00	0.6	6.5
S164T	0.2	0.97	0.8	**5.9**	0.4	0.99	0.6	5.7	0.2	1.00	0.8	6.1
K216Q	0.1	0.98	0.9	**6.7**	0.2	0.95	0.8	6.7	0.1	0.97	0.9	6.7
K216R	0.1	0.99	0.9	**6.9**	0.1	1.00	0.9	6.9	0.2	0.96	0.8	7.0
H138F	0.1	0.99	0.9	**6.9**	0.2	1.00	0.8	6.8	0.1	1.00	0.9	6.8
H138Y	0.2	1.00	0.8	**6.8**	0.2	0.99	0.8	6.8	0.1	0.97	0.9	6.8
Y299F	0.3	0.98	0.7	**6.0**	0.4	0.97	0.6	5.6	0.2	0.97	0.8	6.1
Y299H	0.2	0.96	0.8	**5.6**	0.3	0.95	0.7	5.1	0.2	0.99	0.8	6.1
Active site												
Y212F	0.1	0.98	0.9	**6.6**	0.4	0.99	0.5	6.4	0.1	1.00	0.9	6.6
Y212H	0.3	0.97	0.7	**6.4**	0.3	0.97	0.7	6.5	0.3	0.97	0.7	6.4
K213Q	0.2	0.98	0.8	**6.5**	0.3	1.5	0.7	6.8	0.2	0.98	0.8	6.5
K213R	0.3	0.98	0.7	**6.1**	0.3	0.96	0.7	6.0	0.2	0.98	0.8	6.3
D214M	0.2	0.98	0.8	**6.7**	0.2	0.99	0.8	6.7	0.2	1.00	0.8	6.7
D214A	0.4	0.98	0.6	**6.2**	0.5	0.98	0.5	6.0	0.4	0.99	0.6	6.3
K216Q	0.2	0.98	0.8	**6.7**	0.2	0.95	0.8	6.7	0.2	0.97	0.9	6.7
K216R	0.1	0.99	0.9	**6.9**	0.1	1.00	0.9	6.9	0.2	0.96	0.8	7.0
POR A isoform												
PChlide	0.3	0.98	0.7	**5.7**	0.5	0.97	0.5	5.7	0.2	0.97	0.8	5.8
PChlide - POR A	0.4	0.95	0.6	**6.2**	0.4	0.77	0.6	5.8	0.3	1.00	0.7	6.2
PChlide - POR A - NADPH	0.5	0.81	0.5	**5.0**	0.6	0.99	0.4	5.6	0.6	0.8	0.4	5.1
Active site												
Y215F	0.2	0.98	0.8	**6.2**	0.3	0.97	0.7	6.0	0.1	0.99	0.9	6.3
Y215H	0.2	1.00	0.8	**6.7**	0.3	0.99	0.7	6.6	0.2	0.93	0.8	6.7
K216Q	0.2	1.04	0.8	**6.4**	0.3	0.99	0.7	6.3	0.2	1.00	0.8	6.5
K216R	0.2	0.96	0.8	**6.2**	0.4	1.00	0.6	6.1	0.1	1.00	0.9	6.3
D217A	0.3	0.96	0.7	**5.8**	0.4	1.00	0.6	5.8	0.2	0.97	0.8	5.8
K219Q	0.3	1.05	0.7	**6.3**	0.4	1.00	0.6	6.3	0.1	1.00	0.9	6.3
K219R	0.2	1.00	0.8	**6.6**	0.2	1.00	0.8	6.6	0.2	0.96	0.8	0.6

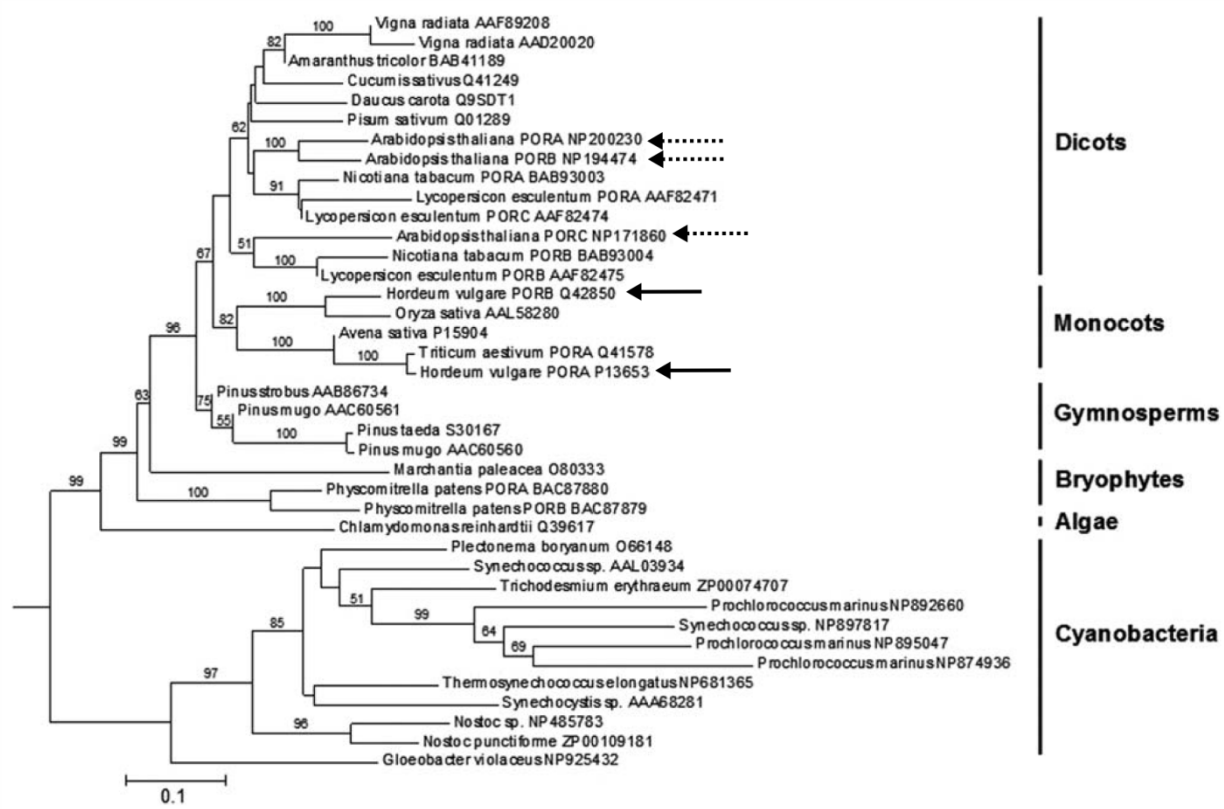

Figure 7.1: phylogenetic tree of light prone POR (LPOR) reconstructed by the neighbor joining method. The bootstrap proportions are reported at the internal nodes. Values under 50% are not shown. The expected number of amino acid substitutions per site are proportional to the branch length. POR A, POR B and POR C from *A. Thaliana* are marked with a dashed arrows. POR A and POR B from *H. vulgare* are marked with arrows. The tree highlights the phylogenetic proximity between the POR A and B from *Thaliana*, in contrast with the distance between POR A and B from *H. vulgare*. (figure modified from Yang et al.[36])

List of Publications

Garrone A[#], Archipowa N[#], Zipfel PF, Hermann G, Dietzek B. Plant Protochlorophyllide Oxidoreductases A and B: CATALYTIC EFFICIENCY AND INITIAL REACTION STEPS. *J Biol Chem*. 2015 Nov 20; **290(**47):28530-9

# Equal contribution

Ginter T, Fahrer J, Kröhnert U, Fetz V, **Garrone A**, Stauber RH, Reichardt W, Müller-Newen G, Kosan C, Heinzel T, Krämer OH. Arginine residues within the DNA binding domain of STAT3 promote intracellular shuttling and phosphorylation of STAT3. *Cell Signal.* 2014 Aug **26**(8):1698-706

Participation at national and international conferences

Oral presentations:

16.09.2014 - **Annual Meeting of the German Biophysical Society** - Lübeck

09.-11.05.2013 - **Annual German Conference on Physical Chemistry** - Karlsruhe

26.-30.08.2012 - **EuCheMS** (European Association for Chemical and Molecular Science) Prague (Czech Republic)

Posters :

31.03.-03.04.2014 - **4th International conference on Microbial Communication** - Jena

12.-14.11.2012 - **Manfred Eigen Gespräche** - Jena

08.-10.10.2012 - **23rd Lecture Conference on Photochemstry** - Postdam

Acknowledgement

Foremost, I would like to thank Prof. Dr. Benjamin Dietzek and PD Dr. Gudrun Hermann for supervise my work along this five years, for the constructive discussions and critics in the laboratory work, analysis of the results and in writing this thesis.

I would like to thank Nataliya Archipowa for her important contribution in the production and characterization at room temperature of the wild type and mutant enzymes as well as Joachim Kuebel who assisted me in set-up the fluorescence experiment and created the software for the fluorescence data analysis. I would also thanks the Genetic and the Microbiology working group for let me use some of their equipment.

My sincere thanks go to all the member of both, biochemistry and fast spectroscopy working group. You all created a fruitful, collaborative but also convivial working atmosphere that supported me in keep going with my PhD work. Furthermore, I would thank Vito Valiante, Tobias Wagner, Julian Schindler, Christian Reichard and Alessandro Tuniz for their very helpful comments on my dissertation.

I am grateful to the Jena Graduate School for Microbial Communication (JSMC) who founded my first three years of work, allowed me to be involved in a numerous extracurricular activities and created an inspiring cross-disciplinary scientific network.

A big big Dankeschön to all my friends and people I got to know in Jena. It was amazing been part of such an international and sparkling group.

My thanks go also to my family, my close friends in Turin and Franziska. You were always next to me despite the distance. I really appreaciate your support along this years.

Declaration of Originality

I hereby certify that I am familiar with the course of examination for doctoral candidates of the faculty of Biology and Pharmacy of the Friedrich Schiller University Jena. I further declare that I have composed and written the dissertation on my own with the assistance of my supervisor PD Frau Dr. Gudrun Hermann. I certify that, to the best of my knowledge, my thesis does not infringe upon anyone's copyright nor violate any proprietary rights and that any material from third part is identify as such and quoted according to the standard referencing practices. Furthermore, I do not enlist the assistance of doctoral consultant as well as no third parties have received either direct or indirect monetary benefits.

I also declare that I have not submitted my dissertation, or a substantially similar one, to any other University or Institution.

Jena, 23.03.2017

_____

Alessio Garrone

Curriculum vitae

Personal data

Name	Alessio Garrone
Birth date:	23.09.1985
Birth place:	Ciriè

High school education

09.1999 - 06.2004	Scientific High School "A. Gramsci" in Ivrea

University education

09.2004 – 12.2007	Bachelor of Science in Biotechnology at the University of Turin (Italy) Thesis title: "Myco-remediation: application of fungi for organic pollutant bioremediation"
01.2008 – 10.2010	Master of Science in Industrial Biotechnology at the University of Turin (Italy) Thesis: "Tailoring a Catechol 1,2-Dioxygenase active site: Catalytic features of novel mutants in positions 69 and 72"
01.2009 – 06.2009	Erasmus exchange student at the University of Umeå (Sweden)
Since 10.2011	PhD student at the University of Jena in collaboration with the Leibnitz Institute for Photonic Technology Jena

Zusammenfassung

Die NADPH-Protochlorophyllid-Oxidoreduktase (POR), EC 1.3.1.33, ist in allen Organismen mit oxygener Photosynthese ein Schlüsselenzym bei der Biosynthese von Chlorophyll. Sie katalysiert in einer lichtabhängigen Reaktion und in Gegenwart des Coaktors NADPH die Reduktion des Protochlorophyllids (PChlide) zum Chlorophyllid (Chlide). Dabei treten in Pflanzen zwei Isoenzymformen auf, POR A und POR B. Die POR A ist als Enzym ausschließlich in der Phase des De-etiolements aktiv, während die POR B konstitutiv exprimiert wird und in licht-adaptierten Pflanzen als Hauptenzym bei der lichtgesteuerten Synthese von Chlorophyll fungiert. Beide Isoenzyme, POR A und POR B, werden hinsichtlich ihrer katalytischen Effizienz und ihres Reaktionsmechanismus verglichen. Untersucht werden heterolog exprimierte Enzyme aus Gerste (*Hordeum vulgare*, L.).

Im Vergleich zur POR A weist die POR B eine 6-fach höhere katalytische Effizienz (k_{kat}/K_M) auf. Ausgehend von gleichen Intermediaten, die bei tiefen Temperaturen „ausgefroren“ werden können, unterscheidet sich der Katalysemechanismus beider Isoenzyme nicht, sehr wohl aber der Temperaturbereich innerhalb dessen diese Intermediate gebildet werden. Die Ergebnisse legen für die POR B eine höhere konformationelle Flexibilität der Proteinumgebung im katalytisch aktiven Zentrum des Enzyms nahe. Im Unterschied zum Reaktionsmechanismus in POR-Enzymen aus Cyanobakterien, die als phylogenetischer Vorläufer der pflanzlichen POR-Enzyme zu betrachten sind, bilden sowohl POR A als auch POR B bei 180 K bereits vollständig reduziertes, aber noch enzymgebundenes Chlide. Das deutet auf einen gekoppelten und, nicht wie bei den Cyanobakterien, sequentiellen H^-/H^+ Transfer hin. Der Grund dafür ist offensichtlich eine im Verlauf der Evolution erfolgte Optimierung des katalytisch aktiven Zentrums.

Um einen detaillierteren Einblick in den Aufbau des katalytisch aktiven Zentrums zu gewinnen, wurde für die POR B mit Hilfe von *in silico* Methoden ein dreidimensionales Strukturmodell entwickelt. In dieses Strukturmodell wurden mit geeigneten *docking*-Methoden auch das Substrat, PChlide, und der Cofaktor, NADPH, über Energieminimierungsprozesse eingepasst. Im katalytisch aktiven Zentrum spielen His-138, Ser-164, Lys-216 und Tyr-299 für die Einbindung des PChlide sowie dessen korrekte Positionierung im ternären Enzym-Substrat Komplex eine wichtige Rolle. His-138 und Lys-

216 interagieren über elektrostatische/Wasserstoffbrückenbindungen mit der Carboxylgruppe der Propionsäureseitenkette am C(17) des PChlide. Ser-164 bildet eine koordinative Bindung zum Mg^{2+}-Zentralion aus und Tyr-299 steht in Wasserstoffbrückenbindungskontakt mit der C(13')=O Gruppe am Cyclopentanonring. Die beschriebenen Wechselwirkungen können in *site-directed* Mutagenese-Experimenten bestätigt werden.

Zum ersten Mal kann für ein POR B Enzym die Beteiligung eines katalytisch aktiven Tyr- und Lys-Restes am Reaktionsmechanismus nachgewiesen werden. Tyr-212 übernimmt die Rolle des H^+-Donators und Lys-216 ist bei der Herabsetzung des pK_a-Wertes der Tyr-OH Gruppe von Bedeutung. Die Seitenketten beider katalytisch aktiven Aminosäuren sind darüber hinaus auch an der korrekten Einbindung des Substrats in das aktive Zentrum, über die möglicherweise ein „Prae"-Übergangszustand geschaffen wird, beteiligt. Die im katalytischen **Y**KDS**K** Motiv ebenfalls enthaltenen Aminosäuren Lys-213, Asp-214, Ser-215 sind auf der der Substratbindungsstelle abgewandten α-Helixregion lokalisiert, weshalb sie nur einen indirekten Einfluss auf die katalytische Aktivität ausüben. Sie sind offenbar für die korrekte Positionierung dieser α-Helix innerhalb der 3-D Struktur verantwortlich.

Darüber hinaus wird gezeigt, wie etliche der im aktiven Zentrum lokalisierten Aminosäuren wichtige reaktive Intermediate (S_X, S_{ICT}) stabilisieren und die direkte Desaktierung der in den S_1-Zustand angeregten Population entlang des reaktiven Desaktivierungskanals möglicherweise unter Vermeidung unerwünschter Nebenreaktionen ermöglichen.